

ABSTRACT

Title of Document: A MULTI-SCALE APPROACH FOR
CHARACTERIZING THE MECHANICAL BEHAVIOR
OF PIN-REINFORCED COMPOSITE SANDWICH
STRUCTURES WITH DIGITAL IMAGE
CORRELATION

Bianca Renee Brandveen, Master's of Science, 2013

Directed By: Professor Hugh A. Bruck
Department of Mechanical Engineering

In the last 10 years, pin-reinforced composite sandwich structures have become an interesting research topic in aerospace and naval engineering because of their low weight and high compressive properties. Current models lack rigorous physical understanding of the mechanics of these structures and do not accurately predict their performance. This hybrid numerical-experimental research approach investigates the compressive and flexural mechanical behavior of these materials and also characterizes and models the mechanical response in the form of full-field displacements and strains using Digital Image Correlation (DIC).

This thesis establishes an experimental mechanics characterization approach spanning several length scales, including: single pins, representative volume elements, contoured beams, and cylindrical shells with 6" radius of curvature. The previously assumed deformation response of pins within the composite was substantiated with 2D and 3D DIC and extrapolated to the macroscale for both straight and contoured composites.

**A MULTI-SCALE APPROACH FOR CHARACTERIZING THE
MECHANICAL BEHAVIOR OF PIN-REINFORCED COMPOSITE
SANDWICH STRUCTURES WITH DIGITAL IMAGE CORRELATION**

By

Bianca Renee Brandveen

Thesis submitted to the Faculty of the Graduate School of the
University of Maryland, College Park, in partial fulfillment
of the requirements for the degree of
Master of Science
2013

Advisory Committee:
Professor Hugh A. Bruck, Chair and Advisor
Professor Abhijit Dasgupta
Professor Sung Lee

© Copyright by
Bianca Renee Brandveen
2013

Foreword

“Trust in the Lord with all your heart, and lean not on your own understanding; in all your ways acknowledge Him, and He shall direct your paths.”

Proverbs 3: 5-6 (NKJV)

My life verse:

“For God has not given us a spirit of fear, but of power and of love and of a sound mind.” 2 Timothy 1:7 (NKJV)

Dedication

To my parents

Donna and Reggie Brandveen

for all of your love, support, advice and guidance throughout my education.

Acknowledgements

First of all, I would like to thank my advisor Dr. Bruck for his support and guidance throughout the process of doing research. I also want to thank my thesis committee members Dr. Dasgupta and Dr. Lee for aiding me in my research and agreeing to be a part of my committee. A big thank you goes out to Mr. Amarildo DaMata for keeping me notified about deadlines, guiding me through graduate school, and inspiring me to keep going since day one. Overall, I thank University of Maryland for providing access to academic resources through the library system such as journals and papers.

Additionally, I offer a thank you to my colleagues and fellow researchers in the AML and MML research group: Ariel Perez-Rosado, Sandip Haldar, Elizabeth Sauerbrunn, Joe Puishys, Robert Kupferschmitt, Graeme Fukuda, and Luke Roberts. You all have certainly made graduate school an interesting and rewarding time in my life.

Thank you Albany Engineered Composites (AEC) for providing the pin-reinforced composite sandwich materials to me. Without you all, this research project would not have been possible. I'd also like to thank Materials Research and Design (MR&D) for assisting with the analytical portion of the research. Additionally, I'd like to thank NAVAIR - Patuxent River for funding this project under contract number N68335-12-C-0301 and agreement number N00421-98-H-1116.

Moreover, I want to thank my family and friends for all of their support and love throughout my matriculation. To my parents, I appreciate all of your helpful advice

that you've given me. To my siblings-- Andrea, Andrew and Danielle—thank you all for reminding me to keep smiling even when things get tough. To James Lankford, thank you for your encouragement, love, patience and understanding throughout my Master's program. You have been there since the very beginning. Words cannot express how thankful I am to have you in my life. To “Dr.” Kathy Lloyd, thank you for giving me helpful resources during my writing process and being there for me emotionally. To Miss Nefretiti Nassar, thank you for all of your advice and support to get me through the “Boston Market” moments during my graduate program.

I would like to give a special “thank you” to the National GEM Consortium and Fermi National Accelerator Laboratory for funding my graduate school education. I couldn't have done this without you all!

To my newfound family at the Black Engineers Society: thank you for all of the support, laughter, encouragement and positivity you've given me throughout my thesis writing process. You guys keep me young. I'll never forget you.

Thank you to my churches, Zion Church - Landover and Mount Olive Baptist Church - Centreville, for providing me with a loving church family who supported and encouraged me throughout my graduate program. Last, but certainly not least, I give all honor and glory to my savior, Jesus Christ. Through His Word, I have received so much wisdom, guidance and strength over the years, and I would be remised to

exclude Him from this exciting phase of my life. Thank you Lord for all You've done for me!

Table of Contents

FOREWORD	II
DEDICATION	III
ACKNOWLEDGEMENTS	IV
TABLE OF CONTENTS	VII
LIST OF TABLES	IX
LIST OF FIGURES	X
LIST OF ABBREVIATIONS	XIV
CHAPTER 1: INTRODUCTION	1
1.1 X-COR AND K-COR PIN CONFIGURATIONS	6
1.2 EXISTING LITERATURE ON PIN-REINFORCED SANDWICH STRUCTURES.....	9
1.2.1 <i>Failure Modes</i>	11
1.2.2 <i>Related Equations</i>	13
1.3 DIGITAL IMAGE CORRELATION	15
1.4 CONTRIBUTIONS.....	16
1.5 THESIS ORGANIZATION	17
CHAPTER 2: EXPERIMENTAL SETUP	18
2.1 CONSTITUENT MATERIAL PROPERTIES.....	18
2.2 PREPARATION AND MANUFACTURE OF K-COR SANDWICH STRUCTURE	20
2.3 EQUIPMENT	21
2.4 PROCEDURE AND METHODS	25
2.4.1 <i>Procedures</i>	25
2.4.2 <i>Methods</i>	28
CHAPTER 3: RELEVANT FINDINGS FROM PRIOR EXPERIMENTS	30
3.1 METHODOLOGY	30
3.2 RESULTS	34
3.2.1 <i>Square Specimens: 2cm x 2cm</i>	34
3.2.2 <i>Square Specimens: 3" x 3"</i>	35
3.2.3 <i>Cross pin Specimens</i>	37
3.2.4 <i>Additional Tests</i>	39
CHAPTER 4: MULTI-PIN REPRESENTATIVE VOLUME ELEMENT COMPRESSION TESTING	41
4.1 <i>METHODOLOGY</i>	43
4.1.1 <i>Free Boundary Condition</i>	43
4.1.2 <i>Glued and Greased Boundary Conditions</i>	45
4.2 RESULTS	45

4.2.1 <i>Free Boundary Condition</i>	46
4.2.2 <i>Glued and Greased Boundary Conditions</i>	55
4.3 DISCUSSION	63
CHAPTER 5: TWO- AND THREE-DIMENSIONAL COMPRESSION TESTING OF SMALL CURVED SPECIMENS.....	65
5.1 <i>METHODOLOGY</i>	66
5.1.1 <i>Design of Experiments</i>	67
5.1.2 <i>Preparation of Curved Sandwich</i>	68
5.1.3 <i>Manufacturing Procedure</i>	69
5.2 RESULTS	71
5.2.1 <i>Load-Displacement Results</i>	71
5.2.2 <i>2D DIC Results</i>	74
5.2.3 <i>3D DIC Results</i>	78
5.3 DISCUSSION	81
CHAPTER 6: TWO- AND THREE- DIMENSIONAL COMPRESSION TESTING OF LARGE CURVED SPECIMENS.....	83
6.1 <i>METHODOLOGY</i>	83
6.2 RESULTS	88
6.2.1 <i>Load-Displacement Results</i>	88
6.2.2 <i>2D DIC Results</i>	91
6.2.3 <i>3D DIC Results</i>	98
6.2.4 <i>Comparison with Small Curved Specimen</i>	106
6.3 DISCUSSION	108
CHAPTER 7: CONCLUSION.....	111
7.1 <i>CONTRIBUTIONS</i>	112
7.2 <i>FUTURE WORK</i>	112
GLOSSARY.....	115
BIBLIOGRAPHY	116

List of Tables

Table 1: Table of constitutive material properties used in FEA model and analysis [2]	20
Table 2: Core attributes for pin-reinforced sandwich structures tested during this research	29
Table 3: Summary of compression testing results for 3” x 3” K-cor sandwiches	37
Table 4: Design of Experiments for first set of RVE compression tests; free boundary condition	44
Table 5: Design of Experiments for the second set of RVE Compression Tests; Greased and Glued boundary conditions	45
Table 6: Summary of Results for RVEs with different boundary conditions prior to transformation to macrostress	64
Table 7: Comparison of stiffness and strength of K-Cor specimens from Chapter 3.	64
Table 8: Design of Experiments for small curved pin-reinforced sandwich structures manufactured at UMD	68
Table 9: Brief summary of results for small curved specimen experiments.....	82

List of Figures

Figure 1: Nomex honeycomb sandwich structure [24].....	2
Figure 2: Pin-reinforced composite sandwich structure [13].....	4
Figure 3: X-Cor sandwich structure [16].....	7
Figure 4: K-cor sandwich structure [16].....	7
Figure 5: Reveal length for a K-Cor pin-reinforced sandwich structure	7
Figure 6: Detail drawing of X-cor and K-cor facesheet adhesion	8
Figure 7: (a) Geometries and properties pertinent to the analysis of a beam in three-point bending, with schematics of the expected failure modes (b) indentation, (c) core shear, and (d) face failure [21]	13
Figure 8: Point Grey Flea 2G CCD Camera	22
Figure 9: Tamron 28-80mm adjustable zoom lens	23
Figure 10: Set of lens extenders: 7mm, 14mm and 28mm	23
Figure 11: C-Mount adapter to attach to the Tamron lens.....	24
Figure 12: Excel program that collects load-displacement data from the Imada load frame.	24
Figure 13: Example of Target Generator calibration image before and after detection in the VIC 3D DIC program	26
Figure 14: Small scale X-pin specimen	32
Figure 15: Sample screen for VIC Gauge software program with a cross pin specimen	32
Figure 16: Undeformed small-scale pin compression specimen in microtensile load frame	33
Figure 17: Undeformed small-scale cross pin compression test with foam cut at the facesheet/core interface.....	33
Figure 18: Graphs showing the global compression response of pin-reinforced composite sandwiches, (a) Load-displacement (b) Stress-strain	35
Figure 19: Axial compression response of 3" x 3" sandwich structure under repeated loading.....	36
Figure 20: Stress-Strain curve for X-pin loading and unloading response.....	38
Figure 21: X-pin specimen with pins experiencing buckling	38
Figure 22: (a) Displacement vector fields from 2D DIC in the RVE specimen, showing bias of deformation transversely whereas axial variation corresponds to higher bending modes. (b) Observed pin shear failure for RVE	39
Figure 23: Change in shape of the top half of the pin, along with increasing stress. (Reference above figure).....	40
Figure 24: Reduced Volume Element (RVE) specimen, showing the unit cell pin structure. This was used for 3D characterization of the compressive behavior. These specimens are 15 mm thick.	41
Figure 25: RVE used for glued and greased end condition. These specimens are 15 mm thick.	42
Figure 26: Sample RVE specimen without foam	43
Figure 27: Experimental setup for RVE experiment	44
Figure 28: Experimental setup for imaging 3-D Digital Image Correlation (DIC)	44

Figure 29: Load-displacement response curve for RVEs with free boundary condition	46
Figure 30: Stress-strain plot for Test 3, 4 and 5 with free boundary condition	47
Figure 31: Strains in the Elastic Region for compression tests with free boundary condition	49
Figure 32: Strain fields at the elastic limit for RVE compression tests with a free boundary condition	51
Figure 33: Strain fields at failure for RVE compression tests with a free boundary condition	53
Figure 34: Strain-Displacement Data for Test 4, free boundary condition.....	54
Figure 35: Global crosshead strain plotted against Pin Strain achieved from 3D DIC. These results also come from the Test 4 data set (free boundary condition).....	54
Figure 36: Vertical displacement field at failure for RVE with free boundary condition	55
Figure 37: Load-displacement curve for greased RVE experiment.....	56
Figure 38: Stress-strain plot for greased RVE experiment	56
Figure 39: Load-displacement curve for glued RVE experiment.....	58
Figure 40 Stress-strain plot for glued RVE experiment.....	58
Figure 41: Stress-strain curve showing the macrostress for RVE test specimens with various boundary conditions	59
Figure 42: Location of pixels where strain and displacement fields were extracted. This image comes from the Test 2 RVE data set with greased boundary condition.	60
Figure 43: Strain-displacement plot of the left pin for Test #2 (greased boundary condition). All values are calculated with VIC 3D.	61
Figure 44: Strain-strain plot of the left pin for Test #2 (greased boundary condition). DIC pin strains were calculated with VIC 3D and global strain comes from Imada load frame.	61
Figure 45: Strain-displacement plot of the right pin for Test #2 (greased boundary condition). All values are calculated with VIC 3D.....	62
Figure 46: Strain-strain plot of the right pin for Test #2 (greased boundary condition). DIC pin strains were calculated with VIC 3D and global strain comes from Imada load frame.	62
Figure 47: The radius of curvature for a curved sandwich structure changes; R can help determine local pin orientations after the sandwich has been thermoformed into shape.	66
Figure 48: End supports for small curved specimen experiments, including: (a) bottom supports and (b) bottom and edge supports	67
Figure 49: Fixture design for shaping sandwich specimens. Screw holes allowed variations of three and four point bending locations when specimen is in the oven.....	69
Figure 50: Fixture allowing for fabrication of shaped K-Cor composites with a single curvature	69
Figure 51: Representative curved specimen with dimensions.....	70
Figure 52: Experimental set up for the flexural test of the K-cor sandwich composite, showing a specimen without foam core.....	71

Figure 53: Load-displacement curve for central loading of curved specimen with foam and bottom boundary condition. Results are from the Test 1 data set.....	72
Figure 54: Global flexural response of the curved K-cor sandwich specimens and comparison with straight sandwich. The elastic deformation, failure initiation and transition to compressive response are indicated.	73
Figure 55: Stress-Strain diagram for small curved sandwiches with and without foam core.....	74
Figure 56: DIC strain field results for load conditions A (top), B (middle) and C (bottom). These results come from the Test 1 data set.	75
Figure 57: Deformation images for (a) elastic region (b) end of elastic region and (c) failure.	76
Figure 58: Failure of a previously tested flat specimen in three point bending. The core shear failure mechanism is indicated in yellow	77
Figure 59: Axial DIC strain fields associated with core shear failure in the previous figure.	78
Figure 60: Data extraction point for Test 1, with coordinate system shown	79
Figure 61: Evolution of DIC facesheet strains as a function of global strain. Results come from the Test 1 data set	79
Figure 62: 3D DIC Strain data for Test 1	80
Figure 63: Whole 6" radius sandwich structure from AEC	84
Figure 64: Whole 6" radius of curvature sandwich structure	84
Figure 65: Schematic of compressive loading condition for 6" radius curved sandwich	85
Figure 66: Schematic diagram of the curved X-cor specimen supported at the bottom and edge	85
Figure 67: End condition for 6" radius flexural experiment. The sandwich was cut to be perpendicular to the facesheet material.....	86
Figure 68: Imada load frame, specimen and caliper	86
Figure 69: Diagram showing how the macro-mechanical DIC images were obtained.	87
Figure 70: The location of the 3D imaging surface	88
Figure 71: Load-displacement response of the curved (6" Radius) X-cor composite sandwich structure under flexure; the elastic stiffness is shown.	89
Figure 72: Global stress-strain results for Test 5 of the 6" radius curved sandwich structure.....	90
Figure 73: Shear strain fields on the X-Cor sandwich specimen as determined by DIC at (a) elastic regime, (b) before failure initiation, (c) failure initiation, and (d) start of plateau regime. The specimen fails by core shear.	93
Figure 74: Vertical displacement fields for a six inch radius of curvature sandwich at (a) elastic region (b) end of the elastic region and (c) failure.....	95
Figure 75: Chosen area for 2D DIC strain and displacement extraction	96
Figure 76: Strains in the x and y direction and shear strain plotted against vertical displacement.	97
Figure 77: A sample specimen that failed by core shear failure and facesheet-core delamination.....	98

Figure 78: Strain fields, as determined by 3D DIC, for (a) within the elastic regime and (b) after the failure initiation.	100
Figure 79: Contour strain plots, as determined by 3D DIC, for (a) the elastic regime and (b) after the failure initiation.	102
Figure 80: Representative image to show the area used to extract strains from 3D DIC.	103
Figure 81: 3D DIC strain versus vertical displacement (ref. Figure 78)	104
Figure 82: Plot of DIC Strain versus global strain (ref. Figure 78)	104
Figure 83: Plot of curvature versus macroscopic load.....	105
Figure 84: The non-normalized load-displacement response for small and large curved sandwich specimens.	107
Figure 85: Stress-Strain plot to show the response of small K-Cor curved sandwiches prepared at UMD and large X-Cor curved sandwiches from AEC.	108

List of Abbreviations

AEC	Albany Engineered Composites
b	base dimension; Used in the inertia equation
d	height dimension; Used in the inertia equation
D	Deflection of a beam, as measured by the Imada load frame
DIC	Digital Image Correlation
E	Young's modulus
e_{xx}	Strain in x-direction and on the x-face
e_{yy}	Strain in y-direction and on the y-face
e_{zz}	Strain in z-direction and on the z-face
e_{xy}	Shear strain in xy plane
FEA	Finite Element Analysis
F, P	Force
GPa	Gigapascals
l	Length
MPa	Megapascals
RVE	Representative Volume Element
R	Radius of curvature
ε	Strain
θ	Angle
ρ	Curvature
σ	Normal Stress
τ	Shear stress

Chapter 1: Introduction

Engineers are constantly fighting the battle to find construction materials that are strong, stiff, and lightweight. This is especially true in the field of aerospace and naval engineering. Aerodynamics requires materials to have complex surface contours, which further complicates the problem. Airplane wings and parts are constantly being optimized to maintain their in-plane and flexural stiffnesses while still decreasing the total vehicle weight. Oftentimes, a change in material can mitigate or completely eliminate the issue of mass management. Lightweight pin-reinforced composite materials provide one avenue for solving this problem.

There are several benefits that can come about when designing with lightweight composite materials, especially in aerospace applications. When designing flight vehicles, there is the potential to increase fuel efficiency and create additional cargo capacity inside of the aircraft by using lightweight composite sandwich structures. In the automotive industry, there is the potential to provide an impact-resistant material for car bodies. Lightweight composites can also be used in shipbuilding. For instance, the Office of Naval Research is currently considering composite sandwich structures for naval ship hulls [3]. Sandwich structures are composed of two thin facesheets, usually composite laminates, and a thick layer of core material sandwiched in between. These materials have great properties: in particular, they are very lightweight, and the facesheet material generally allows the entire structure to be stiff and strong.

Sandwich structures are not a new concept; the idea has existed since 1849. According to Vinson, these types of materials have been manufactured since World

War II when England constructed the Mosquito night bomber with plywood sandwich materials. In that same time period, the United States started designing sandwich structures with reinforced plastic faces and low-density cores. It wasn't until the 1970's that composite sandwich structures were used to construct naval ship hulls in Sweden. Shifting from steel hulls to fiberglass composite construction required thorough experimentation and analysis in both small scale and full-scale tests. These experiments proved that, when properly designed, a composite sandwich hull could be as structurally sound as a hull composed entirely of steel. [4]

Sandwich structures are still being employed today, with most of them being in the form of honeycomb core sandwiches. An example of this form is shown in Figure 1. Honeycomb sandwich structures have a core consisting of open cells in hexagonal or cylindrical shapes that are separated by thin vertical walls. The core is usually made out of aluminum or composite materials like glass-phenolic, glass thermoplastic or Nomex. This type of sandwich structure gives relatively high out-of-plane compression and out-of-plane shear properties and also has a low core density. Because of this combination of properties, the honeycomb sandwich structure has seen lots of growth in recent years. For example, the wetted surface of a Boeing 707 (debuted in 1958) was 8% composite sandwich, whereas 46% of the wetted surface of the Boeing 757/767 (debuted in 1982) is honeycomb sandwich [4].



Figure 1: Nomex honeycomb sandwich structure [24]

While honeycomb sandwich structures have proven to be adequate in many engineering applications, there are still improvements that can be made. Pin-reinforced composite sandwich structures are even lighter and have better resistance to shear loads, in comparison to honeycomb sandwiches. By utilizing a closed-cell polyurethane foam as the core material and reinforcing it with pins, the structure is capable of withstanding higher compressive loads, in comparison to non-reinforced composite sandwich structures. All the while, it can still maintain its low-weight and high bending stiffness characteristics. Furthermore, unlike honeycomb sandwich structures, pin-reinforced composite sandwiches have more core surface area that can be bonded with the facesheet and they are not as sensitive to various environmental conditions.

What Is a Pin-Reinforced Composite Sandwich Structure?

The pin-reinforced composite sandwich structures discussed in this study are composed of three different parts: a foam core, carbon pins, and two carbon fiber facesheets (see Figure 2). The core is a soft and lightweight inner layer that carries the material's transverse shear and compressive loads. The core material can be thought of as the "meat" of the sandwich. The carbon pins, which are inserted at a specific angle through the core, act as stiff rods that add compressive strength to the sandwich structure. The pins also help to support the core. Finally, the laminated carbon fiber facesheets are the "bread" of the sandwich. This stiff outer layer resists both in-plane and lateral loading conditions. The core material separates the two facesheets, thereby

increasing the second area moment of inertia. This causes the sandwich to have a higher bending stiffness with only a slight increase in mass.

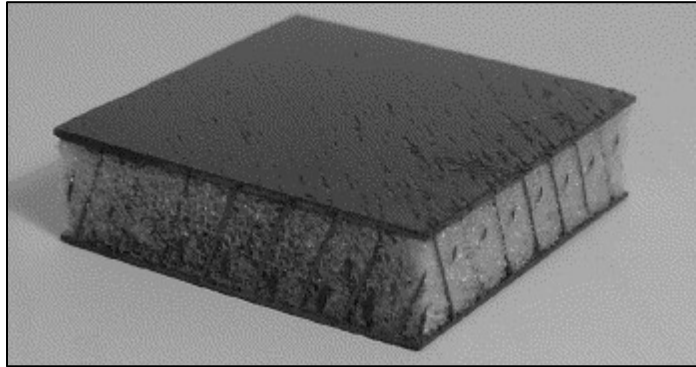


Figure 2: Pin-reinforced composite sandwich structure [13]

As one can imagine, the material properties of sandwich structures depend on the properties of the facesheet, core, adhesive bonding material and pins as well as the final geometry of the sandwich [10]. Further details about the constitutive properties of the pin-reinforced composite sandwich structure are given in *Section 2.1 Constituent Material Properties*.

Why Are Pin-Reinforced Composite Sandwich Structures So Important?

It is important to study and gain understanding of these pin-reinforced composite sandwich structures because of the potential benefits they offer to engineers and designers. As with any engineered composite material, the material properties and failure modes must be determined before the material can be put into the market and used commercially. These types of sandwich structures are difficult to analyze because of the complex nature of their make-up, but their material properties can be characterized by making use of technological advances such as Digital Image Correlation (DIC).

A combination of experimental material testing and DIC analysis was used to conduct this study. A review of the literature revealed that finite element analysis (FEA) has been used to predict these types of properties in the past, but DIC has not yet known to be utilized in determining the structural properties of pin-reinforced composite sandwich structures. [2] This novel approach is discussed further in *Section 1.3: Digital Image Correlation*.

Benefits of Incorporating Pin-Reinforced Foam Cores

There are several benefits to incorporating pin-reinforced foam cores into engineering designs. Studies at Sikorsky Aircraft Company have proven that replacing honeycomb sandwiches with pin-reinforced truss sandwiches can reduce the weight of the vehicle by 10-15% while maintaining the same compression and shear strength [7]. Along with being more lightweight and stiffer than honeycomb cores, pin-reinforced closed cell foam cores have several other benefits. They support transverse shear and impact loads through the thickness, provide a better bonding between the core and facesheet and resist fatigue crack propagation. Additionally, the pin-reinforced composite sandwich structure is an attractive alternative to open cell honeycomb sandwiches because of their high strength-to-weight ratio and increased compressive strength. Furthermore, pin-reinforced composite sandwiches have excellent responses to temperature and moisture, which makes them advantageous over honeycomb sandwiches because they eliminate corrosion and wetness related issues [10].

Problems/Challenges with Composite Sandwich Structures

Pin-reinforced composite sandwich structures have several advantages over honeycomb sandwich structures and other metallic materials when it comes to sandwich design and manufacturability. However, modern-day engineering challenges require composite materials that are stiffer and stronger in the through-thickness direction. At present, sandwich composites tend to have low stiffnesses, strength and impact resistance through the core because of the poor strength of the core material. One way to increase the overall mechanical properties of the composite sandwich structure is to add reinforcing pins by Z-pinning.

Z-pinning is a method that is used to reinforce a composite sandwich structure with small rods that protrude through the core and into (or onto) the facesheet [8]. The pins can be made from unidirectional carbon fiber composite or other high strength materials like titanium. Commercially, these Z-pins are known as X-Cor and K-Cor. More information about the different types of Z-pins is given in the next section.

1.1 X-Cor and K-Cor Pin Configurations

As previously mentioned, there are two ways to reinforce the through-thickness of composite sandwich structures with pins. In industry, they are known as X-Cor and K-Cor. The X-Cor configuration, shown in Figure 3 below, exhibits superior skin to core bonding because the tips of the rods penetrate through both of the facesheets. With this process, no additional bonding is required because the pins are protruded into the facesheet before curing. With K-Cor sandwiches (Figure 4), the

reinforcing pins are made to be longer than the foam thickness, creating an extended length known as the reveal length. A sketch of the reveal length is given in Figure 5.

X-COR:

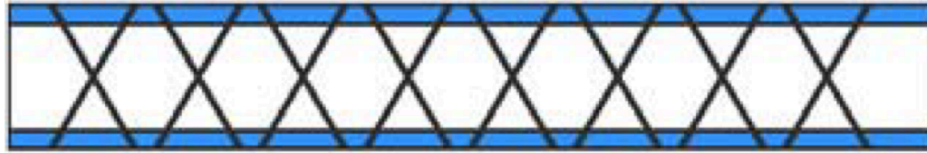


Figure 3: X-Cor sandwich structure [16]

K-COR:

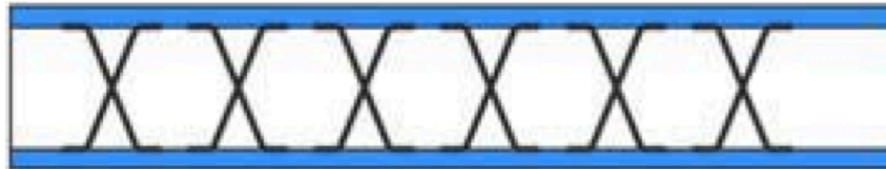


Figure 4: K-cor sandwich structure [16]

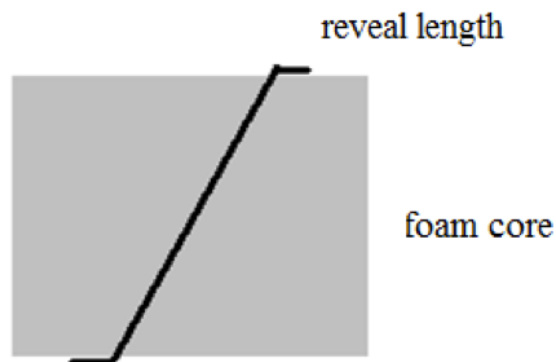


Figure 5: Reveal length for a K-Cor pin-reinforced sandwich structure

The ends of these pins are pressed onto the facesheet, which allows for exceptional flexibility in laminating and bonding the core to the facesheets [16]. In general, X-Cor sandwich structures utilize pins with a diameter of 500 microns while K-Cor sandwiches usually have pins that are more than 500 microns in diameter [11]. A more detailed view of the pin-facesheet connection is given in Figure 6.

Both the X-Cor and K-Cor arrangements create a pyramidal truss-like structure throughout the foam core of the composite sandwich structure. The pattern repeats throughout the entire sandwich structure, forming a unit cell of pins. In order to fully understand, some definitions must be given first. The pyramidal truss configuration - and thus, pin density - is described by two parameters: pin insertion angle and cell interval length. Pin density is the weight of the pins inside of a unit volume of sandwich structure material. Intuitively, higher pin densities create close packed pin configurations and tend to create stronger sandwich structures. The angle that the pins make with respect to the vertical is defined as the pin insertion angle. In this study, pins are set at a 30-degree angle (60 degree angle from the horizontal). The cell interval, which is also the side length of a unit cell, is the distance between adjacent pins of the same orientation in a sandwich structure.

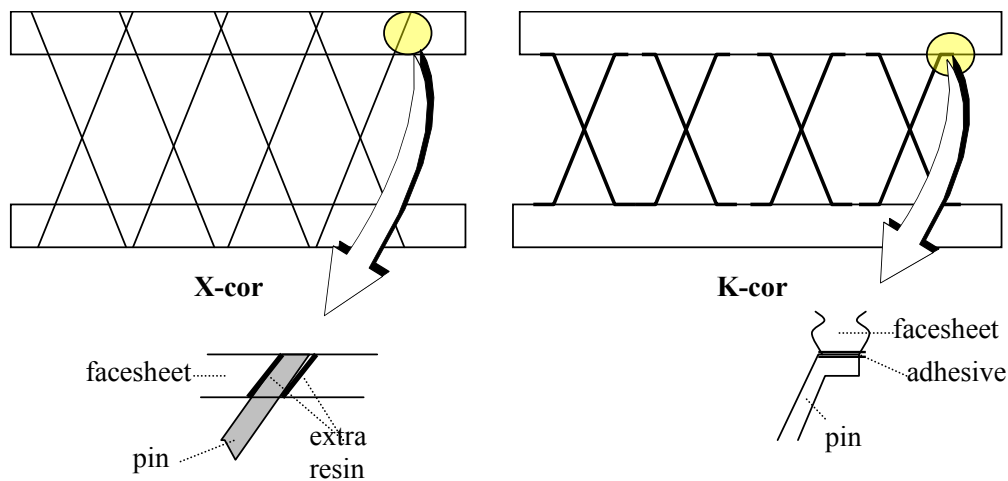


Figure 6: Detail drawing of X-cor and K-cor facesheet adhesion

1.2 Existing Literature on Pin-Reinforced Sandwich Structures

Sandwich structures are characterized by their compressive stiffnesses and strengths, so it is important to study how reinforcing the core in various ways changes these material properties. Alternative methods of reinforcing a sandwich structure using pins have been explored, in addition to the aforementioned X-Cor and K-Cor pyramidal structure. For instance, some use vertical pins, cross pin pairs, and tetrahedral arrangements [2]. Cross pins are a set of two oblique pins in a unit cell. Tetrahedral arrangements contain three oblique pins in a unit cell, with one in the direction of width and two in the direction of length. Still, other studies have been conducted with a pyramid-shaped arrangement in which a set of four pins all meet at a single location on the facesheet [19].

Due to the idea that pin-reinforced composite sandwich materials could completely replace honeycomb cored sandwiches, initial testing with these materials focused on dynamic and impact loading. The basic conclusions after studies from Marasco, Cartié et al show that 1) the mechanical properties of pin-reinforced sandwiches are strongly influenced by the pin insertion angle and 2) the bond strength between the core and facesheet is the limiting factor under tension and three-point bending [13].

To date, most of the studies for obtaining compressive material properties for reinforced sandwich structures are analytical and use experimental data to back up their models. These studies are meant to understand the compressive strength and stiffness for reinforced sandwiches. A. P. Mouritz [9] studied the effect of Z-pinning on through-thickness compression properties for sandwich structures with different

pin materials such as carbon nanotubes, composite, Steel, Aluminum and Titanium. He found that the pins are extremely effective at improving the compression properties and that carbon nanotube pins outperformed the other pin materials in terms of compressive modulus and compressive strength. Composite pins performed much better than Titanium pins and Aluminum pins were shown to have the lowest performance characteristics.

Still, other researchers have developed comprehensive analytical models by using FEA and empirical relationships to determine the stiffness of pin-reinforced composite sandwich structures. D.D. Cartié and Fleck tested X-Cor sandwich structures under quasi-static compressive loads and represented the pins as a beam-column upon an elastic foundation in their buckling analysis. During testing, an X-ray CAT scan machine was used to examine how the pins deformed under compressive loading. Their study showed that the maximum strength that pin-reinforced composite sandwich structures can achieve is determined by the elastic behavior of the reinforcing pins.

A more recent study by Rice, Fleischer and Zupan [21] demonstrates how they created a failure mode map to determine the initial failure mode of pin-reinforced sandwich cores. Based on geometry, yield strengths and force to initiate failure, the map can determine whether the pin-reinforced sandwich structure will fail via indentation, core shear failure or facesheet delamination. Further explanation about these failure modes is given in the next section. In the same study, these researchers also determined that pin reinforced cores were stronger in three-point bend than aluminum honeycomb, metal foam and PVC foam sandwich structures.

Of all of the research that has been conducted with pin-reinforced composite sandwich structures over the years, none have utilized Digital Image Correlation to characterize the material's response to compressive loading. Daniel and Gdoutos [10] used Moire' fringe patterns to visualize displacements as loads were being applied to a test specimen in three-point bend. This full-field optical method works well, but it does not give quite as much information as DIC for pin-reinforced sandwiches due to the highly variational geometries and directions within these sandwiches. A 2011 study by Nanayakkara, Feih and Mouritz [8] used acoustic emission monitoring, scanning electron microscopy, and X-ray computed tomography to image pin failure under a compressive loading condition. The study determined that some of the pins are damaged during elastic loading by longitudinal splitting and/or kinking, but they are still able to withstand a significant compressive load.

1.2.1 Failure Modes

Sandwich structures can be brought to failure by a number of different failure mechanisms, including: core shear failure, facesheet-core debonding, tensile or compressive failure of the facesheet, indentation failure, buckling, and wrinkling of the compression facesheet. Pin-reinforced composite sandwich structures tend to fail mostly by indentation, facesheet delamination and core shear failure. Indentation occurs when localized loads induce localized stresses sufficient enough to cause core failure. Facesheet delamination occurs when interlaminar shear stresses or out-of-plane strains are large enough to cause the facesheet to separate from the core. Failure modes can be visualized and identified by using DIC.

Figure 7 on the next page shows three examples of common failure modes: (b) indentation, (c) core shear failure and (d) facesheet delamination. Of these, core shear failure is the most common failure mode amongst sandwich structures. It occurs in short beams when the maximum shear stress experienced is equal to the shear strength of the core material. This failure mode becomes more prevalent when shear and compressive stresses are localized. [10]

Although there are many failure modes that can affect the sandwich structure, the mode of failure also depends on the loading state. When a specimen is placed in four-point bending or out-of-plane compression, neither facesheet delamination nor indentation is induced. In that case, only core shear failure will occur. On the other hand, specimens loaded in three-point bend can induce all three of the failure modes depending on the material properties and geometry of the composite sandwich. The standard laminated composite plate failure theory does not accurately describe how composite sandwich structures fail. For this reason, more complex failure criteria for pin-reinforced composite sandwich structures must be developed.

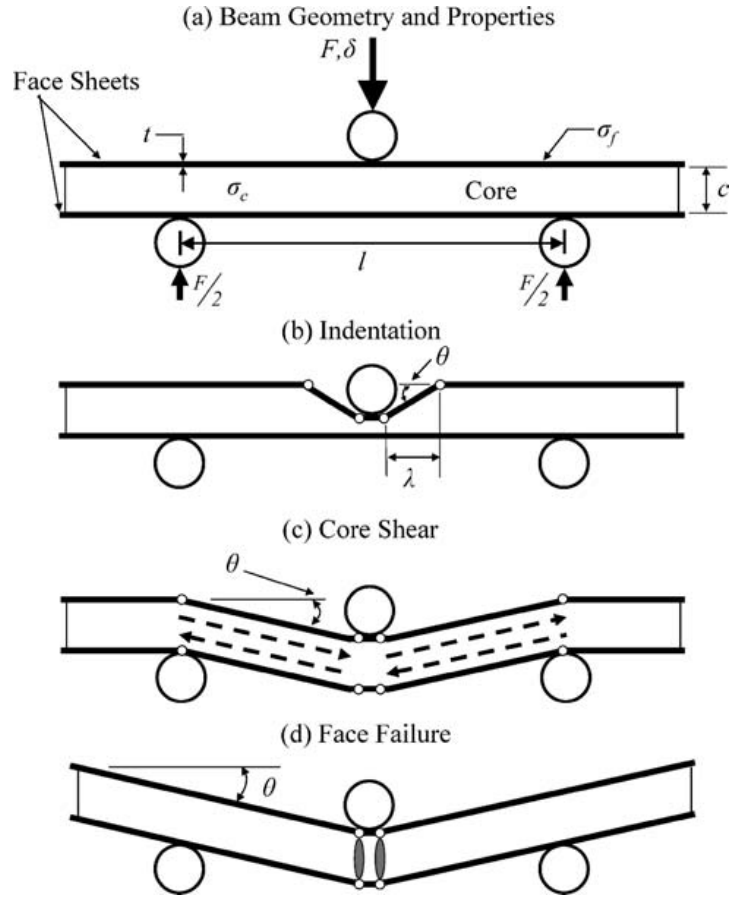


Figure 7: (a) Geometries and properties pertinent to the analysis of a beam in three-point bending, with schematics of the expected failure modes (b) indentation, (c) core shear, and (d) face failure [21]

1.2.2 Related Equations

The compressive modulus (stiffness) of a pin-reinforced composite sandwich structure can be determined empirically using the rule of mixtures formula as defined by Mouritz [9]. Each of the pultruded carbon pins is inserted at an angle (θ), so we must express the compression modulus of the pins with (Eq. 1). The through-thickness strength can be calculated by a similar relationship, given in (Eq. 2).

$$E_c = E_f f_f + E_p f_p \quad (\text{Eq. 1})$$

where E_f and E_p are the elastic modulus of the foam core and pins, respectively, and f_f and f_p are the volume fractions of foam and pins inside of the core, respectively. E_c is the compressive modulus of the composite.

$$E_p = \left[\frac{\cos^4 \theta}{E_x} + \frac{\sin^4 \theta}{E_y} + \left(\frac{1}{G_{xy}} - \frac{2 \nu_{xy}}{E_x} \right) \sin^2 \theta \cos^2 \theta \right]^{-1} \quad (\text{Eq. 2})$$

where θ is the inclination angle of the pin from the direction of the compressive load.

In-plane loading and bending moments can be related to in-plane curvatures and strains by using the following relations:

$$\begin{bmatrix} N_x \\ N_y \\ N_{xy} \end{bmatrix} = \begin{bmatrix} A_{11} & A_{12} & A_{16} \\ A_{12} & A_{22} & A_{26} \\ A_{16} & A_{26} & A_{66} \end{bmatrix} \begin{bmatrix} \varepsilon_x^0 \\ \varepsilon_y^0 \\ \varepsilon_{xy}^0 \end{bmatrix} + \begin{bmatrix} B_{11} & B_{12} & B_{16} \\ B_{12} & B_{22} & B_{26} \\ B_{16} & B_{26} & B_{66} \end{bmatrix} \begin{bmatrix} K_x \\ K_y \\ K_{xy} \end{bmatrix} \quad (\text{Eq. 3})$$

$$\begin{bmatrix} M_x \\ M_y \\ M_{xy} \end{bmatrix} = \begin{bmatrix} B_{11} & B_{12} & B_{16} \\ B_{12} & B_{22} & B_{26} \\ B_{16} & B_{26} & B_{66} \end{bmatrix} \begin{bmatrix} \varepsilon_x^0 \\ \varepsilon_y^0 \\ \varepsilon_{xy}^0 \end{bmatrix} + \begin{bmatrix} D_{11} & D_{12} & D_{16} \\ D_{12} & D_{22} & D_{26} \\ D_{16} & D_{26} & D_{66} \end{bmatrix} \begin{bmatrix} K_x \\ K_y \\ K_{xy} \end{bmatrix} \quad (\text{Eq. 4})$$

For compression tests, the modulus E_z and strength Z_t can be determined as long as the cross-sectional area and gage length are known. These quantities, as described by Carlsson and Kardomateas [23], are given by:

$$E_z = \frac{\sigma_z}{\varepsilon_z} \quad (\varepsilon_z \ll 1) \quad (\text{Eq. 5})$$

where σ_z is the load divided by the cross-sectional area and ε_z is the strain in the z direction.

$$Z_t = \frac{P_{ult}}{A} \quad (\text{Eq. 6})$$

where P_{ult} is the failure load of the specimen and A is the cross-sectional area [23].

For structures with simply supported end conditions, the buckling equation is as follows. Here, F is the critical force required for buckling, E is the elastic modulus, I is the second area moment of inertia, and L is the length of the column. For the pins in these sandwich structures, the critical load is ~68 N, as calculated by Virakthi [2].

$$F = \frac{4EI\pi^2}{L^2} \quad (\text{Eq. 7})$$

1.3 Digital Image Correlation

Digital image correlation (DIC) is a widely accepted high-performance computational tool that analyzes the pixel-to-pixel difference between digital images to calculate strain and deformation. This method has been used to characterize inhomogenous and non-uniform deformations at varied length scales and for several different applications and materials [20]. No matter what the application is, stress can be calculated from the strains by assuming a constitutive stress-strain relationship. This powerful software allows us to calculate strain without the use of strain gauges attached to the composite material.

Unlike strain gauges that only give the strain at a point, DIC can determine the full strain fields. This is like having an infinite number of strain gauges. With DIC, a subset of a random pattern is tracked by using an algorithm and later, the displacements can be computed. Each subset represents a scalar displacement value within the displacement field. Differentiation of the displacement field gives the strain field. This software has proven effective in this research due to the ease of use, scalability and fast calculation time.

This project makes use of multi-scale DIC technology by way of two-dimensional and three-dimensional Digital Image Correlation. 2D DIC is used to calculate in-plane values and 3D DIC can compute out of plane strains and displacements. Some experiments solely relied on 2D or 3D DIC, while others utilized both at the same time.

1.4 Contributions

A lack of experimental data on the micro-mechanical scale of pin-reinforced composite sandwich structures as well as the effects of contouring have prompted this research; therefore, the DIC method is presented to give the full-field strain and displacement response of these novel composite structures. The goals of this research are three-fold: property characterization, effect of carbon pins, and the response of the macro-scale material. The main purpose of this study is to characterize the mechanical behavior of both X-Cor and K-Cor pin-reinforced composite sandwich structures and analyze their behavior under compressive loading conditions with DIC. This study also seeks to understand the effect that reinforcing carbon pins have on load-bearing capacity and how these interactions impact the surrounding foam and facesheet. The final goal for this research is to extrapolate the micro-mechanical behavior to the macro-scale response. By characterizing the local micro-mechanical response of the carbon pins and sandwich structure, we can gain a better understanding of the global macro-mechanical behavior of the pin-reinforced composite sandwich structure.

This study is significant because it provides insight into the pin and pin-reinforced core mechanical responses that define pin-reinforced composite sandwich

structures. Moreover, this study validates and connects the FEA results from previous research with experimental data to prove the accuracy of the homogenized core approach. Lastly, this study provides a strong comparison for composite sandwich bending theory.

This is the first time that DIC will be used for this type of research. Using DIC on pin-reinforced structures is a special imaging challenge due to the highly complex 3D geometry that spans over the small discrete features of the sandwich. These features, which have highly variable orientations to the macro-scale geometry, vary from 500 microns all the way up to 30 centimeters.

1.5 Thesis Organization

This thesis is a detailed report of multi-scale compression and bending experiments for pin-reinforced composite sandwich structures. It is organized into seven chapters. The subject matter has already been explained briefly in the introduction chapter. Chapter 2 encompasses all of the experimental setup and details the properties of the constituent materials. The subsequent chapters numbered 3 through 6 discuss the experimental setup and results from each type of test at different length scales. Lastly, Chapter 7 concludes the document by providing a review of the work and presents opportunities for future developments on this topic.

Chapter 2: Experimental Setup

Several different types of experiments were conducted during this research program. Each experiment is set up in a similar fashion; they test what the material's response is for different sizes and configurations. Materials were tested under compressive loading as well as three-point bending. The full-field strain and displacement responses are measured with 2D and 3D DIC. Test materials were provided by Albany Engineered Composites (AEC), based out of Rochester, New Hampshire.

2.1 Constituent Material Properties

Composite structures are made up of several different materials, each having varying properties. When these materials combine, they form a composite that typically has better properties than the constituent materials themselves. Pin-reinforced composite sandwich structures are designed to be stiff, strong and lightweight, however the exact compressive properties have yet to be clearly established.

As with any composite, the mechanical properties of the individual components must be assessed before any attempt can be made to quantify the properties of the bulk composite structure. To this end, a description of the constituent materials for the pin-reinforced composite sandwich is given below in Table 1.

The core material used for these experiments was a closed cell Rohacell 31 foam [11]. This particular foam is highly resistant to water penetration. It has a

density of 31 kg/m^3 (1.9 lb/ft^3) and a compressive strength of 0.393 MPa (57 psi). The elastic modulus of this foam is 36 MPa , so it is very compliant. This foam core is strong enough in compression that it can support the facesheet with out of plane deflection, and is considered to be isotropic. [15]

Two different facesheets were used for these experiments. For specimens prepared at UMD, a woven fabric carbon-epoxy composite facesheet from DragonPlate was used. The layup appears to be a $0 / -45 / 0 / 45 / 0$, where each layer is approximately 0.138 mm thick. In total, the laminate composite facesheet is 1.1 mm thick. For specimens delivered by Albany Engineered Composites (AEC), the carbon fiber-epoxy facesheets were 0.75 mm thick and had a layup of $45 / 0 / -45 / 0 / 45 / 0$. In either case, both of the facesheets of a single sandwich have equal thickness.

The properties of the carbon fiber pins will be briefly described here, and the properties are given in the table below. The 8606 carbon fiber pins were tested under a tensile load at the University of Maryland. (These pins are also called T650-35). The elastic modulus for these pins was experimentally determined to be 155.2 GPa . The maximum stress that the pin held during the tensile test was 1.3 GPa . [12] For most of the experiments described in this thesis, the pin density used was 1.4 lb/ft^3 and 1.8 lb/ft^3 unless otherwise stated.

The epoxy that was used to bond the facesheet and core together is a West System epoxy resin 105 and hardener 206. These were mixed with a 5:1 ratio. The epoxy adhesive was cured at $200 \text{ degrees Celsius}$ for approximately 24 hours. The

Young's modulus of this epoxy is 3.17 GPa and it has a poisson's ratio of 0.35. The compression yield strength is 79 MPa [2].

The following table of material properties stems from the progress report from previous research conducted at UMD. All of the values were found in literature and were not measured directly with experiments. These same properties were used in the FEA model as well.

Table 1: Table of constitutive material properties used in FEA model and analysis [2]

	8606 Carbon Pin (T650-35)	Carbon Fiber Facesheet	Rohacell 31 Foam Core
Elastic Modulus, E_1	156.5 GPa	156.5 GPa	36 MPa
Elastic Modulus, E_2	156.5 GPa	12.96 GPa	36 MPa
Poisson's Ratio, ν_{12}	0.23	0.23	0.38
Shear Modulus, $G_{12} = G_{21}$	6.96 GPa	5.309 GPa	12.76 MPa
Shear Modulus, G_{23}	4.30 GPa	n/a	12.76 MPa

2.2 Preparation and Manufacture of K-Cor Sandwich Structure

During the course of this research program, the Multiscale Measurements Laboratory (MML) at the University of Maryland, College Park fabricated several different sizes of pin-reinforced sandwich structures. Results from Chapter 3, 4, and 5 all use material that was fabricated at MML. Albany Engineering Composites (AEC) provided the foam core that contained through thickness reinforcement of carbon rods. The woven carbon fiber laminates were obtained from The Composite Store [14]. The manufacturing procedure is explained below.

1. Heat the oven to 80 degrees Celsius.
2. Using the band saw, cut the foam and facesheet into the necessary size. You should cut out two identical facesheets and one foam core.
3. Prepare an epoxy mixture with 5 parts West System epoxy resin 105 and 1

part slow hardener 206, by mass.

4. Apply the epoxy to each facesheet and attach the pin-reinforced foam core.
5. Insert the specimen into the oven. Add a weight on top to allow for an even distribution of the epoxy. Let the specimen cure in the oven for 30 hours.
6. After the time has elapsed, carefully remove the specimen from the oven.

2.3 Equipment

All of the equipment that was used to carry out these experiments is listed below in bullet point format. There are also pictures of certain equipment below the list as a visual reference.

- Point Grey CCD cameras to capture images (Figure 8)
 - Flea 2 (mono, 1.4 MP, 30 fps)
 - Flea 2G (mono, 1.3 MP, 30 fps)
- Tamron Lenses (Figure 9)
 - 75-300 mm adjustable zoom lens
 - 28-80 mm adjustable zoom lens
- Lens extenders (Figure 10)
 - 14 mm
 - 21 mm
- 1394b FireWire cables
- C-Mount Adapters (Figure 11)
- Imada MX 500 load frame with Z2H-440 2 kN load cell
 - Load cell has resolution of 0.1 kg
- Caliper to measure the loading point displacement

- Edmund Optics MI-150 high intensity fiber optic illuminator
- PC equipped with MS Excel and DIC Software
- Software used:
 - Correlated Solutions: [VIC 2D 2010, VIC 3D 2009, VIC Snap 2010, Target Generator, VIC Gauge]
 - Point Grey [FlyCap]
 - sw2xmodified Excel spreadsheet program (See Figure 12 below)
- Oven

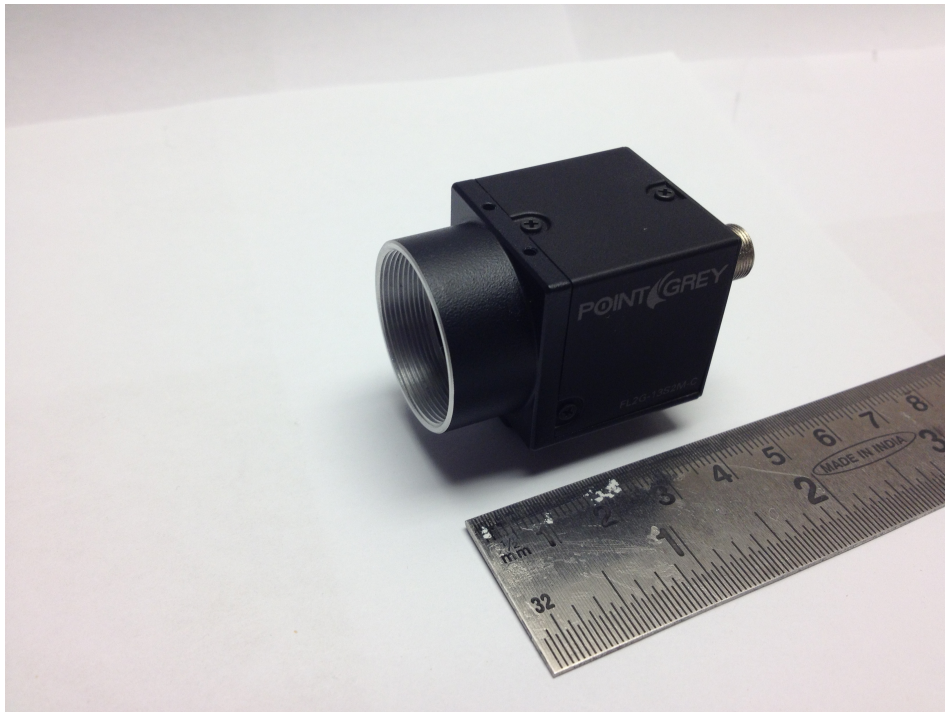


Figure 8: Point Grey Flea 2G CCD Camera



Figure 9: Tamron 28-80mm adjustable zoom lens



Figure 10: Set of lens extenders: 7mm, 14mm and 28mm

2.4 Procedure and Methods

The procedure for carrying out this compression experiment with Digital Image Correlation (DIC) must be followed exactly, lest any steps be forgotten.

2.4.1 Procedures

To calibrate the two cameras for 3D DIC:

1. Plug in the cameras to the computer using the FireWire cables.
2. Set up cameras so that they can fully capture the specimen you wish to take pictures of. It may be helpful to shine the fiber optic lamp on the specimen to make sure the lighting is adequate.
3. Ensure that the cameras and lenses are clean (no smudges) and that the lenses are zoomed in on the part of the specimen that you wish to analyze.
4. Generate a target using the Target Generator software. (The dimensions for the target will change, depending on how big the specimen is.) Print out the target and tape it to a flat surface like cardboard. An example of a target is shown in Figure 13.
5. Remove the specimen from the test stand and replace it with the appropriately sized target.
6. Using VIC Snap, capture images of the target. Ensure that the entire target can be seen in the image and that the three dots are clear. Capture about 15 images.
7. Import these calibration images into the VIC 3D file
8. In VIC 3D, click “Calibration”
9. Select the target size that you used from the dropdown menu.

10. Click “Analyze”
11. Check the calibration score. The score is the average error in pixels, so lower scores are better than higher scores. Good scores are displayed in green and bad scores are displayed in red. If the score is good, continue to step 12. If the score is bad, you must recalibrate the cameras by repeating steps 6-11.
12. Do not touch or move the cameras, as this will change the calibration values and cause you to re-calibrate the cameras.

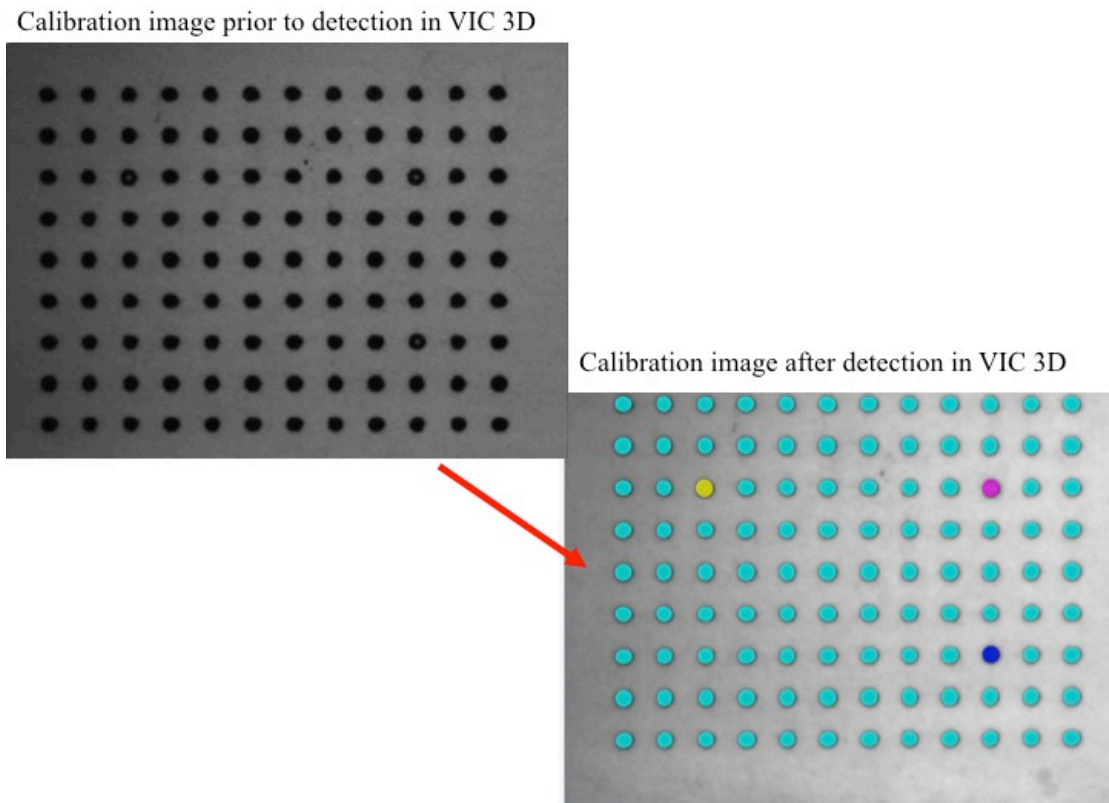


Figure 13: Example of Target Generator calibration image before and after detection in the VIC 3D DIC program

To run the experiment with a specimen:

1. Apply a speckle pattern to the specimen by using spray paint. White spray paint typically works well, since you are painting onto a black surface. The smaller the speckle pattern is, the better your results will be. Large regions of color are not detected well within the DIC program. To minimize reflections in the images, flat paint and/or anti-reflection coatings are recommended.
2. Post-calibration, insert the specimen into the test stand.
3. Open the load-displacement Excel program (sw2xmodified.xls) on the computer. In the setup, set the data capture rate to be every 0.5 seconds.
4. Open VIC Snap on the computer. Set up the program so that it will capture images every 0.5 seconds.
5. Turn on the Imada and caliper. Zero the equipment.
6. Set the Imada to a slow loading condition, preferably 0.55 mm/s.
7. With the indenter barely touching the specimen, start the compression.
8. BEFORE THE INDENTER TOUCHES THE SPECIMEN, simultaneously, start recording with VIC Snap and the load-displacement Excel spreadsheet.
9. Start compressing the specimen. Compress until fracture / failure.
10. Remove the load.
11. Stop recording in VIC Snap and the load-displacement Excel spreadsheet.

To analyze the speckle images using VIC 2D and VIC 3D:

1. Import the images into the VIC 2D or 3D program, just as before with the calibration images.
2. Select a reference (undeformed) image.

3. Choose an area of interest (AOI) for the program to find data points within.
4. Place a start point somewhere within the AOI.
5. Click the Run button
6. (Optional) Add post-processing options, like calculating strain or curvature.
7. Click “Run”.

2.4.2 Methods

Throughout this research program, several different sizes and types of pin-reinforced sandwich structures were tested. These are all summarized in Table 2 below. With the exception of the straight sandwich specimen tested in Chapter 5, every experiment was a quasi-static compression test that conformed to the ASTM C365 standard. Each of these test specimens had a 15 mm thick core, 0.50 mm diameter pins and ~1 mm thick facesheets. The pins consistently rested at a 60-degree angle from the horizontal. The material properties of the facesheet, foam and pins have been described previously in this chapter.

Table 2: Core attributes for pin-reinforced sandwich structures tested during this research

Thesis Chapter #	Core type	X-Cor or K-Cor	Boundary conditions and other characteristics
3	Cross-pin (with foam)	K-Cor	N/A
	Cross-pin (without foam)	K-Cor	N/A
	Cross-pin (with cut foam)	K-Cor	N/A
4	RVE without foam	K-Cor	Greased end condition
	RVE without foam	K-Cor	Glued end condition
	RVE without foam	K-Cor	Free end condition
5	Small curved sandwich without foam	K-Cor	Restrained end condition
	Small curved sandwich without foam	K-Cor	Bottom supported end condition
	Small curved sandwich with foam	K-Cor	Restrained end condition
	Small curved sandwich with foam	K-Cor	Bottom supported end condition
	Straight sandwich with foam	K-Cor	3-point bend *
6	Large curved sandwich	X-Cor	Restrained end condition

* The 3-point bend test was conducted without any restriction on the boundary condition.

Chapter 3: Relevant Findings from Prior Experiments

Previous experiments within this research program have provided some background for characterizing the mechanical behavior of pin-reinforced composite sandwich structures. These tests experimentally determined the elastic modulus through three-point bending and compression testing. The use of 2D Digital Image Correlation (DIC) was helpful as a computational analysis tool in this portion of the project. The DIC strain and displacement results were computed, which gave rise to important mechanical behavioral properties such as compressive stiffness and compressive strength. These results are being provided to give background and context to the remainder of the work in this thesis.

3.1 Methodology

Three types of pin-reinforced composite sandwich structures were considered during this phase of the research: 2 cm x 2 cm (0.79" x 0.79") K-Cor squares with pin density of 1.5 lb/ft³, 3"x3" squares with pin density of 0.9 lb/ft³ and small-scale cross pin specimens. The 2 cm x 2 cm K-Cor squares were tested so that the compressive strength, elastic modulus and maximum compressive stress of the pin-reinforced composite sandwich structure could be identified. These sandwiches were measured to be 1.4 cm (0.55") thick. The 3"x3" square specimens were tested in order to fully realize what the material response would be at the macro-scale. These experiments made use of 2D DIC in order to characterize the in-plane displacements along and transverse to the axis of the specimen. 2D DIC was also useful in determining the bending deformations and subsequent shear and axial strain distributions. The cross

pin experiments were conducted so that we could understand how the pins react under compressive loading without the foam core supporting it. For these tests, 2D DIC was employed to show the deformation and buckling of the carbon fiber pins. Three types of reduced representative volume element (RVE) cross-pin specimens were utilized: sandwiches without foam core, sandwiches with foam core and sandwiches with the core cut away at the facesheet-core interface.

The 2 cm x 2 cm K-Cor specimens were tested until failure by applying a compressive loading condition. The load and crosshead displacement were measured with the equipment stated in Chapter 2. These values were later transformed into strain and stress by utilizing geometric relationships. Similarly, the 3"x3" square specimens were tested in compression by loading and unloading. The size of these sandwiches required the use of a larger load cell in order to bring the specimen to failure, so these experiments were conducted in a different laboratory than the others.

The small-scale cross pin specimens were prepared from a block of thermoformed K-Cor sandwich structures. The specimens, each consisting of two pins in a crossed configuration, were cut from a larger sandwich. This crossed configuration, shown in Figure 14, was selected in order to minimize the in plane rotation of the pins due to shear deformations [12]. Each specimen was 20.7 mm wide, 21.0 mm tall and 6.4mm thick.

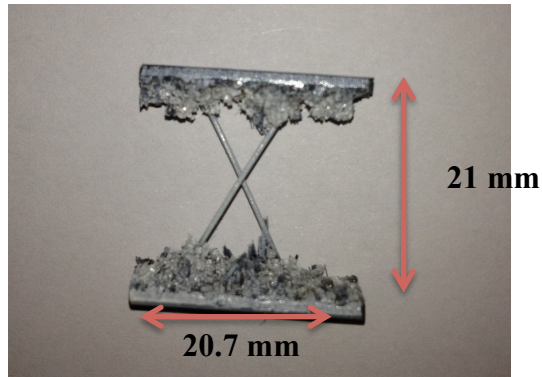


Figure 14: Small scale X-pin specimen

In each experiment, the cross-pin configuration was loaded and unloaded. The load-displacement response was collected and stored using the equipment stated in Chapter 2. The strains and displacements were computed using VIC Gauge (Figure 15), which is another 2D computational imaging tool similar to DIC.

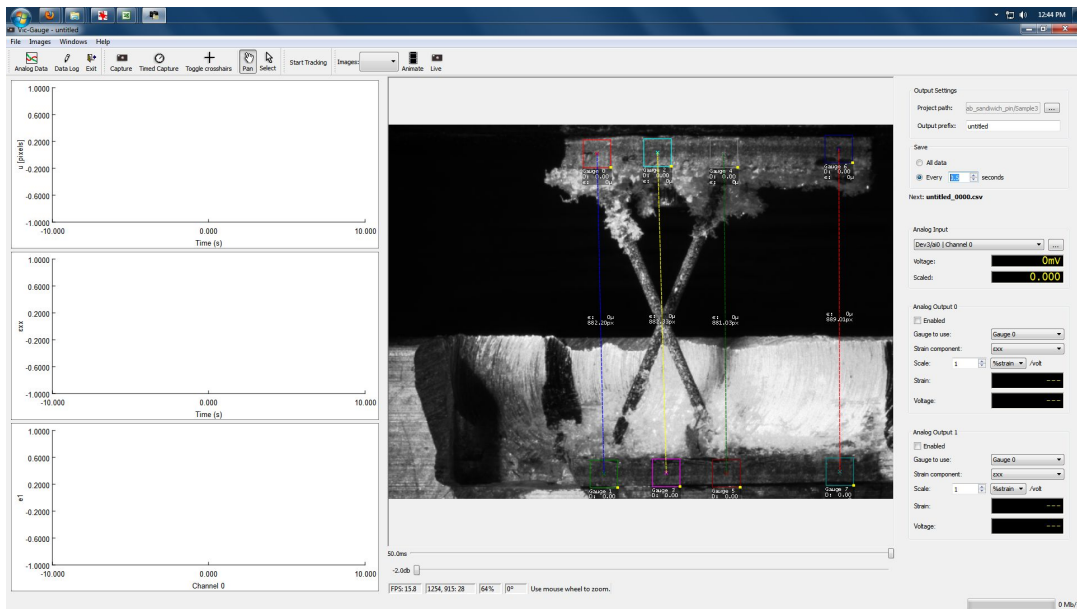


Figure 15: Sample screen for VIC Gauge software program with a cross pin specimen

Figure 16 shows what an undeformed cross pin configuration looks like as it rests in the microtensile test frame. This 5-pound load capacity microtensile test frame isolates the small-scale specimens from the mechanical response of the pins.

Figure 17 shows an undeformed cross pin sandwich that has the foam cut away at the facesheet/core interface.

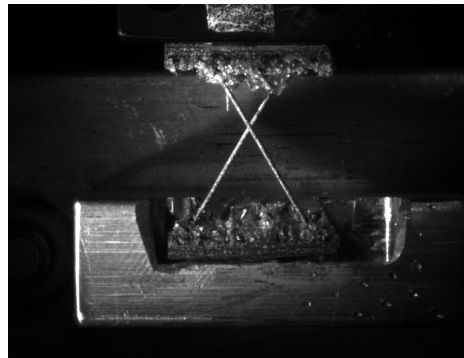


Figure 16: Undeformed small-scale pin compression specimen in microtensile load frame

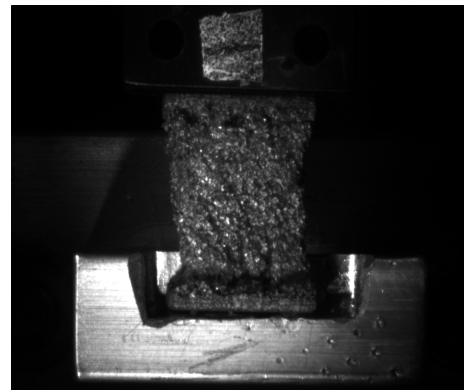


Figure 17: Undeformed small-scale cross pin compression test with foam cut at the facesheet/core interface

Regardless of what type of loading the specimen is under, the compressive response can be translated from the microscale to the macroscale by the following relationship:

$$\text{Macrostress} = \frac{\text{Load} * \text{pin correction factor} * \text{foam factor}}{\text{area of RVE}} \quad (\text{Eq. 8})$$

$$\text{Macrostress (MPa)} = \left(\frac{\text{Load(N)} * 2 * 1.57}{(0.16\text{in})^2} \right) \left(\frac{2.2}{9.8} \right) \left(\frac{6904}{1,000,000} \right) \quad (\text{Eq. 9})$$

where the pin correction factor is used to adjust for the number of pins tested relative to the number of pins in the RVE, and the foam factor is used to adjust for the effect of the core material on the compressive strength. The compressive strength is obtained by comparing the stress of a full-scale specimen before and after pin failure occurs when the foam is the only load-bearing component. Therefore, the foam core factor can be envisioned as using a “linear rule-of-mixtures” assumption for the mechanical behavior of the core in order to convert the results from the small-scale specimens to the macro-scale, and is essentially a measure of the load partitioning in the composite foam core using isostrain assumptions.

It is important to note that when using Equation (8) for RVE-scale specimens, the pin multiplication factor may be less than one due to using more pins than in a single RVE, and that further adjustment may also be needed to account for the orientation of the excess pins (i.e., a pin at an angle of 30° will bear about 85% of the load that a pin oriented at 0° will bear).

3.2 Results

3.2.1 Square Specimens: 2cm x 2cm

The initial tests involving the 2 cm x 2 cm square specimens provided some insight into how the K-Cor pin-reinforced composite sandwich structure fails under compressive loading. Load-displacement and stress-strain plots are given below in Figure 18. Keep in mind that the ordinate axis on the load-displacement curve is given in kilograms instead of Newtons. From these plots, it is evident that the maximum stress is 4.2 MPa and the compressive stiffness is 129 MPa. This compression behavior was significantly less than the 3-point bending response. (For

this same material in three-point bend, the maximum stress was 37.2 MPa and the stiffness was 2.9 GPa.) Interestingly, there is a sharp decrease in load-bearing capacity after the elastic limit is reached. At this time in the test, a loud snap sound was heard, denoting pin failure.

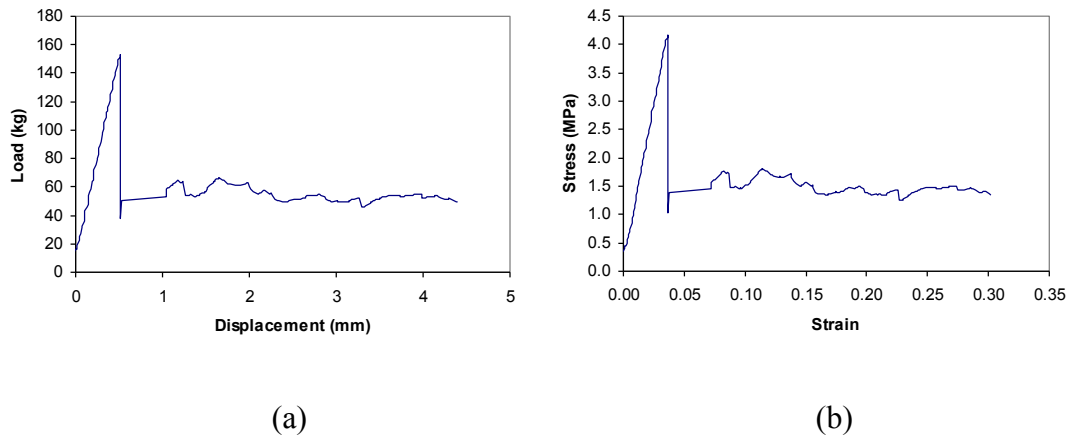


Figure 18: Graphs showing the global compression response of pin-reinforced composite sandwiches, (a) Load-displacement (b) Stress-strain

3.2.2 Square Specimens: 3" x 3"

The 3"x3" square specimens were tested under repeated compressive loading and unloading to understand the effects of the nonlinear behavior on the elastic response. As shown in Figure 19, the modulus varied throughout the experiment and it changes after the onset of nonlinear deformation. In the first loading cycle, the material exhibits a stiffness of 580 MPa and then transitions to 100 MPa as nonlinear deformation sets in. In the final loading cycle, the initial stiffness drops to 160 MPa and later becomes 40 MPa.

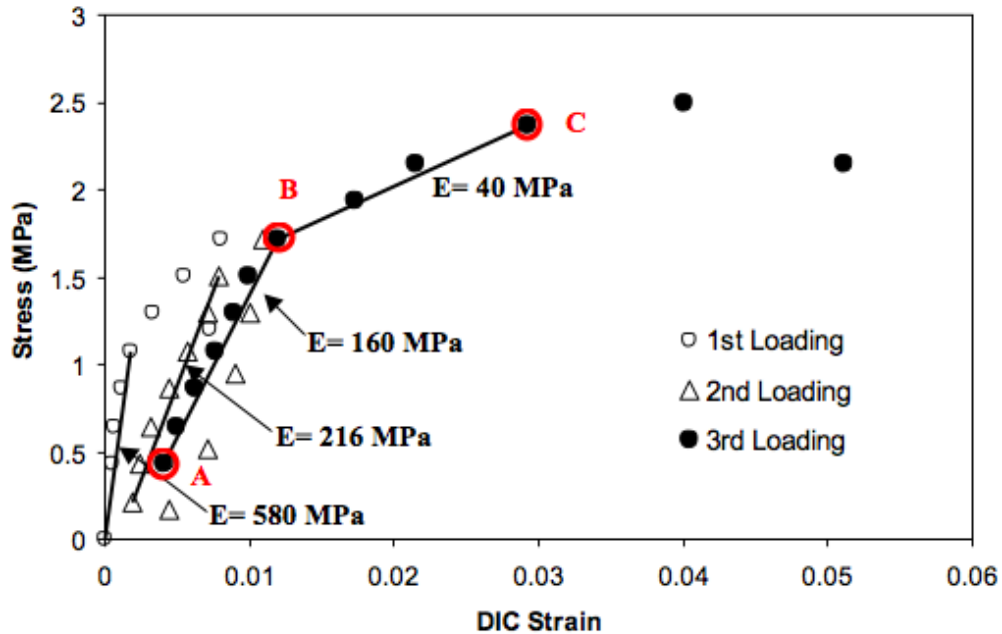


Figure 19: Axial compression response of 3" x 3" sandwich structure under repeated loading

It is clear that the decreased modulus represents a failure point for this particular sandwich structure. After the onset of buckling on the pin's surface, the core became locally damaged. The use of DIC displacement and strain fields proves that there is a direct correlation between this decreased modulus and how strain is distributed throughout the core.

This experimental study also investigated the effect of pin density on elastic modulus. Sandwiches were tested with pin densities of 1.5, 1.8, 4 and 8 lb/ft³. For the most part, the test specimens appear to have an increased elastic moduli and maximum stress with increased pin density under compressive loading (see Table 3). Therefore, pin density directly affects the compressive properties of pin-reinforced composite sandwich structures. These uncorrected values do not account for compliance of the Imada test frame.

Table 3: Summary of compression testing results for 3" x 3" K-cor sandwiches

Pin Density (lb/ft³)	Average Max Stress (MPa)	Elastic Modulus / Compressive Stiffness (MPa)	Yield Stress (MPa)
1.5	1.55	79.24	1.70
1.8	2.03	68.26	1.30
4	1.47	104.17	1.15
8	3.37	138.90	2.94

3.2.3 Cross pin Specimens

The results from the cross pin compression tests as well as a full-scale specimen's loading-unloading experiment are shown in Figure 20 below. The dark blue line refers to a cross pin specimen that was adhered to the load frame using glue. Specimens with foam around the pin were tested in order to determine what effect the foam constraint has on the pin deformation. As you can see, the stress-strain response for the cross pin experiments begins to approach the full-scale specimen loading-unloading test as the amount of foam core is increased. This experiment shows close correlation between the full-scale specimen and the crossed configuration, therefore proving that the compressive stress-strain response for K-Cor composite is scalable. Due to the limited capacity of the load frame, the small-scale specimens could not be compressed to their maximum load bearing capacity.

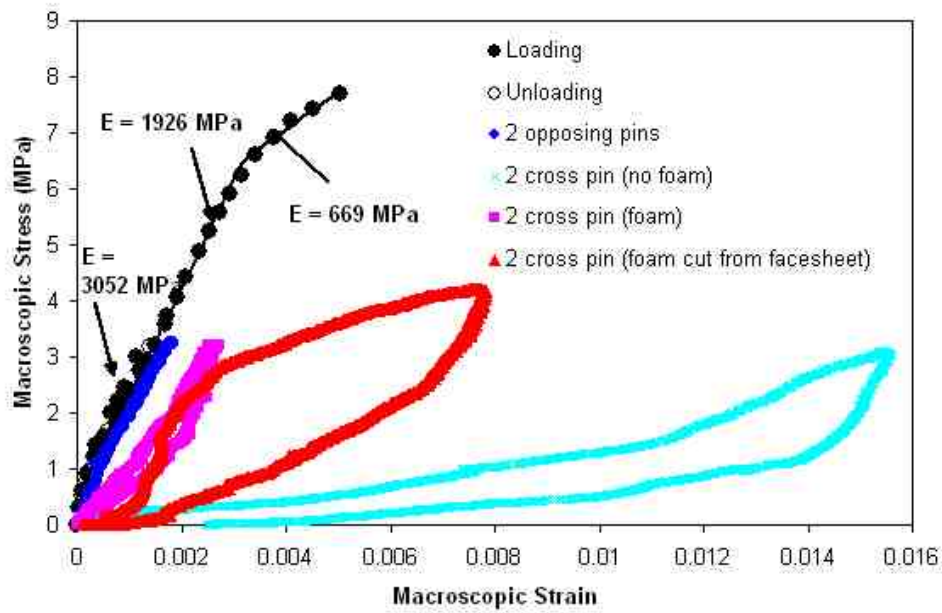


Figure 20: Stress-Strain curve for X-pin loading and unloading response

Figure 21 below shows what a typical specimen looks like after it has been compressed in the microtensile test frame. The carbon pins tend to buckle and fail after reaching a critical load. For specimens without foam, they tended to fail around 3 MPa. Test specimens with foam failed around 3 MPa as well, but they did not experience nearly as much strain as the specimens without foam. Typically, failure was observed at the pin-facesheet interface.

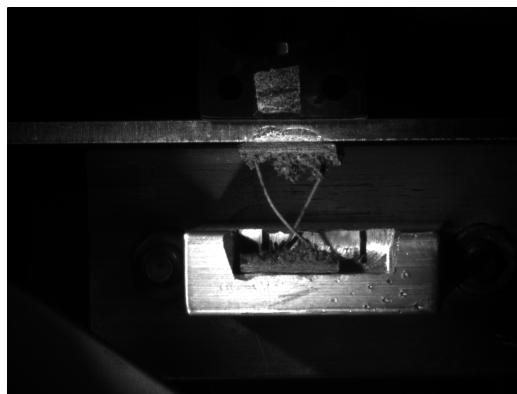


Figure 21: X-pin specimen with pins experiencing buckling

3.2.4 Additional Tests

In addition to the experiments mentioned above, initial testing of pin-reinforced composite sandwich structures were conducted without foam. The specimens were imaged and analyzed with 2D DIC and formed the basis for the experiments in Chapter 4 of this thesis.

It was shown that pin buckling mode shapes could be determined by utilizing 3D DIC on a representative volume element sized sandwich structure. The results from this experiment are shown in Figure 22 and Figure 23 below.

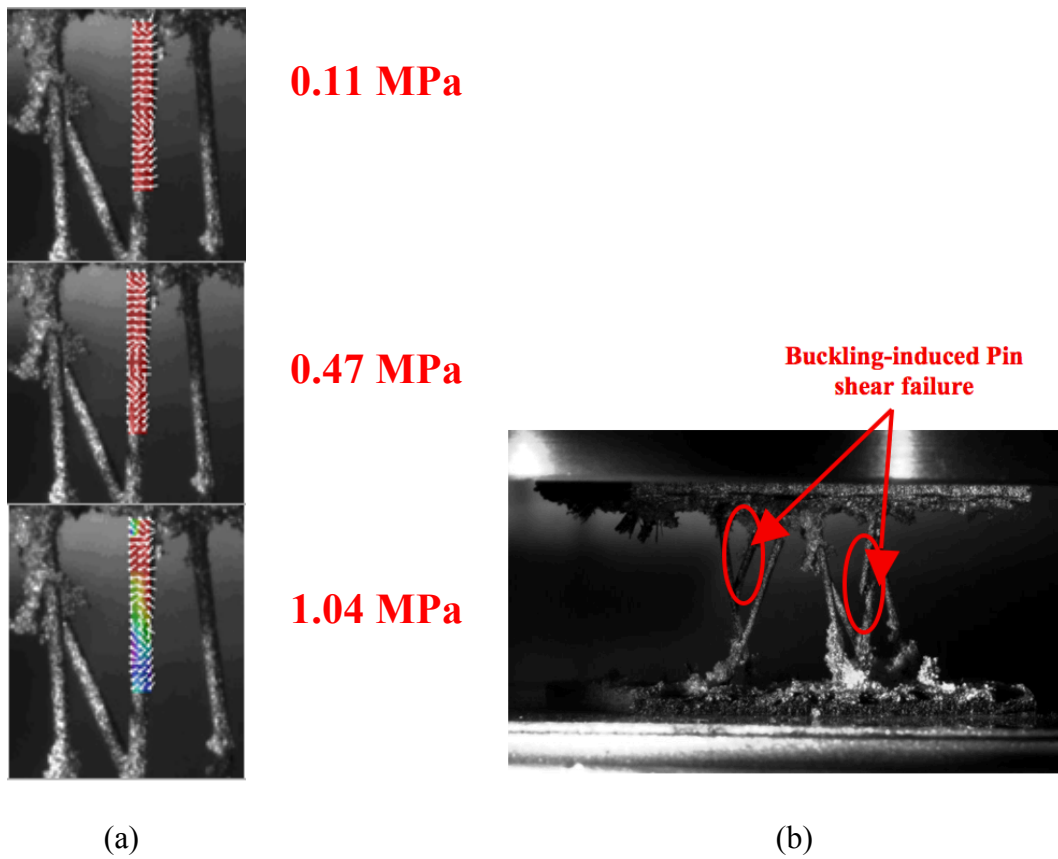


Figure 22: (a) Displacement vector fields from 2D DIC in the RVE specimen, showing bias of deformation transversely whereas axial variation corresponds to higher bending modes. (b) Observed pin shear failure for RVE

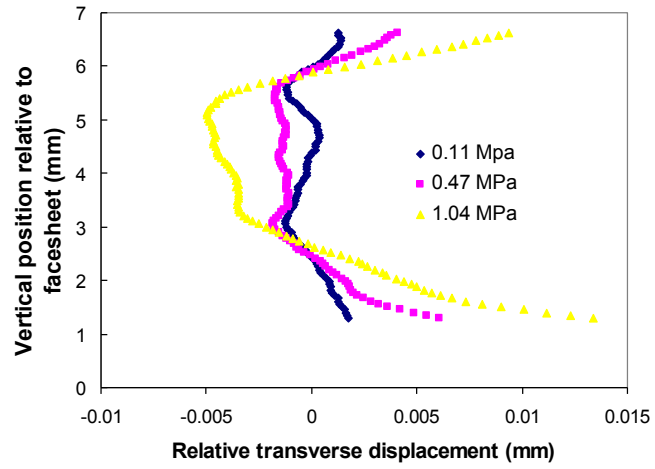


Figure 23: Change in shape of the top half of the pin, along with increasing stress. (Reference above figure)

Chapter 4: Multi-pin Representative Volume Element

Compression Testing

Chapter 3 discussed the results for the cross-pin and other small-scale experiments, so it only makes sense to increase the size and look at a representative volume element (RVE) next. An RVE is the smallest unit for which a single unit cell can represent the full specimen on a micro-mechanical scale. The RVE-scale compression experiment described in this chapter indicates how the multiple pins in a unit cell scale up to the global response of a bulk pin-reinforced composite sandwich structure.

These RVE experiments tested the mechanical response of two sizes of K-Cor composite sandwiches and three different boundary conditions: free, glued and greased. The free condition indicates that no grease or glue was used on the facesheet surfaces during that experiment. All of the tests were performed with the foam core removed. The foam was removed manually by using tweezers, without doing any damage to the carbon fiber pins. The two sizes of pin-reinforced composite sandwich are given in Figure 24 and Figure 25 below, along with some dimensions.

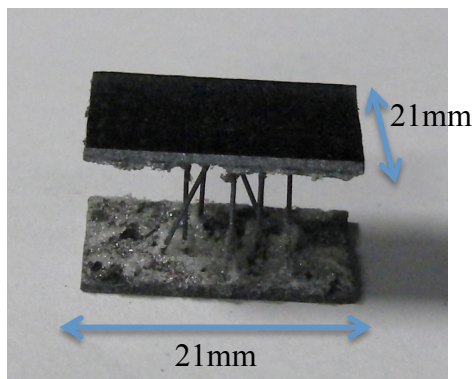


Figure 24: Reduced Volume Element (RVE) specimen, showing the unit cell pin structure. This was used for 3D characterization of the compressive behavior. These specimens are 15 mm thick.

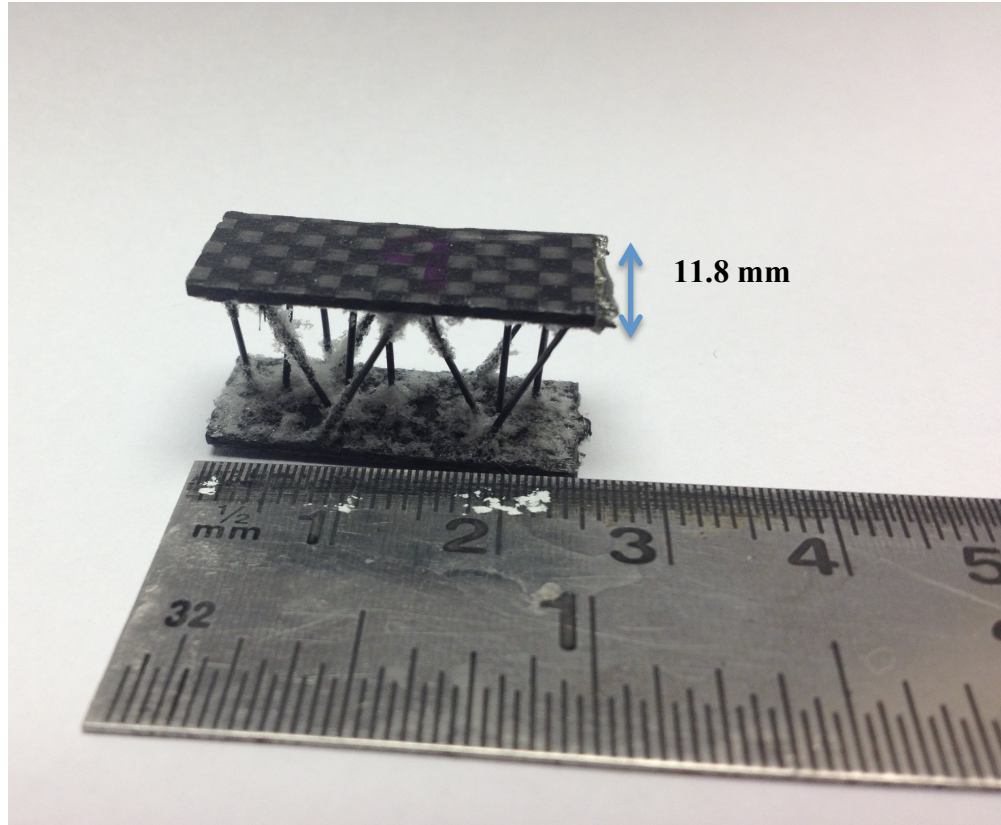


Figure 25: RVE used for glued and greased end condition. These specimens are 15 mm thick.

A three dimensional DIC experiment was devised to test the compressive response of the pin-reinforced composite sandwich structure and determine the local interaction between the pins and facesheet. 3D DIC was chosen for this experiment so that we could observe the bending response and curvature of the pins as they accumulated load. With 3D DIC, we can see the strain over curved surfaces, so this was a great benefit when imaging these small carbon fiber pins.

In order to properly image these specimens with the cameras, it was necessary to add a set of lens extenders. This created a high magnification condition on the carbon fiber pins. The high magnification setting also became useful when analyzing the images with DIC.

4.1 Methodology

4.1.1 Free Boundary Condition

A multi-pin representative volume element (RVE) was cut and developed from a larger K-Cor sandwich composite specimen. These RVE-scale specimens consist of a unit cell of pins, shown in Figure 26 below. The experimental set-up with 3D imaging is shown in Figure 27 and Figure 28 below. The set-up uses all of the same equipment that was used to test the crosspin reinforced composite specimens with the exception of the microtensile machine. Instead of the microtensile tester, the Imada load frame, explained in Chapter 2, was utilized for this test. Two cameras were necessary, since this was a 3D imaging test.

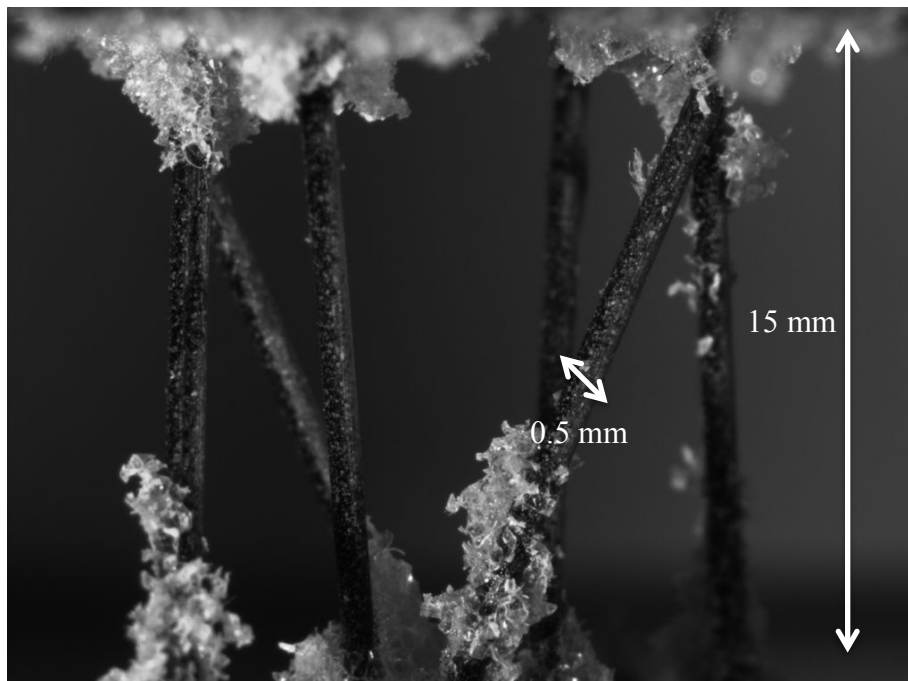


Figure 26: Sample RVE specimen without foam



Figure 27: Experimental setup for RVE experiment



Specimen

Figure 28: Experimental setup for imaging 3-D Digital Image Correlation (DIC)

The first set of experiments utilized test specimens that were 21 mm x 21 mm on the facesheets and 15 mm thick. Specimens in this test had a free boundary condition. The design of experiments is given in the table below.

Table 4: Design of Experiments for first set of RVE compression tests; free boundary condition

Square tops (21 mm x 21 mm)		
Test #	Magnification	Number of Pins
1	21 mm	6
2	21 mm	10
3	21 mm	6
4	21 mm	6
5	14 mm	6 (longer pins)

4.1.2 Glued and Greased Boundary Conditions

The second set of experiments utilized test specimens that were 11.8 mm x 25.3 mm on the facesheets and 15 mm thick. For these tests, the first 4 specimens had the greased boundary condition and the last 4 had the glued boundary condition. Each of these experiments used the 14 mm lens extenders and the Imada test frame as shown in Figure 28. The design of experiments is given in Table 5 below.

Table 5: Design of Experiments for the second set of RVE Compression Tests; Greased and Glued boundary conditions

Test #	# of pins
Greased Experiment	
Test 1	8
Test 2	8
Test 3	9
Test 4	10
Glued Experiment	
Test 5	8
Test 6	7
Test 7	9
Test 8	7

4.2 Results

Results from the experiments are given below in the form of load-displacement charts, stress-strain diagrams, DIC plots, and strain-displacement plots. The first results presented are from the compression experiments with a free boundary condition. Afterwards, the results from the compression test with a greased boundary condition are shown.

4.2.1 Free Boundary Condition

4.2.1.1 Load-Displacement Results

Testing the free end condition under compressive loading gives the following load-displacement curve (Figure 29). Only Tests 3, 4 and 5 are plotted because those three produced the most consistent results and DIC data could be gathered from all of those experiments as well. Out of these three experiments, Test 4 gave the most conclusive data, so strain and displacement results were extracted from that data set. Those results are given below in Figure 31, Figure 32 and Figure 33. The load-displacement curve shows an elastic region with a stiffness of 150 N/mm. Shortly thereafter, around a vertical displacement of ~ 0.6 mm, the pins within the sandwich structure fracture and cause the load-bearing capacity of the structure to decline. After that, there is a bit of variation in the response because the number of broken pins in the structure affects the amount of force applied on the surviving pins.

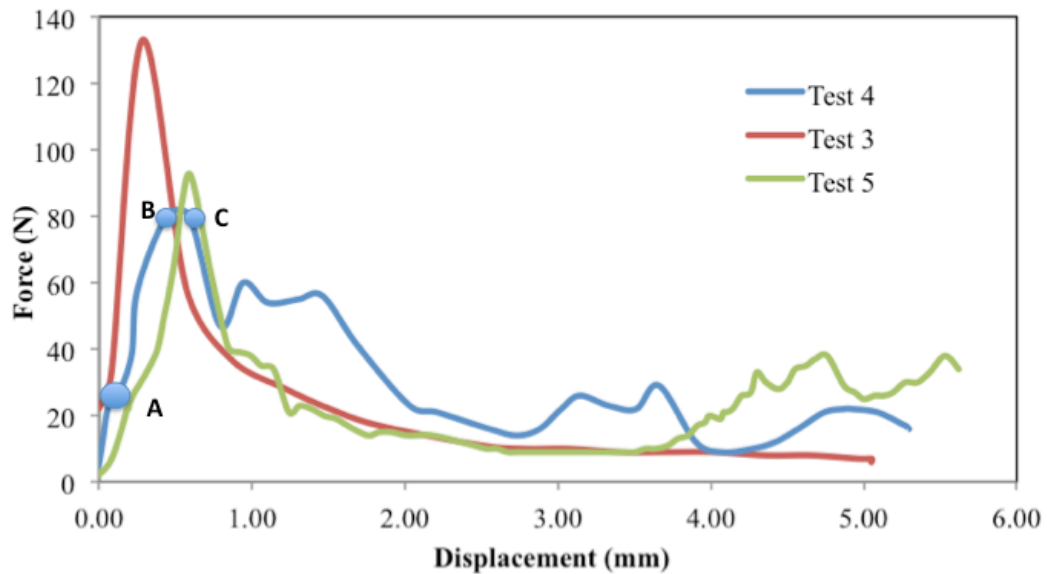


Figure 29: Load-displacement response curve for RVEs with free boundary condition

Incorporating the dimensions of the RVE to the plot given above provides us with the stress-strain diagram in Figure 30. From this plot, the compressive stiffness was calculated to be 13 MPa within the elastic region. As is shown from the graph, the maximum stress that the RVE sandwich without foam could hold was 0.18 MPa. (This is the same as compressive strength.) For added comparison, the cross pin and 3”x3” sandwiches achieved a maximum stress of 3 MPa and 1.7 MPa respectively. Keep in mind that the RVE-scale experiments are expected to reach lower stresses because there was no foam present to strengthen the sandwich structure. Further, the cross pin specimens were not tested until failure. The RVE loads have been translated to macroscopic stress by use of Equation 8. The results of that transformation are shown in Figure 41.

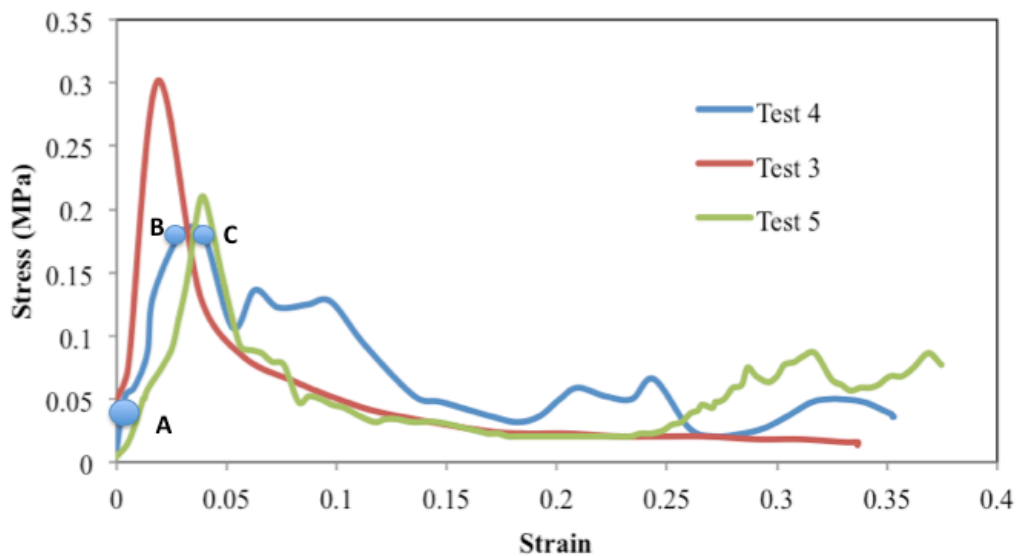
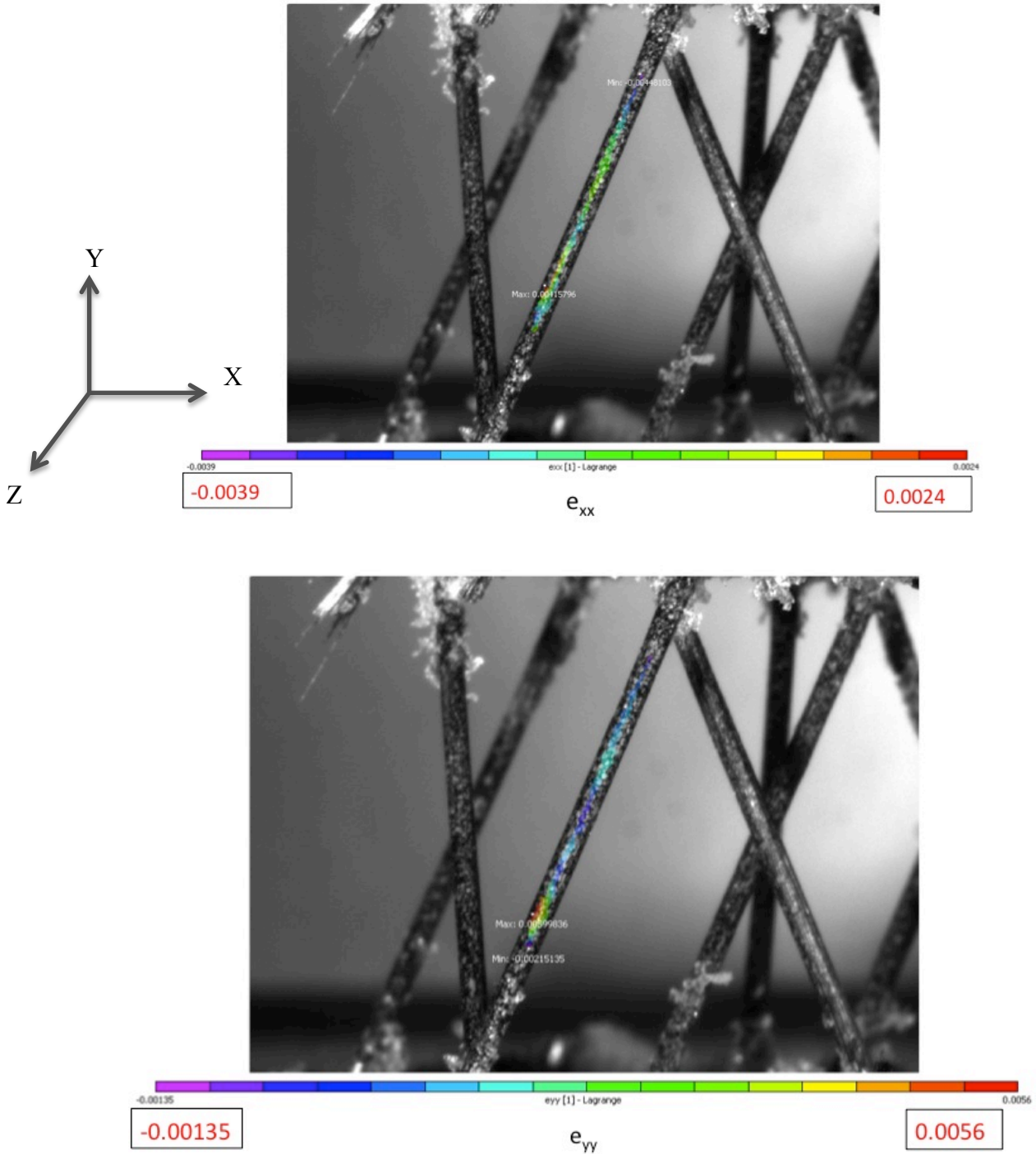


Figure 30: Stress-strain plot for Test 3, 4 and 5 with free boundary condition

4.2.1.2 DIC Results

Two dimensional strain fields are shown in Figure 31 through Figure 33.

These results are given in 2D form to show an overlay of the strains on the deformed pin structure, however they were all obtained by using VIC 3D.



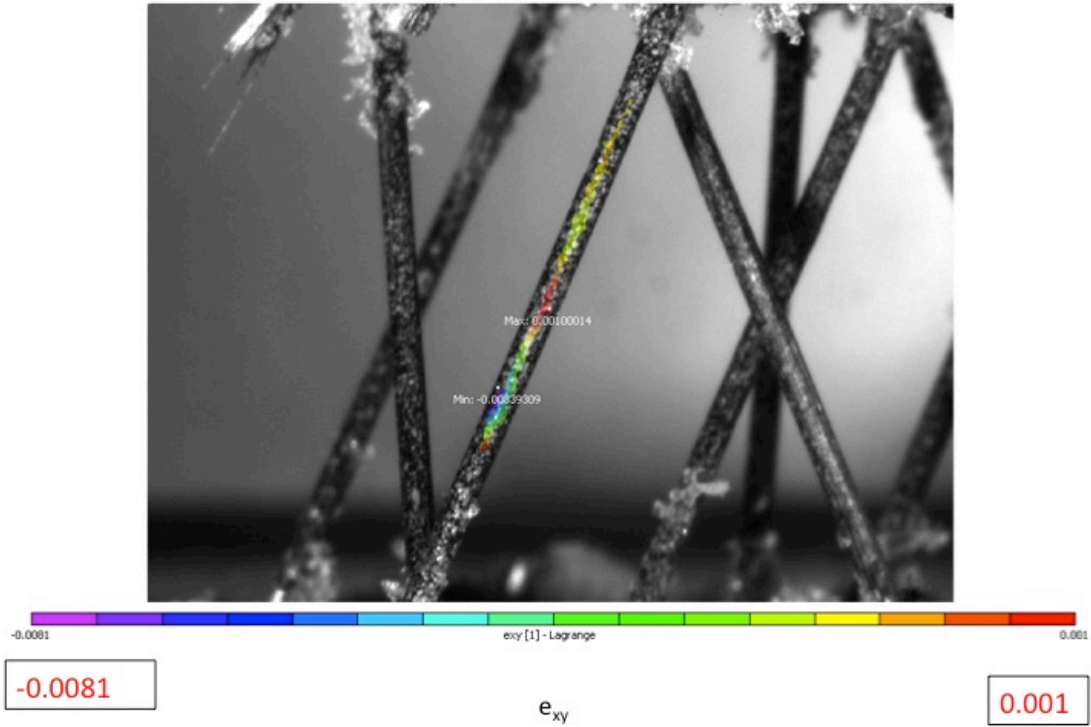
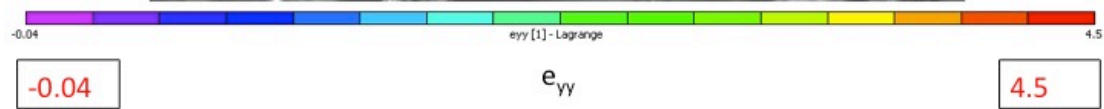
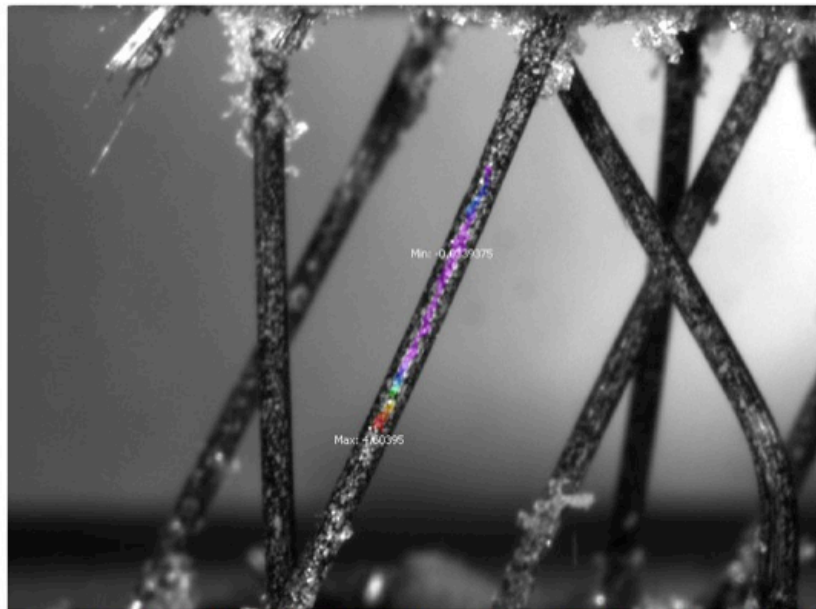
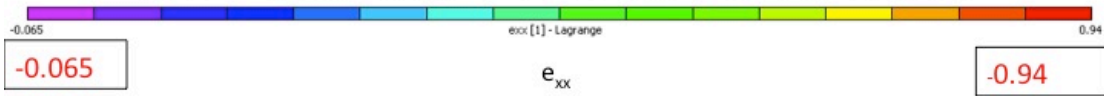
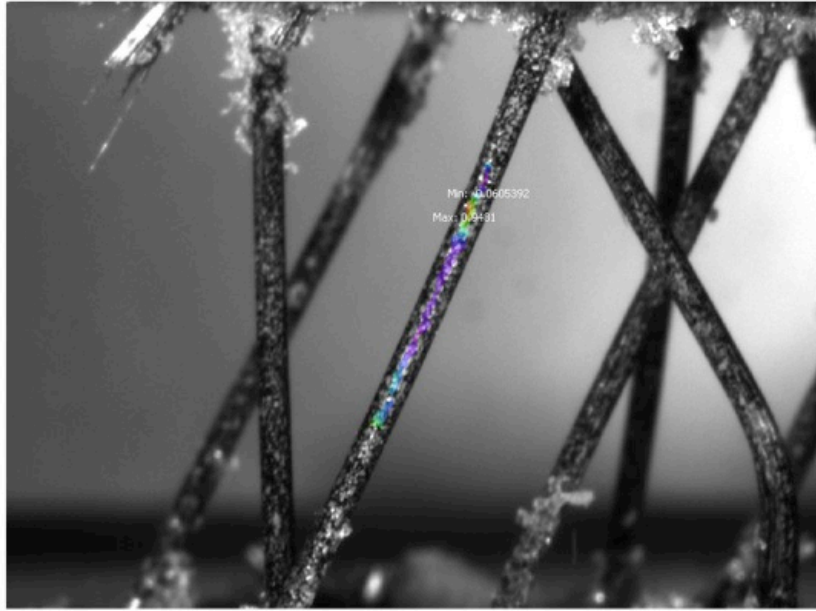


Figure 31: Strains in the Elastic Region for compression tests with free boundary condition

The axial, transverse and shear strains for the elastic region are shown in Figure 31. At this point in the experiment, the specimen was experiencing a force of 23 N. The transverse strain (e_{yy}) reaches 0.5% near the bottom of the pin and the shear strain (e_{xy}) is 0.1% at the same location.



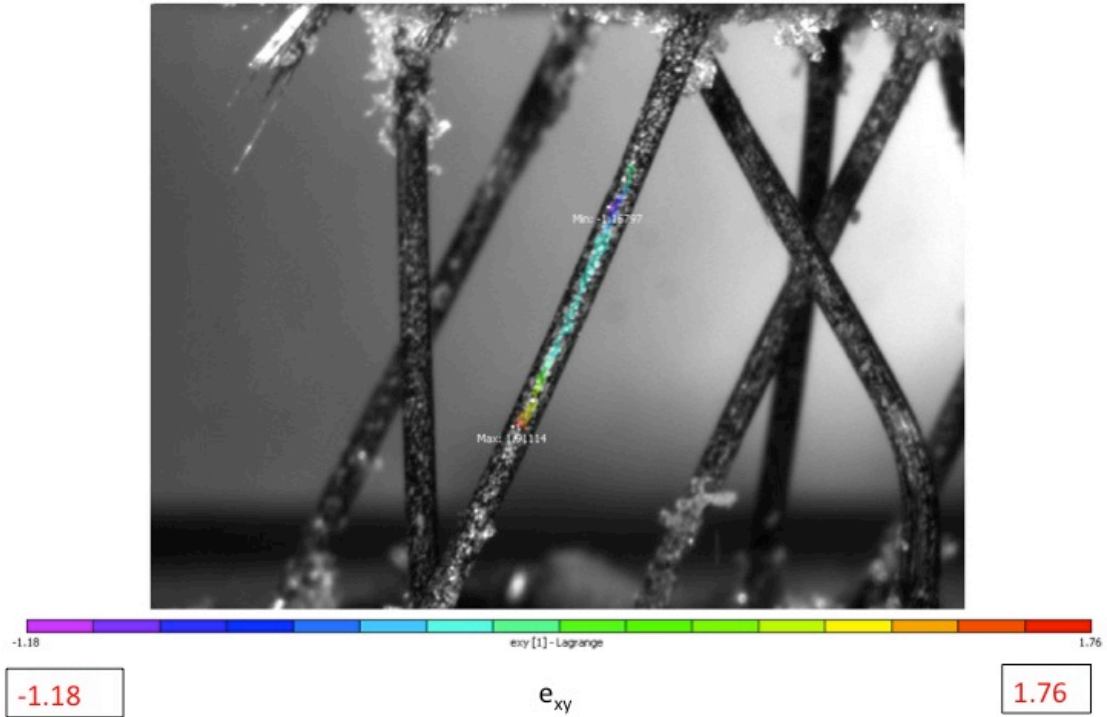
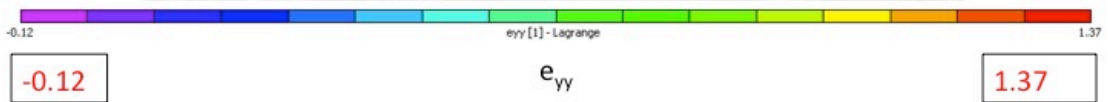
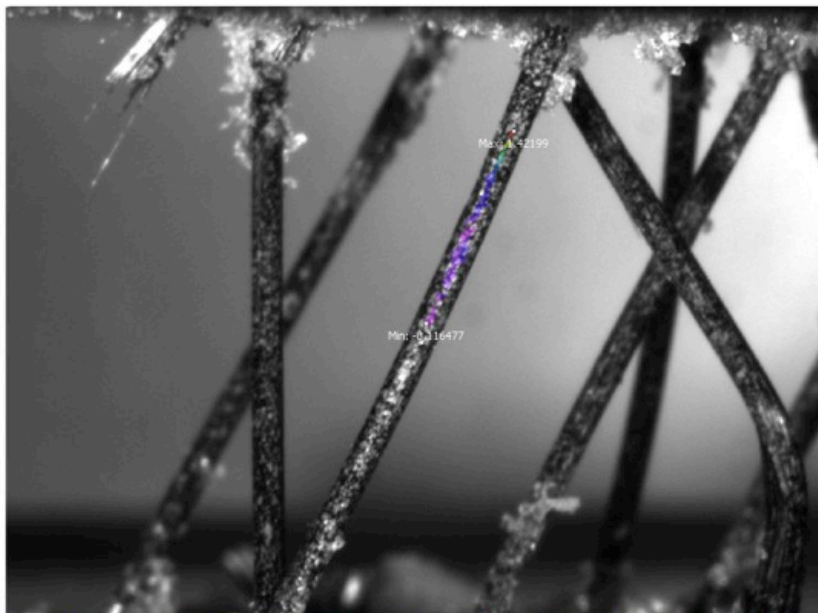
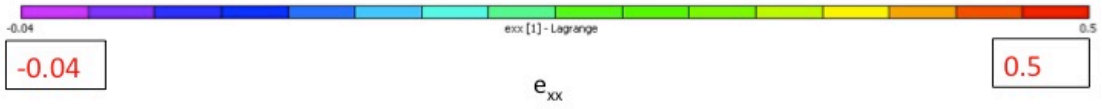
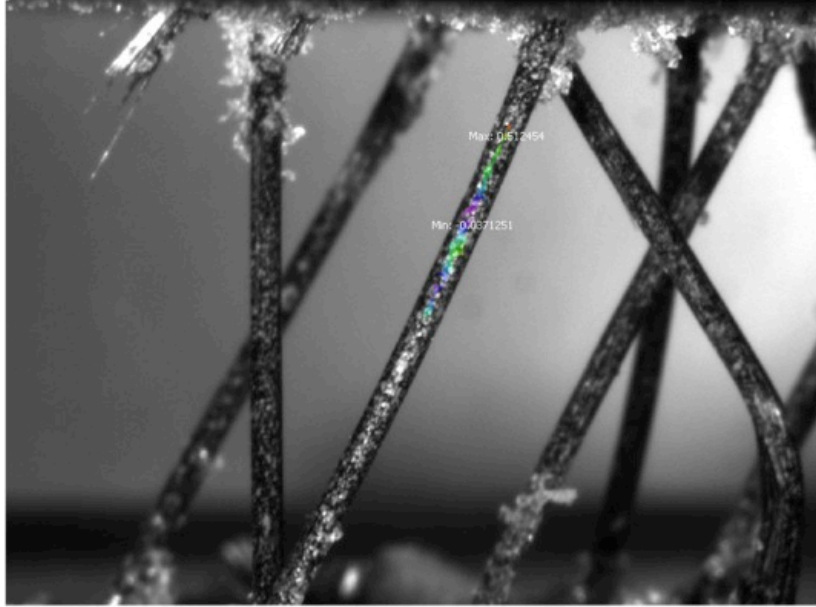


Figure 32: Strain fields at the elastic limit for RVE compression tests with a free boundary condition

Figure 32 shows the axial, transverse and shear strains for the elastic limit. The compressive force was equal to 80 N at this time. The figures show that the transverse strain is estimated to be -4% over most of the pin. DIC produced a maximum transverse strain of 450%, but this is only for a few pixels within the image of the pin. This is an error that can be attributed to the small size of the pin area and weak speckle patterning. This same error also occurs for the shear strain and axial strain DIC results. On an unrelated note, the pin on the rightmost side of the images is buckling. This is probably what led to the failure of the sandwich structure.



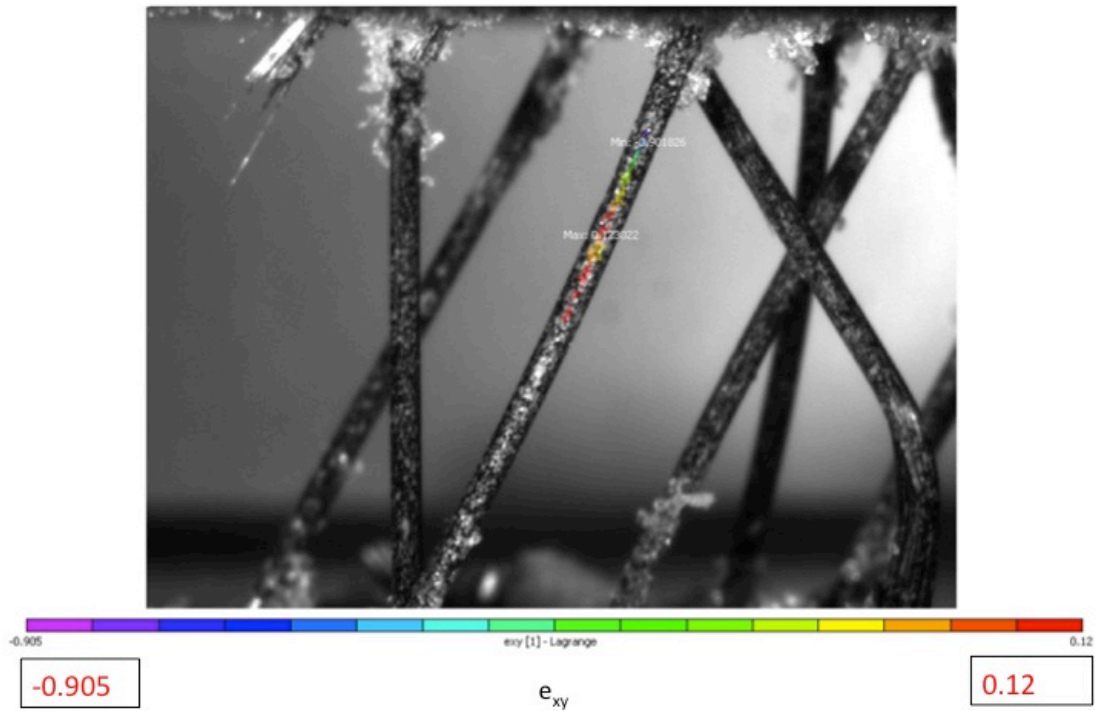


Figure 33: Strain fields at failure for RVE compression tests with a free boundary condition

Similar to the other strain field images presented above, Figure 33 shows the axial, transverse and shear strains at failure. This occurred at a load level of 80 N. The pin on the far right has buckled and split open; this causes the entire sandwich to fall over towards the right. DIC reports the maximum shear strain to be 12%.

The 3-dimensional DIC program, along with the images acquired during testing, show how the carbon fiber pins deform, buckle and fracture during compressive loading. Figure 34 is a plot of strain in one of the pins as calculated by VIC 3D against vertical displacement of that pin. The strains all remained relatively low throughout the test, even at failure. The sandwich failed at a displacement of 0.45 mm under a load of 80 N. As the figure shows, the maximum shear strain at failure is only 0.3%. At this point, the global crosshead strain as was collected from the Imada is 5% (Figure 35).

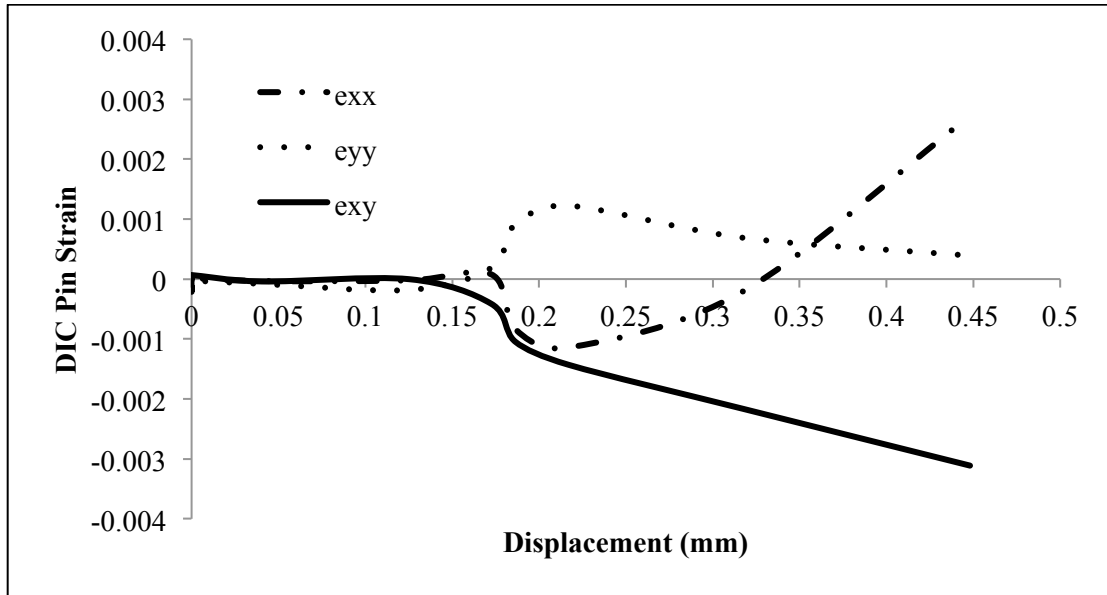


Figure 34: Strain-Displacement Data for Test 4, free boundary condition

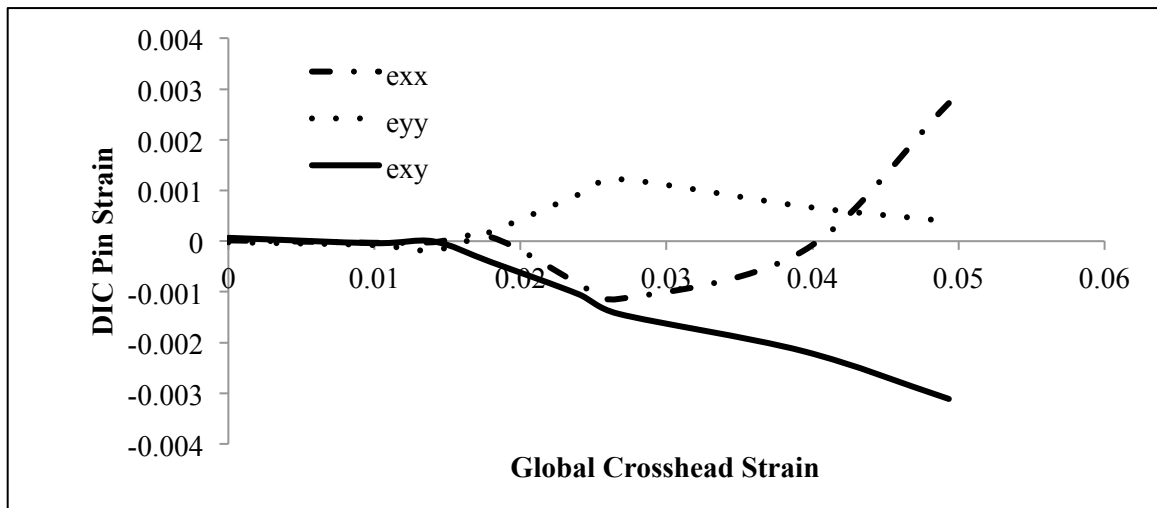


Figure 35: Global crosshead strain plotted against Pin Strain achieved from 3D DIC. These results also come from the Test 4 data set (free boundary condition)

The vertical displacement field at failure, V , is shown in Figure 36. Arrows on the pin show the direction in which the pin is deforming. In this particular test, the sandwich structure began to slip at the surface, causing the pin to fall over towards the right.

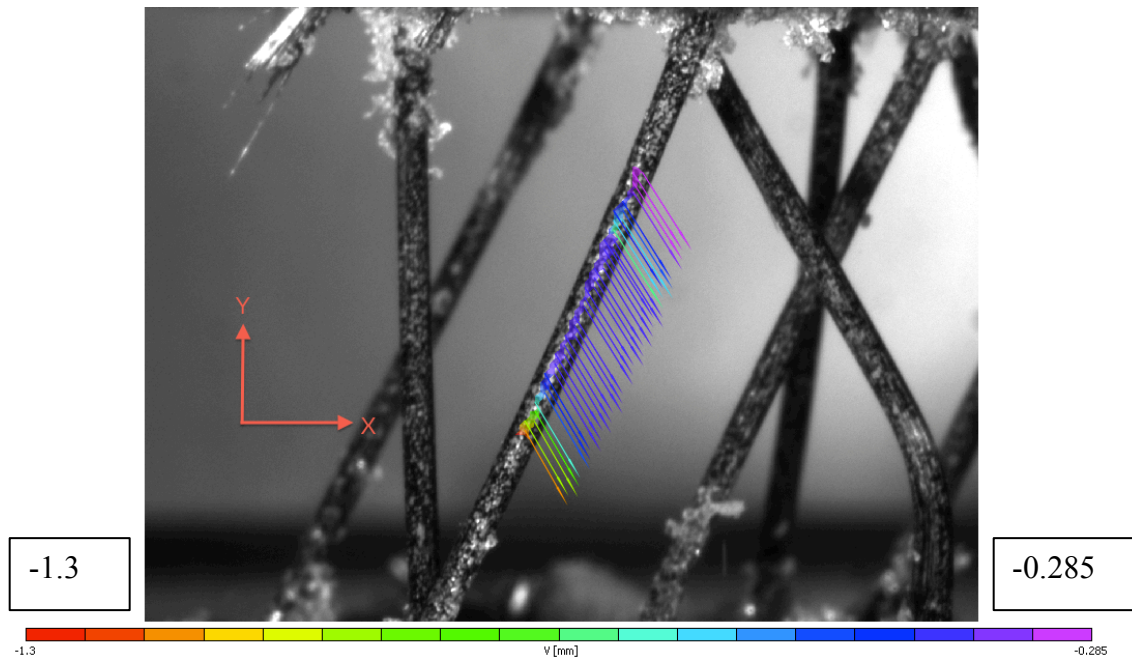


Figure 36: Vertical displacement field at failure for RVE with free boundary condition

4.2.2 Glued and Greased Boundary Conditions

4.2.2.1 Load-Displacement Results

Figure 37 shows the load-displacement plots for test specimens with a greased boundary condition. From this plot, it is evident that the maximum load that this material can hold is a little less than 250 N. The DIC results presented later in this chapter will include the results from Test 2, which contains 8 pins in its structure. This specimen failed at a load of 198 N with a global vertical displacement of 0.65 mm. The corresponding stress-strain plot for the greased RVE-scale specimens is presented directly below, in Figure 38. From this plot, the compressive stiffness for Test 2 is determined to be 12.05 MPa and the compressive strength is 0.663 MPa.

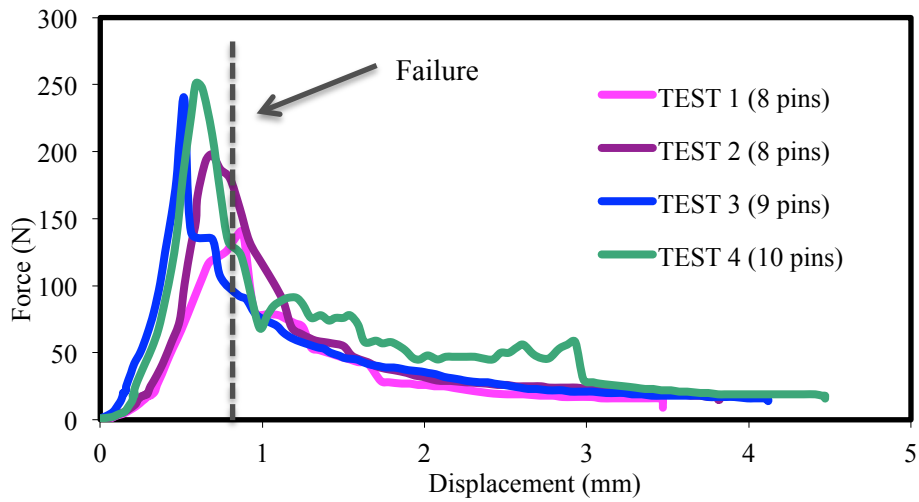


Figure 37: Load-displacement curve for greased RVE experiment

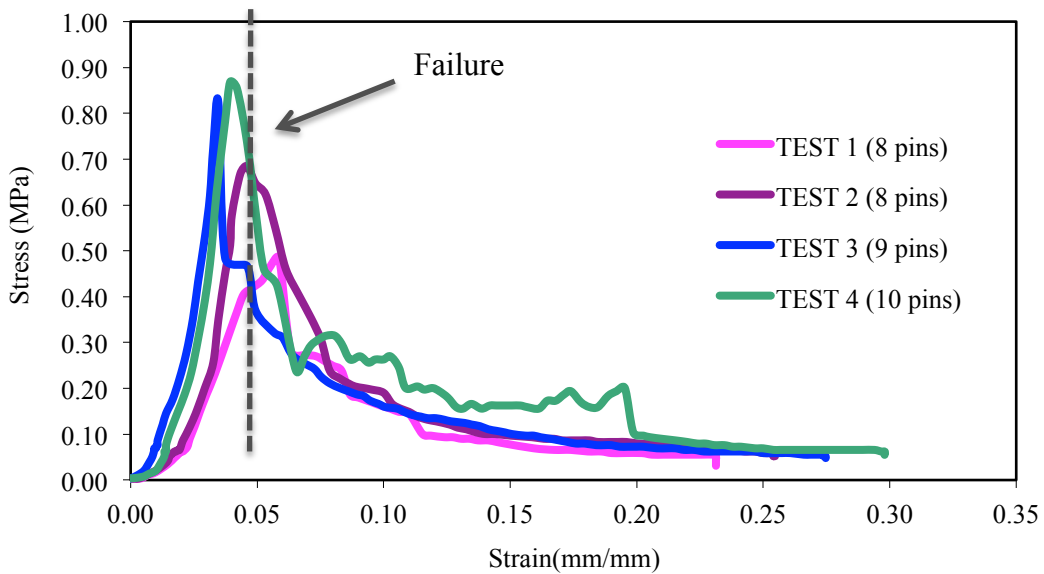


Figure 38: Stress-strain plot for greased RVE experiment

To complete the experiment, additional compression tests were also executed for pin-reinforced composite sandwich structures of the same size. Instead of employing a greased boundary condition, these specimens were glued to the load frame with super glue. The load-displacement plot and stress-strain diagrams are seen below in Figure 39 and Figure 40. Unfortunately, the DIC results for the glued

boundary condition were not sufficient enough to present any results here. For this reason, only the load-displacement and stress-strain plots are shown.

The load-displacement plot shows that the maximum force is ~ 180 N for Test 7 and ~ 120 N for Tests 5, 6 and 8. The sandwich structure failed at a global vertical displacement of 0.45 mm for Test 7, whereas the others did not fail until the displacement reached 1.25 mm. The maximum stress exhibited was ~ 0.65 MPa for Test 7 and 0.4 MPa for the remaining experiments. The compressive stiffness for the glued boundary condition experiments is 37.13 MPa.

A plot of the transformed values of load to macroscopic stress for all of the boundary conditions is given in Figure 41. This plot shows that the compressive stiffness for the RVE with a free boundary condition is 74.6 MPa and the compressive strength is 1.71 MPa. This is comparable to the 3" x 3" sandwich with a pin density of 1.5 lb/ft^3 that was studied in previous experiments, which had a compressive stiffness of 79.24 MPa and a compressive strength of 1.7 MPa. The stiffness is 146.6 MPa and 485.1 MPa for the greased and glued end conditions, respectively. The compressive strengths are 8.33 MPa and 8.61 MPa for the greased and glued end conditions, respectively.

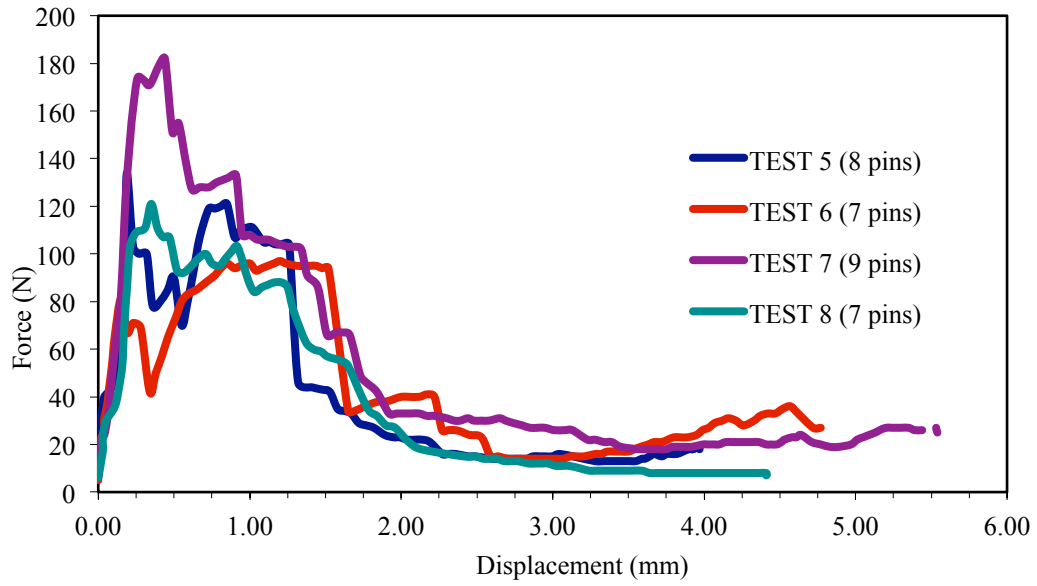


Figure 39: Load-displacement curve for glued RVE experiment

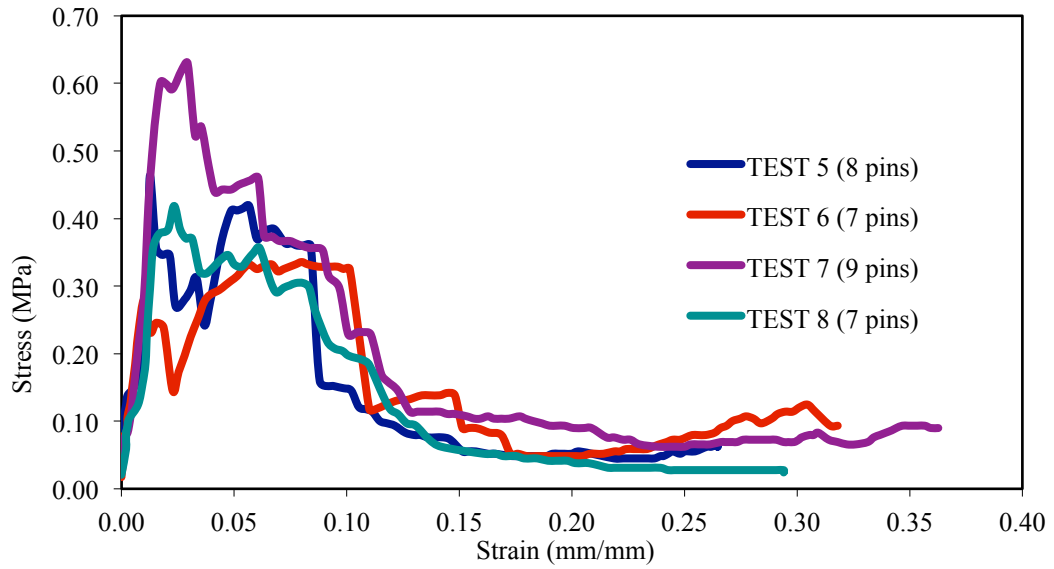


Figure 40 Stress-strain plot for glued RVE experiment

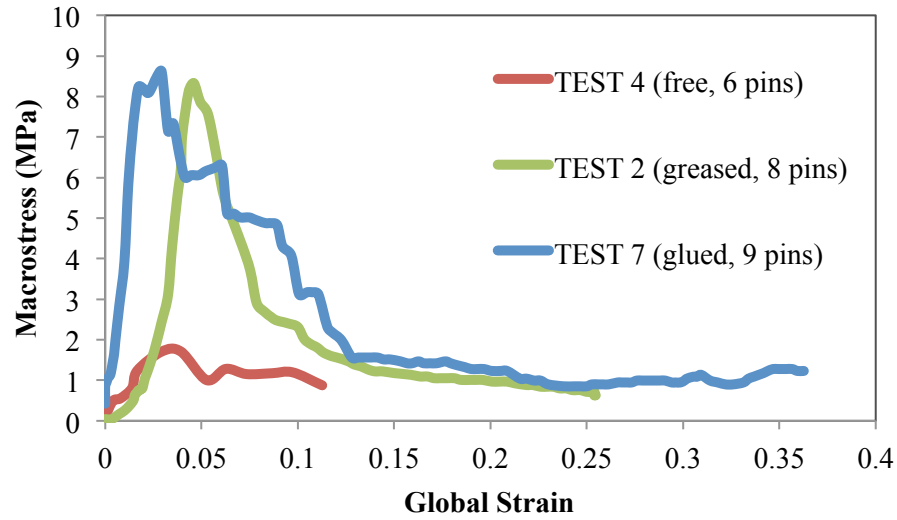


Figure 41: Stress-strain curve showing the macrostress for RVE test specimens with various boundary conditions

4.2.2.2 DIC Results

Full-field strain and displacement data was extracted from the two points in Figure 42 to see how the pin-reinforced sandwich structure responded to compressive loading with a greased boundary condition. Both the left pin and the right pins give good information and detail about the strain as the sandwich carries load. This particular test specimen carried a maximum load of 198 N before failing.

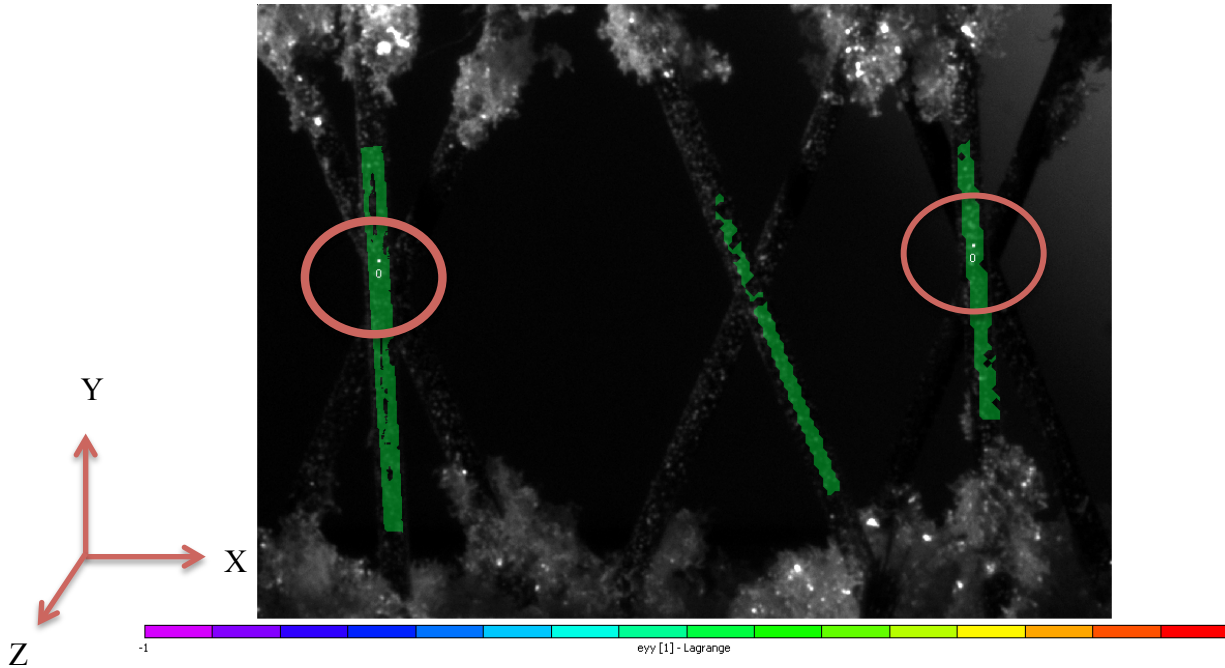


Figure 42: Location of pixels where strain and displacement fields were extracted. This image comes from the Test 2 RVE data set with greased boundary condition.

The strain-displacement plots for the left and right pins are given below in Figure 43 and Figure 45, respectively. From these plots, you can see that the dominant strain in the left pin is e_{xx} , achieving a maximum strain of 11%. e_{yy} is the dominant strain in the right pin, reaching a value of 9.5%. At the time of failure, both the left and right pins had displaced by ~ 0.7 mm. The plots show a deviation in the strains around 0.4 mm because the central pin burst open around that time. Strain-strain plots are also presented in order to give better understanding of how the pin strains evolve relative to the global strains (Figure 44 and Figure 46).

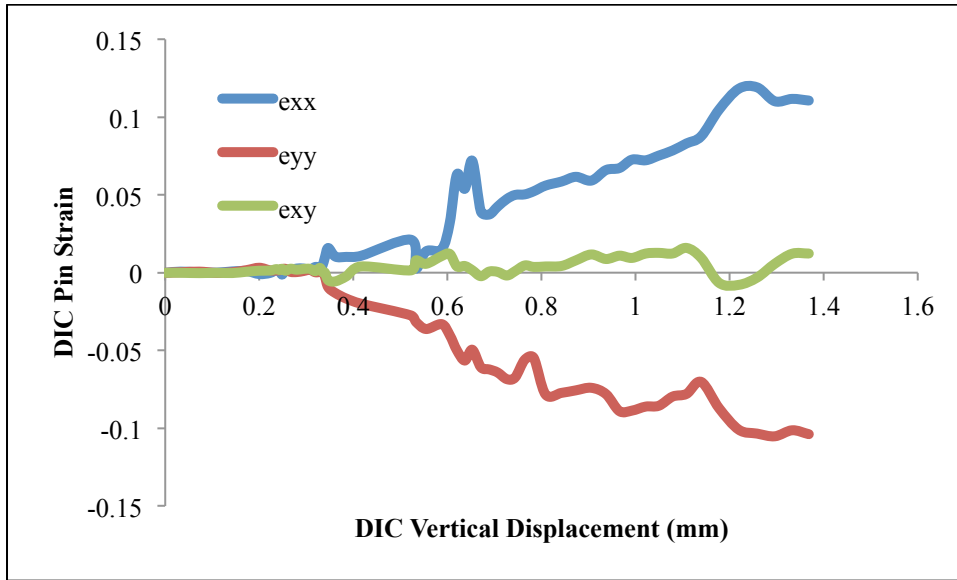


Figure 43: Strain-displacement plot of the left pin for Test #2 (greased boundary condition). All values are calculated with VIC 3D.

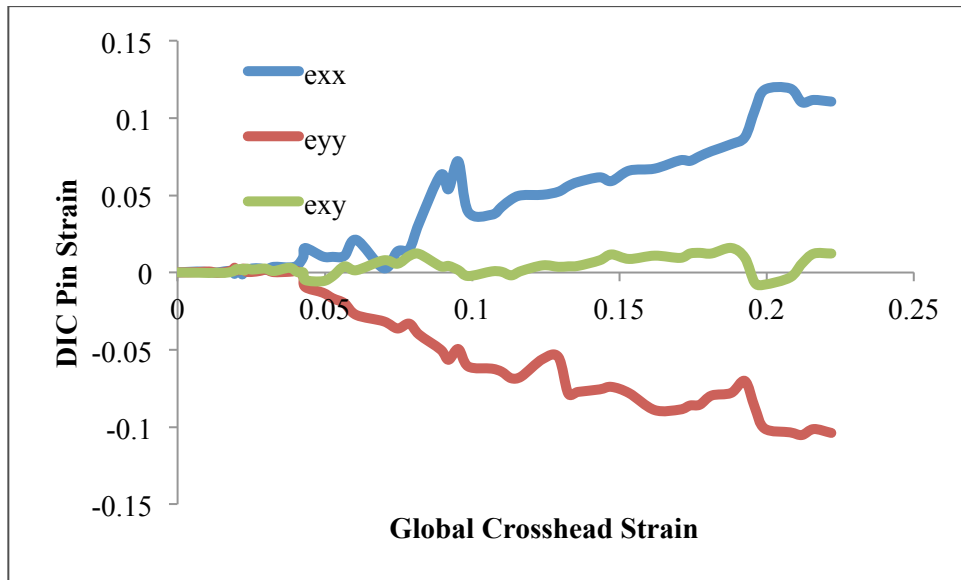


Figure 44: Strain-strain plot of the left pin for Test #2 (greased boundary condition). DIC pin strains were calculated with VIC 3D and global strain comes from Imada load frame.

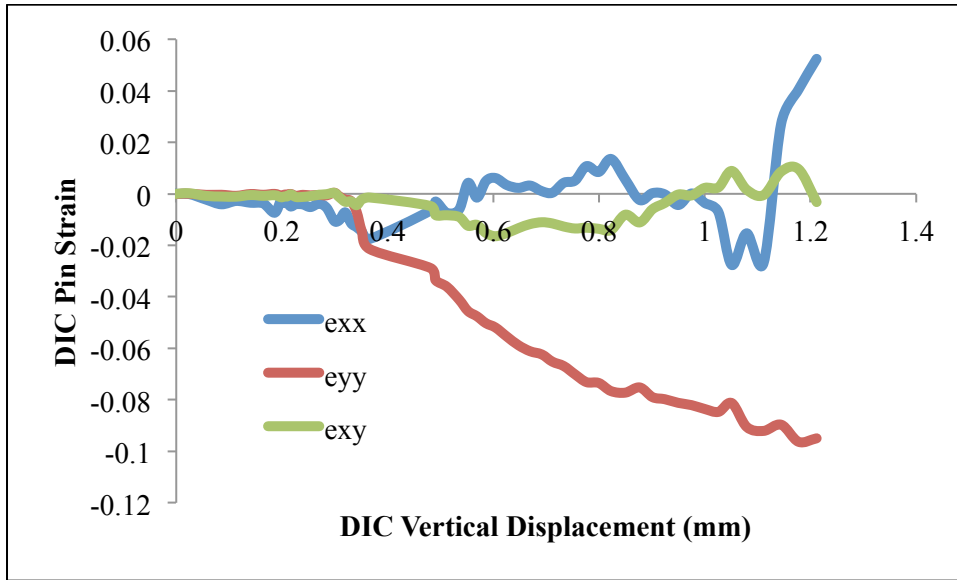


Figure 45: Strain-displacement plot of the right pin for Test #2 (greased boundary condition). All values are calculated with VIC 3D.

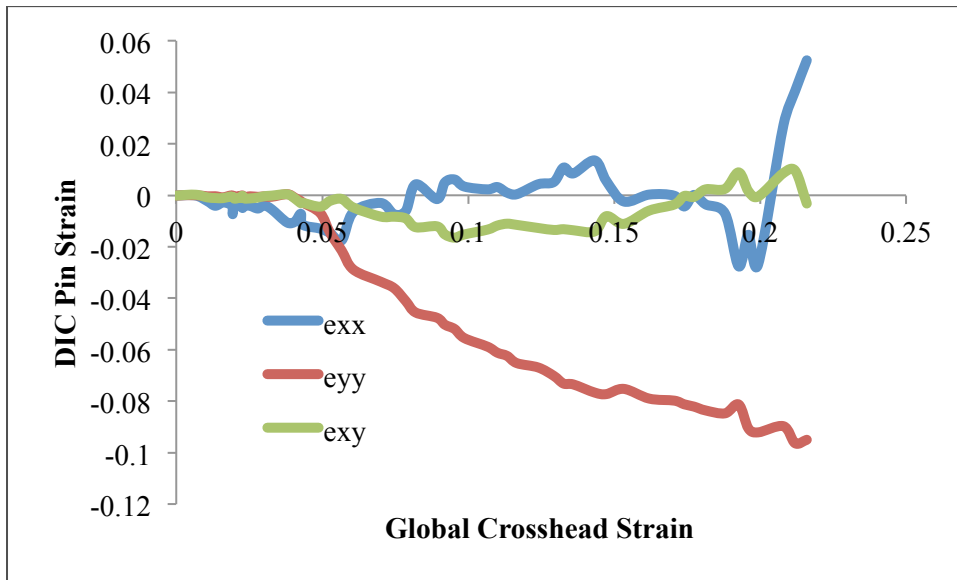


Figure 46: Strain-strain plot of the right pin for Test #2 (greased boundary condition). DIC pin strains were calculated with VIC 3D and global strain comes from Imada load frame.

4.3 Discussion

In this experiment, representative volume elements (RVEs) were tested under compressive loading with various boundary conditions, including: free, greased and glued. All experiments were performed with the foam core removed in order to isolate the pin response within the sandwich. These tests were carried out in order to determine how the pins locally deform and accumulate strain. To achieve this result, 3D DIC was used so that the strain could be determined over the curved pin surface.

The results of this experiment show that the representative volume element (RVE) specimens exhibit similar qualities to the cross pin and 3"x3" macroscale sandwiches. Although the cross pin tests achieved higher stresses, the RVE sandwiches can reach higher loads because of their increased size and number of pins. The experiment also proved that significant full-field strain and displacement fields could be extracted by using 3D DIC. This concept will be extended to shaped sandwich structures in the next few chapters.

In the RVE pin experiments, failure was generally initiated due to pin buckling or kinking. DIC shows that strains remain below 1% before failure initiation, but this changes as the amount of compressive load is increased. The dominant strains in the greased compression test at failure are the transverse and axial strains, with values of 11% and 9.5%, respectively.

This experiment also explored the relationship between boundary conditions and compressive properties. It was determined that the compressive stiffness is not affected by the boundary condition; however, the compressive strength varied largely. Results are tabulated below in Table 6.

Table 6: Summary of Results for RVEs with different boundary conditions prior to transformation to macrostress

	Test 4 (Free)	Test 2 (Greased)	Test 7 (Glued)
Maximum shear strain at failure	12%	9.5%	N/A
Maximum load (N)	80	198	180
Compressive Stiffness (MPa)	13	12.1	37.1
Compressive Strength (MPa)	0.18	0.663	0.65

The results obtained from this experiment can be directly compared to the results from previous small-scale experiments given in Chapter 3. The results are tabulated in Table 7, showing the compressive stiffness and compressive strength as they change with pin density. The first four rows listed come from previous data and the last three rows are results from this research program. In this table, the data from Chapter 4 has been adjusted to show a macro-scale response. Even after transformation, the results from Chapter 3 have much higher stiffnesses and strengths.

Table 7: Comparison of stiffness and strength of K-Cor specimens from Chapter 3

Core Type	Pin Density (lb/ft³)	Compressive Stiffness (MPa)	Compressive Strength (MPa)
<i>K-Cor w/ foam</i>	1.5	79.24	1.70
<i>K-Cor w/ foam</i>	1.8	68.26	1.30
<i>K-Cor w/ foam</i>	4	104.17	1.15
<i>K-Cor w/ foam</i>	8	138.90	2.94
<i>K-Cor without foam (free boundary condition)</i>	1.8	8.96	0.28
<i>K-Cor without foam (greased boundary condition)</i>	1.8	37.06	0.78
<i>K-Cor without foam (glued boundary condition)</i>	1.8	29.76	0.64

Chapter 5: Two- and Three-Dimensional Compression Testing of Small Curved Specimens

Up until now, we have been discussing experiments and results for straight or otherwise flat pin-reinforced composite sandwich structures. In real-life applications, these sandwich materials will be deployed in various shapes that may include curves. Therefore, it is imperative that we test these materials to understand and model their flexural response to compressive loading and examine their failure modes.

According to Vinson [4], shell sandwich structures have a significantly different behavior than plate and beam structures because there is a bending boundary layer under a laterally distributed load. In this case, bending stresses are superimposed on the membrane stresses over a small region near any structural, load, or material discontinuities. Regardless of where the discontinuities lie, shells tend to buckle at a fraction of the load predicted by standard analytical methods.

When pin-reinforced composite sandwich structures are curved, the local orientation of the pins changes, as shown in Figure 47 below. When the sandwich is thermoformed into a curved shape, the pins remain straight and the deformation occurs within the foam. The radius of curvature, R , can be used to define local pin orientations. As we were waiting for AEC to supply the singly curved test specimens, we fabricated our own K-Cor curved sandwiches in the Advanced Manufacturing Lab (AML) at the University of Maryland, College Park. An explanation of how the sandwiches were formed is given below in *Sections 5.1.2 and 5.1.3*.

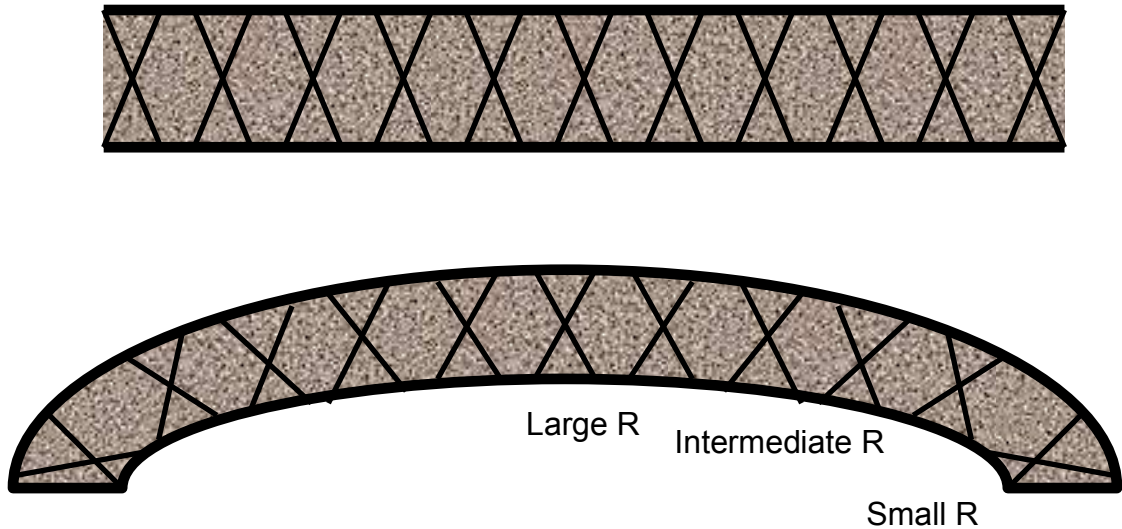


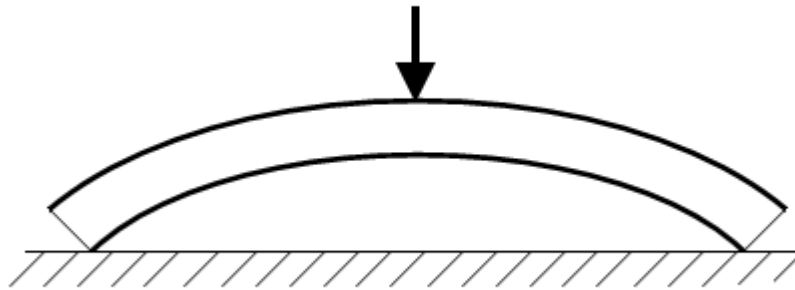
Figure 47: The radius of curvature for a curved sandwich structure changes; R can help determine local pin orientations after the sandwich has been thermoformed into shape.

These experiments tested the response for two different types of curved sandwiches: ones with foam core and ones without the foam core. The foam core was dissolved using aqueous Sodium Hydroxide. Use of this solution did not weaken or damage the carbon fiber pins. To model the global behavior, we utilized 2D and 3D DIC. The 2D DIC was used to observe the failure response at the specimen face and obtain the deformation in the through thickness direction of the sandwich. 3D DIC allowed us to see how the sandwich curved and flexed throughout the test.

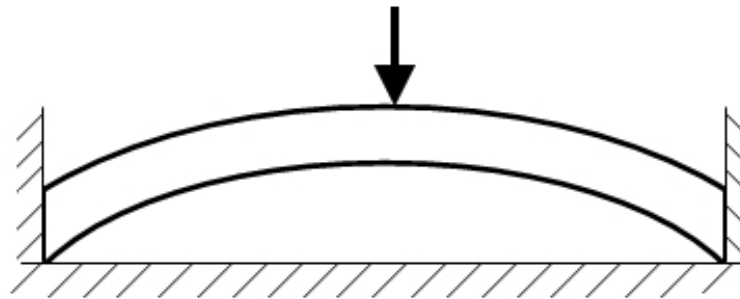
5.1 Methodology

For this experiment, flexural tests were performed with two boundary conditions: (a) supported on the bottom, and (b) supported at the bottom and the edge (See Figure 48 below). Two types of curved sandwiches were investigated, including

curved sandwiches with foam core, curved sandwiches without foam core. For added comparison, flat sandwiches with foam core were tested in 3-point bend. Each of the curved test specimens was the same size and curvature. During testing, a central load was applied to the specimen.



(a) Curved K-cor specimen supported at the bottom



(b) Curved K-cor specimen supported at the bottom and edge/end

Figure 48: End supports for small curved specimen experiments, including: (a) bottom supports and (b) bottom and edge supports

5.1.1 Design of Experiments

With the exception of the tests from Chapter 3, the experiments discussed in earlier in this thesis were all conducted with the foam core removed. In the same fashion, the small curved sandwich structure design of experiments was formed to show how the pins react to compressive loading without the foam core. Additional

tests were executed with the foam core intact in order to see the effect of foam core on stiffness and strength.

Table 8: Design of Experiments for small curved pin-reinforced sandwich structures manufactured at UMD

Test Number	Foam or no foam?	Boundary condition
1	Foam	Bottom
2	Foam	Bottom
3	Foam	Edge support
4	No foam	Edge support
5	No foam	Bottom support
6	Foam	N/A (3-point bend)

5.1.2 Preparation of Curved Sandwich

The curved pin-reinforced sandwiches were formed from DragonPlate woven fabric carbon fiber-epoxy facesheet and K-cor foam with a pin density of 1.8 lb/ft³. Specimens were formed in an oven heated to 200 degrees Celsius (the upper softening point for Rohacell foam) in a three-point bend fixture. The foam and facesheet were pre-heated at this temperature to allow the foam to deform without fracturing. The facesheet and foam were attached with West System epoxy resin 105 and slow hardener 206 with a 5:1 ratio by mass, respectively.

The three-point bend fixture, seen below in Figure 49 and Figure 50, utilized three screws that created intimate contact with the facesheets throughout the length of the specimen. With this fixture, a curved specimen with a maximum radius of curvature of 0.0072/mm was formed. The procedure for creating this specimen is described in the following section.

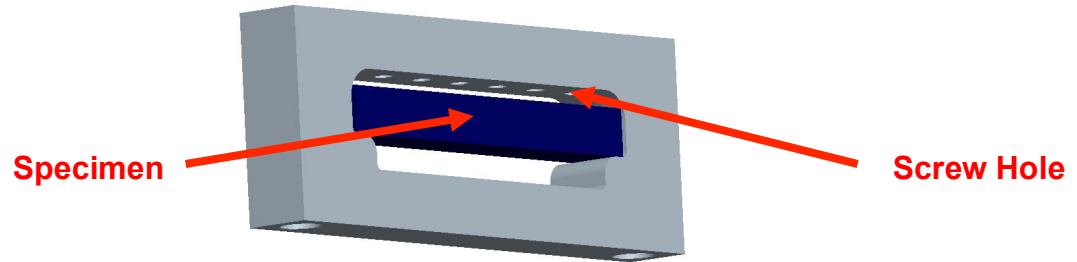


Figure 49: Fixture design for shaping sandwich specimens. Screw holes allowed variations of three and four point bending locations when specimen is in the oven

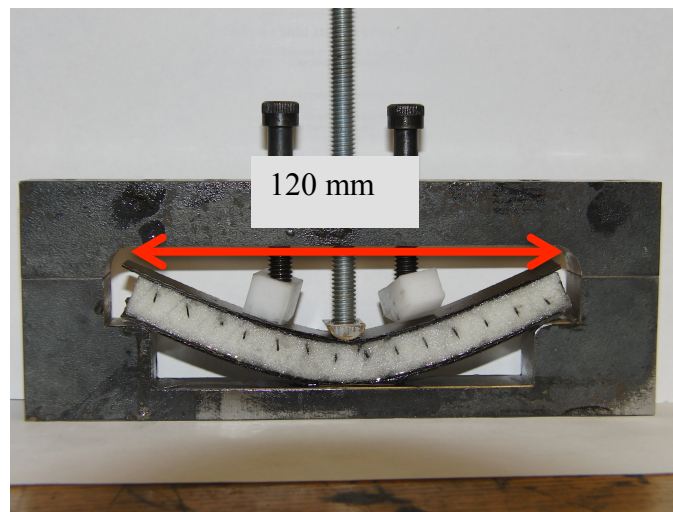


Figure 50: Fixture allowing for fabrication of shaped K-Cor composites with a single curvature

5.1.3 Manufacturing Procedure

1. Using the band saw, cut the foam and facesheet into the necessary size. You should cut out two identical facesheets and one foam core. (20 mm wide and ~130 mm long)
2. Insert the three parts into the fixture and apply a load with the three screws.
3. With the oven set to 200 degrees Celsius, insert the fixture and specimen into the oven for 15-20 minutes.
4. After the time has elapsed, carefully remove the fixture from the oven. Twist the screws down 2 full twists or ~2mm. Be careful not to twist too far because

the foam core may fracture.

- Repeat steps 3-4 for about 90 minutes, or until the specimen touches the bottom of the fixture (like in Figure 50 above). Once it reaches the bottom of the fixture, it is fully bent and you can proceed to step 6.
- Create the epoxy mixture with 5 parts West System epoxy resin 105 and 1 part slow hardener 206.
- Remove the fully bent specimen from the fixture. Apply the epoxy.
- Insert the specimen back into the fixture.
- Put the fixture back into the oven. Allow the specimen to cure for 20-24 hours.

After the specimen has cured in the oven for 24 hours, it can be removed. Then, the foam core can be dissolved by using an aqueous solution of Sodium Hydroxide. The final structure—less the foam—is shown in Figure 51. All of the specimens were of approximately the same dimensions (span = 120 mm, thickness = 15.5 mm, width = 20 mm). For these sandwich structures, the curvature was 0.0072/mm. Figure 52, below, shows the experimental test setup for this flexural test.

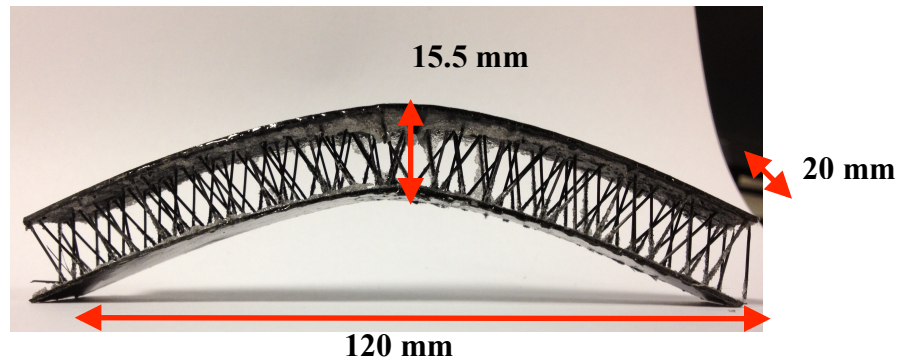


Figure 51: Representative curved specimen with dimensions

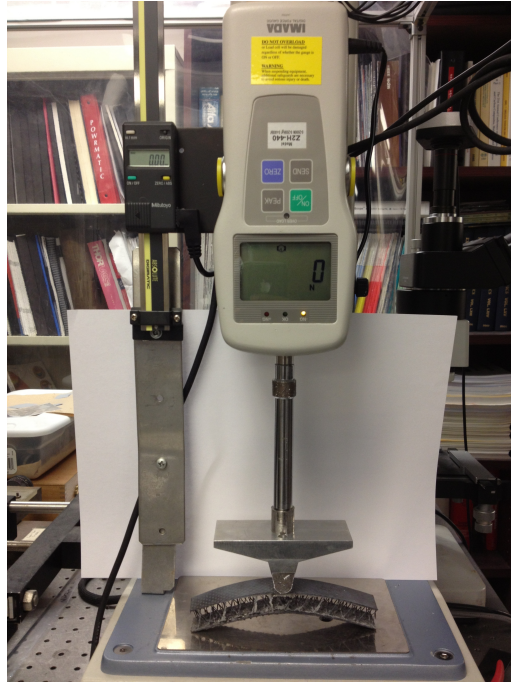


Figure 52: Experimental set up for the flexural test of the K-cor sandwich composite, showing a specimen without foam core

5.2 Results

Results from the experiments are given below in the form of load-displacement charts, stress-strain diagrams, DIC plots, and strain-displacement plots. Presented here are the results from Test 1 (with foam included) and Test 5 (no foam).

5.2.1 Load-Displacement Results

Figure 53 shows the load-displacement results for Test 1, which has the foam core intact. For the curved sandwiches that did not have the foam removed after manufacturing, the load-displacement response was comparable to flat specimens during initial deformations. The curved sandwiches demonstrated a similar elastic load limit and showed a related load-displacement response as compared to flat specimens. Point A on the plot shows where the material exhibits a linear elastic response. The peak force shown by the small curved sandwich before the elastic limit

was reached (point B) is ~ 400 N and the stiffness is determined to be 210 N/mm. The maximum load bearing capacity for this sandwich was a little over 800 N.

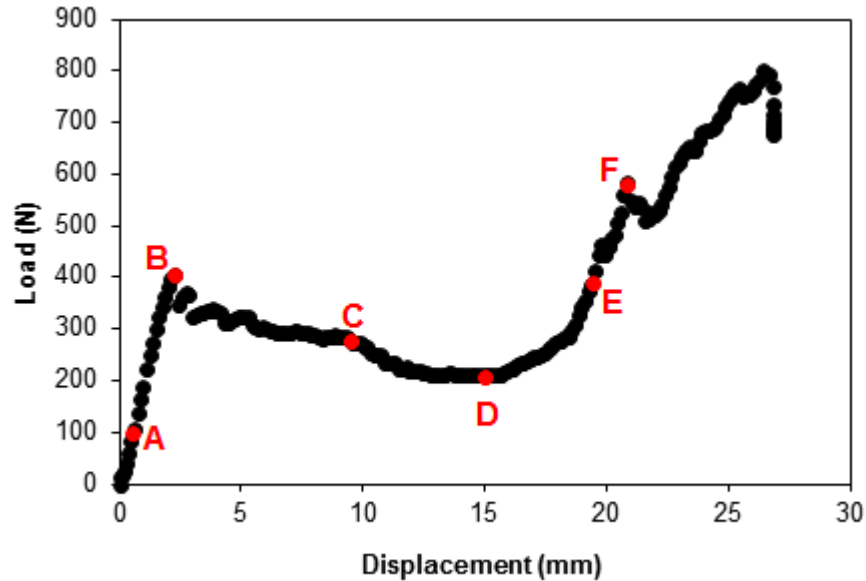


Figure 53: Load-displacement curve for central loading of curved specimen with foam and bottom boundary condition. Results are from the Test 1 data set.

Unlike the flat specimens, the curved sandwich's load bearing capacity was gradually decreased after reaching the elastic limit (from point B to point D) instead of showing an abrupt drop. This probably occurred because the curved specimen induced a bending moment that was akin to the flat specimen in three-point bending. At point D, there seems to be a steady accumulation of elastic load again as the sandwich starts to experience a truly compressive load.

The global load-displacement response of the curved sandwich under two different boundary conditions is expressed in Figure 54 below. More details about these observations will be given when discussing the 2D and 3D DIC results. From the load-displacement curve, it is evident that the global stiffness of these curved sandwiches is ~ 210 N/mm with foam and 75 N/mm without foam. The figure also

includes some preliminary FEA results for a pin-reinforced composite sandwich structure without foam. Note that the boundary conditions do not significantly affect the global flexural response.

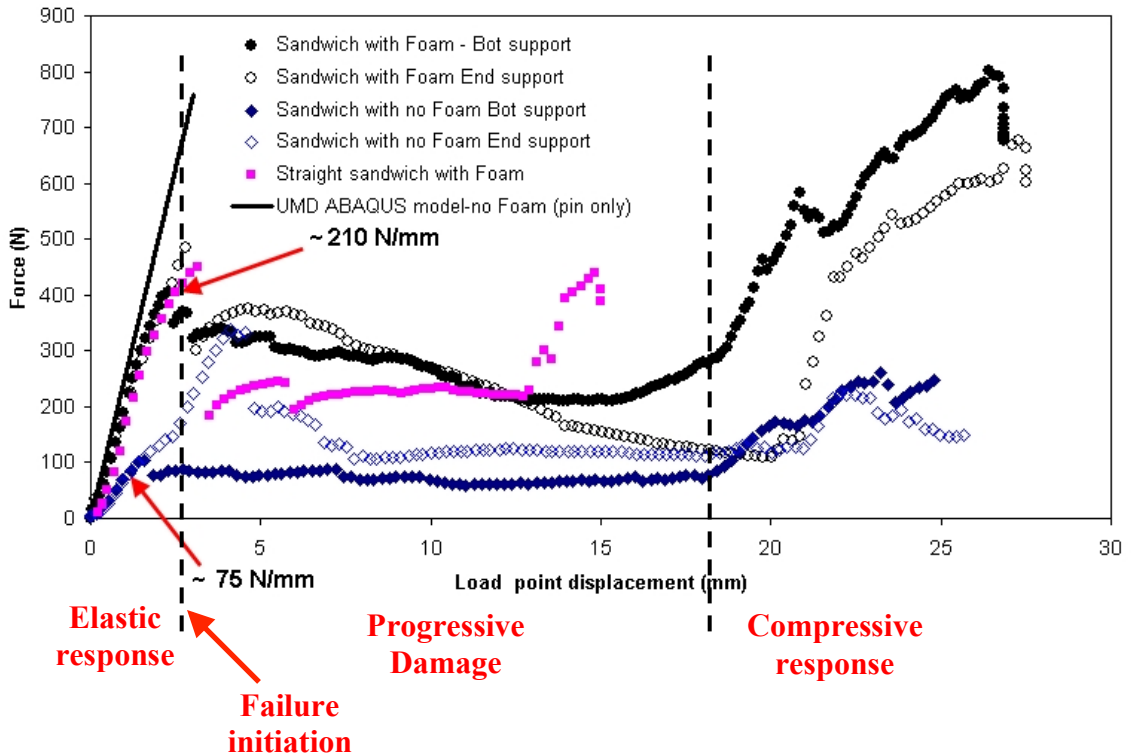


Figure 54: Global flexural response of the curved K-cor sandwich specimens and comparison with straight sandwich. The elastic deformation, failure initiation and transition to compressive response are indicated.

The effect of the end supports is solely realized in terms of maximum load bearing capacity. For sandwiches with and without foam, the maximum load bearing capacity is higher when the edge of the sandwich is supported (see Figure 48 (b) from Section 5.1). The load bearing capacity of the curved sandwich with foam that is constrained at the ends is significantly higher than its end-supported counterpart without foam. This occurs because the foam provides shear resistance when it is present in the sandwich.

The stress-strain results from Test 1 and Test 5 are shown below in Figure 55. Both tests were conducted with a “bottom support” boundary condition. Test 1 is a curved sandwich with foam core; Test 5 does not have foam core included. The stress-strain diagram shows that the compressive stiffness is about 172 MPa and 66 MPa for Test 1 and Test 5, respectively. The maximum compressive load for these sandwiches was determined to be 406 N in curved sandwiches with foam and 101 N in curved sandwiches without foam.

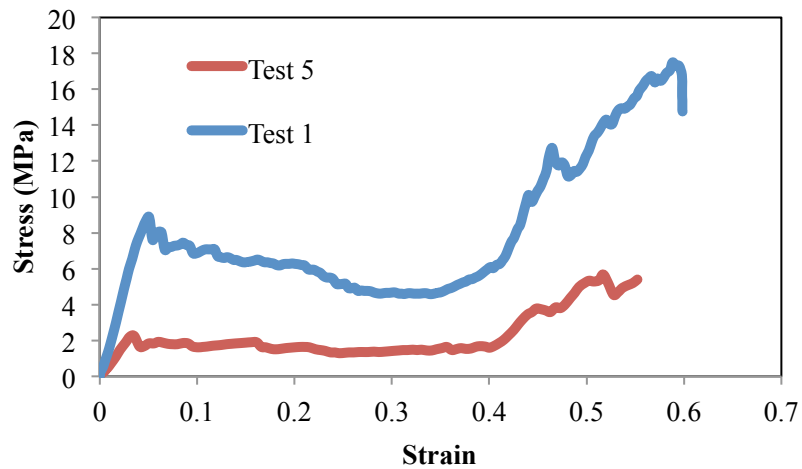


Figure 55: Stress-Strain diagram for small curved sandwiches with and without foam core

5.2.2 2D DIC Results

The two-dimensional DIC results for a curved sandwich structure with foam core are displayed below in Figure 56. These images are in reference to the graph in Figure 53 and come from the Test 1 data set. DIC shows that the loading behavior at point A is perfectly elastic and the strain fields demonstrate a concentrated shear strain on the right side of the specimen. At this same location, there is also a significant contribution from compressive strain in the loading direction (y).

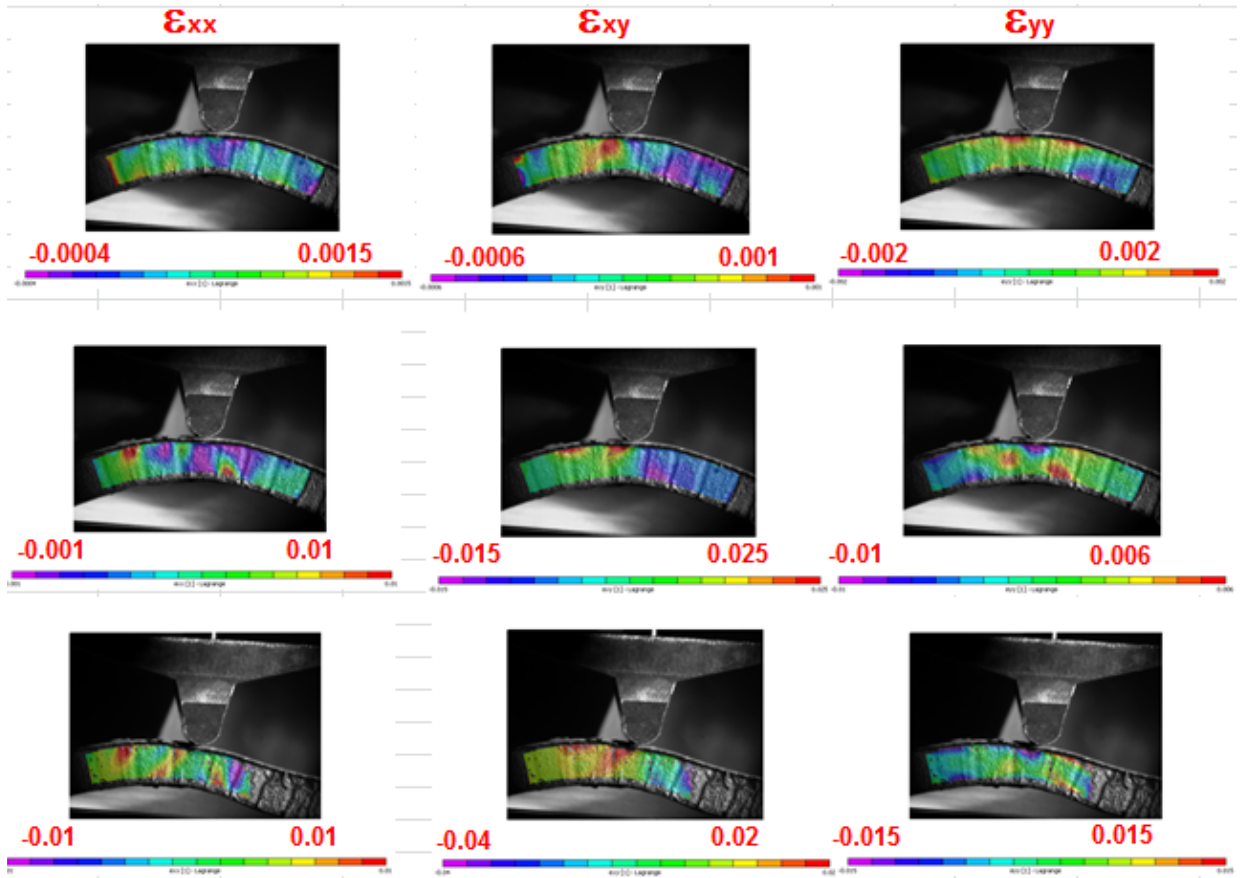
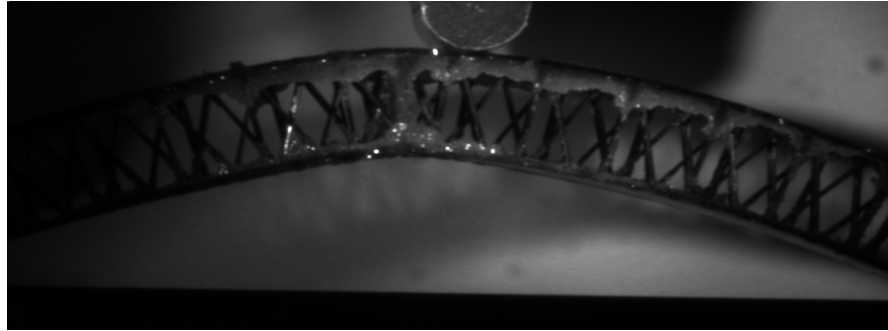


Figure 56: DIC strain field results for load conditions A (top), B (middle) and C (bottom). These results come from the Test 1 data set.

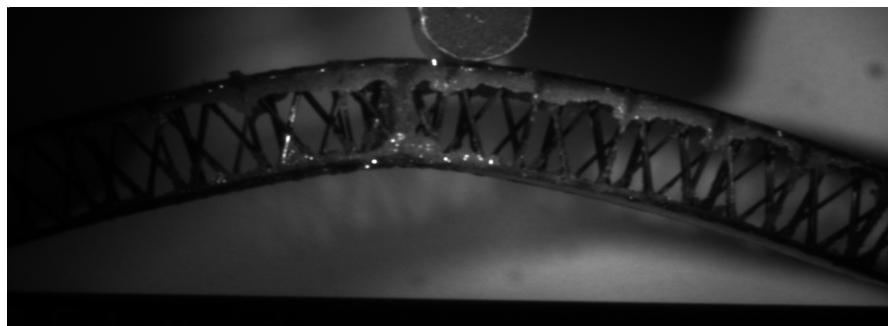
At the elastic limit point B, the shear strain (ϵ_{xy}) increases by an order of magnitude with only a small change in the compressive strain in the y-direction (ϵ_{yy}). The axial strain (ϵ_{xx}) increases by an order of magnitude right beneath the central loading point. An edge delamination comes about at Point C as the load bearing capacity is decreased. In DIC, this appears on the right side of the specimen where shear strain is localized and concentrated. It is at this point that the specimen loses its shape and becomes asymmetrical.

Unfortunately, the 2D digital images that were captured for Test 5 were not clear enough to analyze with DIC. The lighting and level of magnification simply were not adequate enough to properly image the pins. Although this data set was

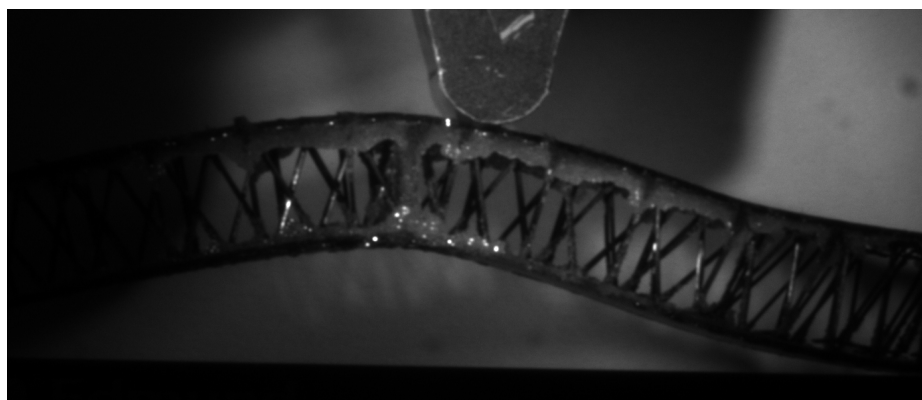
inconclusive, the deformation images can still be presented (Figure 57). By themselves, they show that the facesheet buckled on one side of the specimen and the pins became detached from the facesheet during testing.



(a)



(b)



(c)

Figure 57: Deformation images for (a) elastic region (b) end of elastic region and (c) failure.

5.2.2.1 Comparison with Flat Specimen

The 2D DIC results for small curved sandwiches show a significant amount of shear strain accumulating on one side of the central loading point that eventually led to delamination. This type of behavior was not observed with previously tested flat specimens in three-point bending (see Figure 58 and Figure 59). These flat specimens demonstrated an abrupt load reduction at their elastic limit and later, core shear failure. In contrast, the curved sandwiches showed more of a smooth transition while the load bearing capacity was decreasing. Near the failure point, the DIC axial strain fields for the flat specimens indicated a concentration of strain. This is most likely because the pins buckled before the core material could shear.

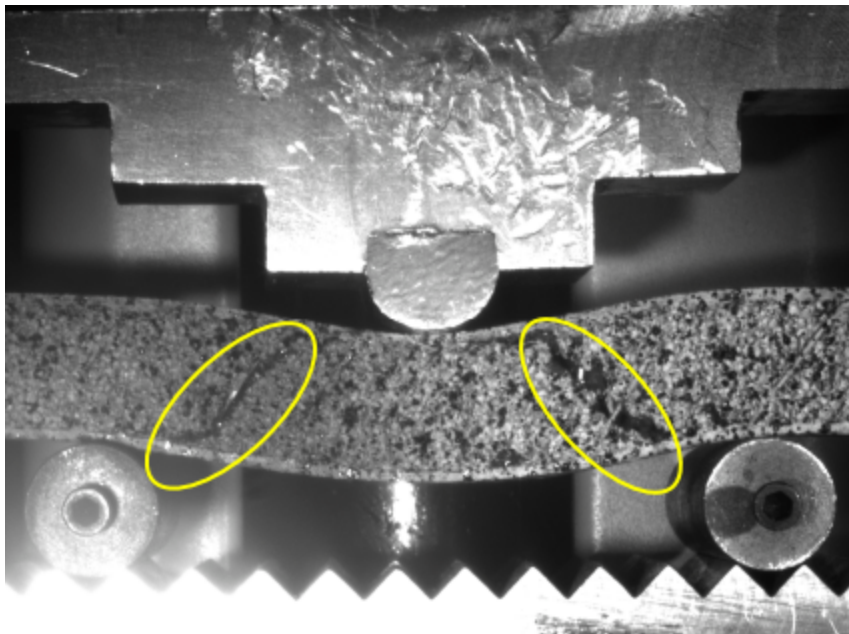


Figure 58: Failure of a previously tested flat specimen in three point bending. The core shear failure mechanism is indicated in yellow

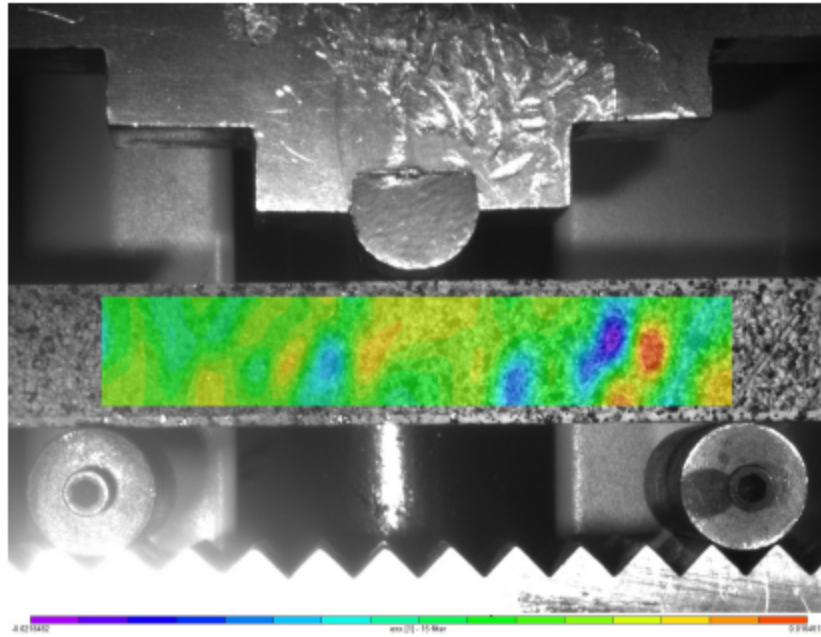


Figure 59: Axial DIC strain fields associated with core shear failure in the previous figure.

5.2.3 3D DIC Results

Strain and displacement data were extracted for a specific point on the facesheet surface for Test 1 and Test 5. For sake of brevity, only the results from Test 1 will be presented. The strain and displacement results emanate from the point on the facesheet given in Figure 60. Additionally, the evolution of DIC strain was plotted against global strain in Figure 61.

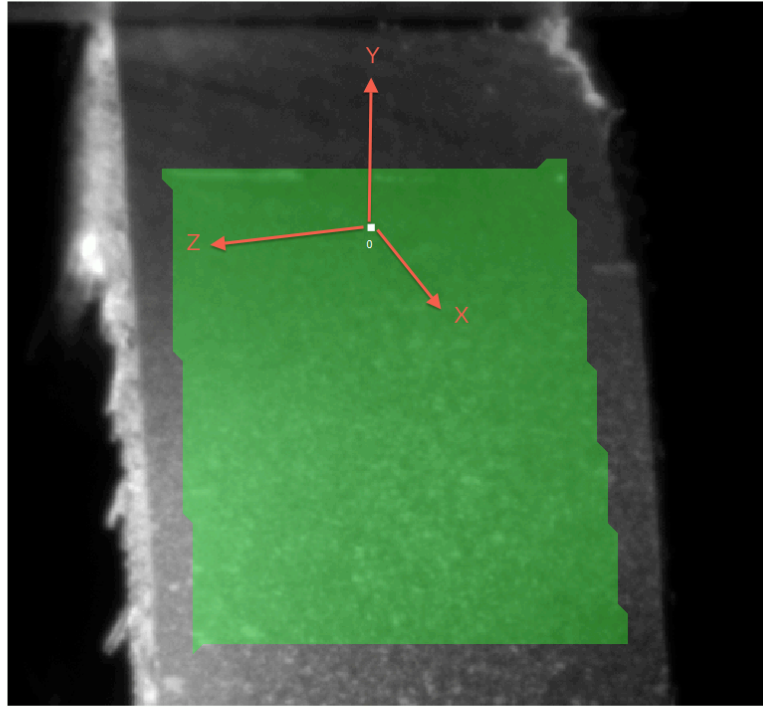


Figure 60: Data extraction point for Test 1, with coordinate system shown

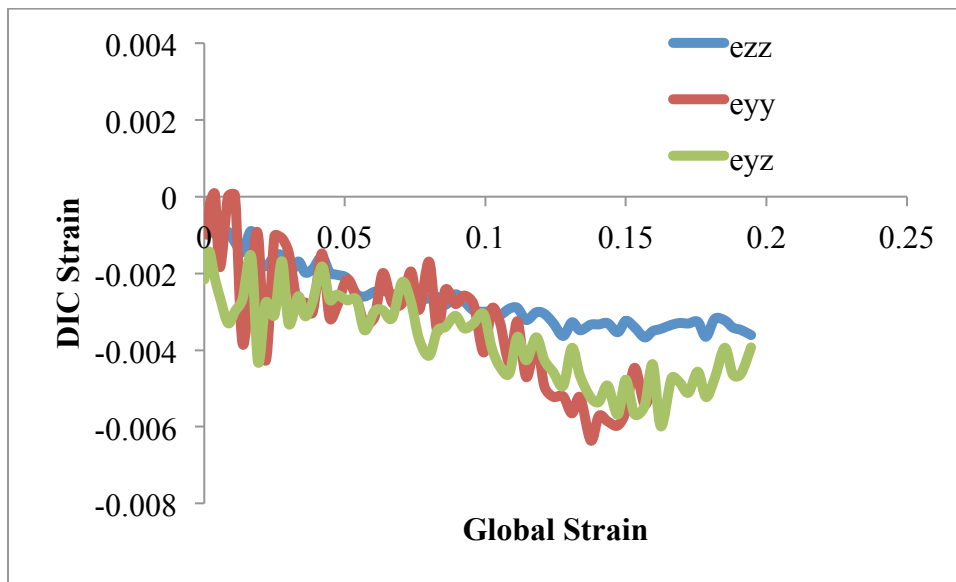


Figure 61: Evolution of DIC facesheet strains as a function of global strain. Results come from the Test 1 data set

Figure 62 below shows the 3D DIC strain fields at three different points in the Test 1 experiment: A) within the elastic region, B) at the elastic limit and C) at

failure. There is significant variation in the strains at point A, especially for the ϵ_{zz} strains. From these images, it is evident that the strains remain relatively low (less than 1%) until point C. At failure, the DIC data becomes a bit uncorrelated, but it still gives important information about the curvature of the facesheet. The shear strain is close to zero at failure. The maximum strain at failure is attributed to ϵ_{yy} which has a value of -2.9%. (The 8.6% strain value comes from decorrelation of the image).

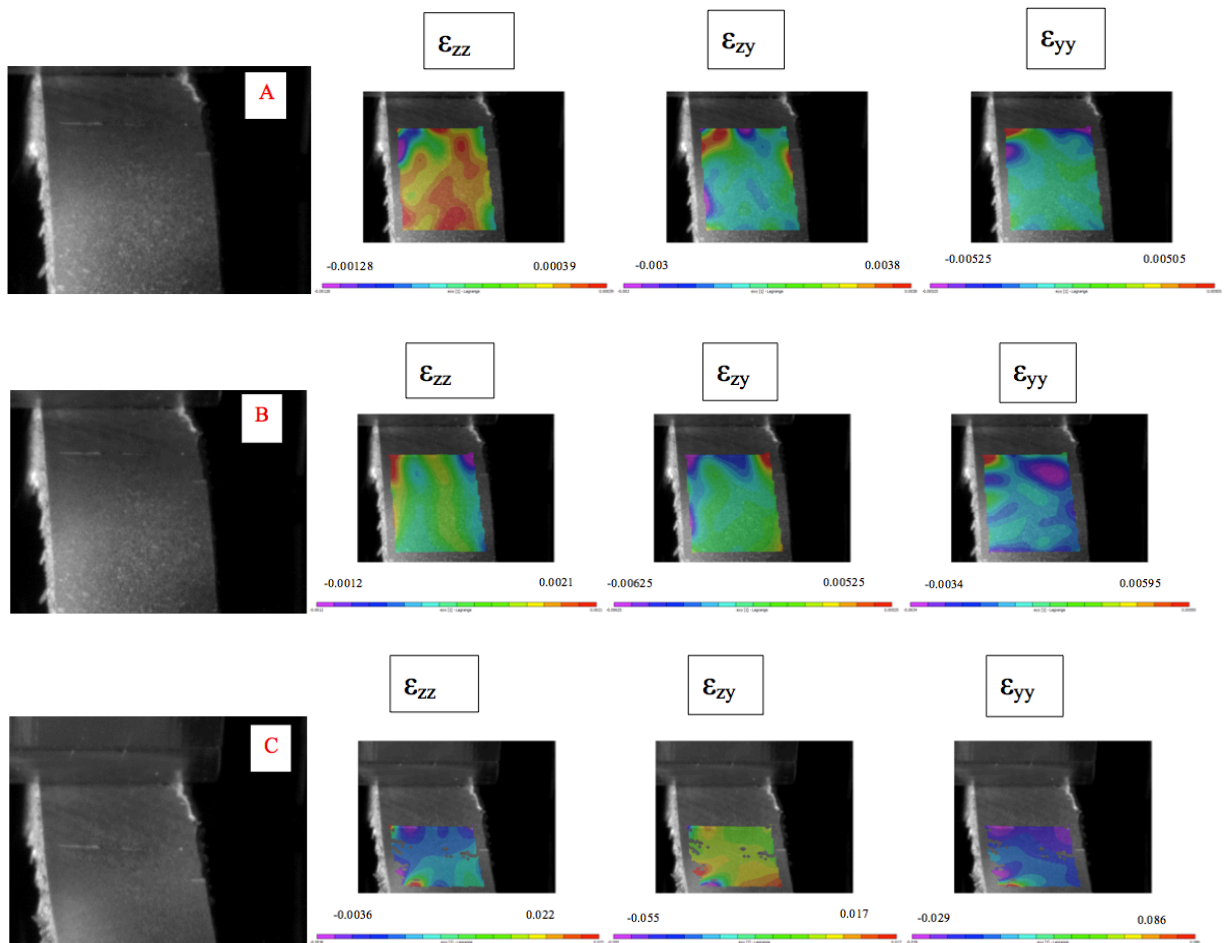


Figure 62: 3D DIC Strain data for Test 1

5.3 Discussion

In this phase of the research, contoured pin-reinforced composite sandwich structures were manufactured, tested under compressive loads, and characterized using 2D and 3D Digital Image Correlation. These K-cor curved sandwiches were designed to have a radius of curvature of 0.0072/mm. The resulting load-displacement plots for the curved sandwiches exhibit a very similar response to flat specimens in three-point bend. The small curved specimens demonstrated a strong localized presence of shear strain that may have been caused by pin buckling. These concentrated shear strains led to core shear failure and is observed from the 2D DIC strain results at the location where the material failed.

The localized shear strain response in 2D DIC generally shows the location at which a curved sandwich structure will fail by core shear failure. Clearly, there is a correlation between the location of concentrated shear strains and failure initiation sites. Failure initiation was typically observed by shear at the center of the material where the curvature is maximized. This behavior was verified with 2D DIC results for test specimens with and without foam core. A large accumulation of shear strain typically led to core shear failure and delamination for these materials. The table below shows the maximum strain at failure, the compressive stiffness and compressive strength for two experiments. Test 1 was an experiment involving a curved sandwich structure with the foam core intact and Test 5 was conducted without any foam inside of the sandwich.

Table 9: Brief summary of results for small curved specimen experiments

	Test 1	Test 5
Maximum shear strain at failure (2D)	-4%	N/A
Maximum shear strain at failure (3D)	-5.5%	-1.8%
Compressive Stiffness (MPa)	172	66
Maximum Load (N)	406	101

3D DIC results show that the strains on the facesheet surface remain less than 1% until failure. Surprisingly, the shear strains are close to zero at failure. The maximum strain at failure is actually attributed to the transverse strain e_{yy} , which has a value of -2.9%.

As it turns out, the effect of the end supports is not significant. The resulting DIC data and load-displacement curves show no differentiation between specimens that are supported on the bottom and on the bottom and sides. This is the case for test specimens with and without the foam core. The end supports only affect the maximum load bearing capacity of the sandwich after the sandwich experiences a “crushing” compressive load.

Chapter 6: Two- and Three- Dimensional Compression Testing of Large Curved Specimens

In order to fully realize the mechanical properties for pin-reinforced composite sandwich structures and validate the previous results, it is important to test these materials on a larger scale. A company called Materials, Research & Design (MR&D) sent us a set of large X-Cor composite specimens to test under compressive load conditions. The material was fabricated by AEC. These singly curved cylindrical materials were tested on the macro-scale with 2D and 3D DIC to analyze deformations near the load point.

6.1 Methodology

For this experiment, a singly curved composite sandwich structure with a six-inch radius was tested. As received, the whole 6” radius sandwiches each weigh 1.07 pounds. Unfortunately, these curved sandwich structures were not perfectly cylindrical, so the radius of curvature actually changes depending on which part of the sandwich you look at. (If it were perfectly cylindrical, the sandwich would be 6 inches tall.) For the sake of consistency, the curved sandwich will be called “6 inch radius curved sandwich” structure throughout the rest of this document. More detailed information about the radius of curvature for these sandwiches is given in *Section 6.2.3.2 Strain at a Specific Location*. The actual height of the curved sandwich is 4.25 inches.

The 6-inch radius curved sandwiches were cut into five identical 3-inch wide test specimens. Each test specimen is 4.25 inches (10.8 cm) tall and 12 inches (30.48

cm) wide. From there, they were tested under compressive load and analyzed with 2D and 3D Digital Image Correlation (DIC). A schematic of the whole specimen is given in Figure 63, along with an image of the actual structure in Figure 64.

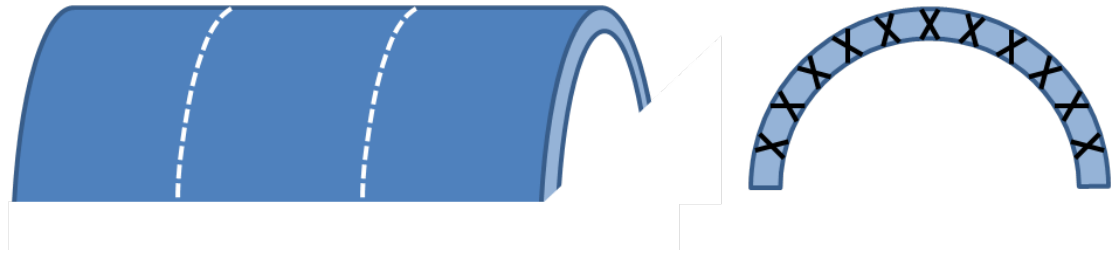


Figure 63: Whole 6" radius sandwich structure from AEC



Figure 64: Whole 6" radius of curvature sandwich structure

Each 3" wide specimen was tested under a compressive loading condition, as shown in Figure 65 below. The ends of the cylinder were cut flush with the surface so that the test stand base could support the structure. Flexural tests were performed with the specimens being supported at the bottom and edges as shown schematically in Figure 66 below.

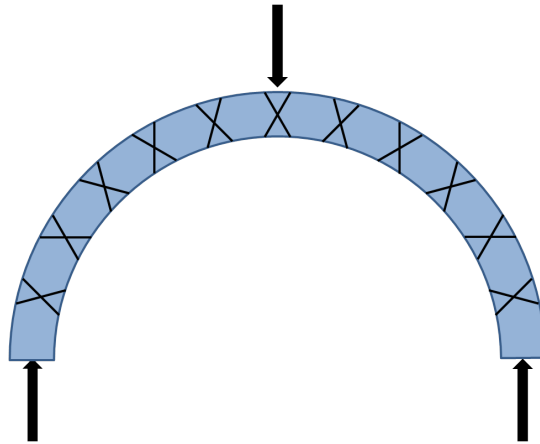


Figure 65: Schematic of compressive loading condition for 6" radius curved sandwich

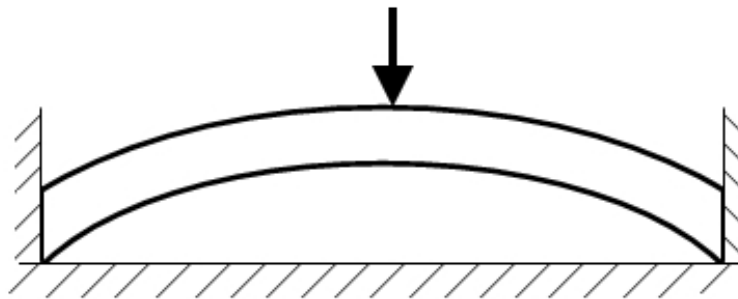


Figure 66: Schematic diagram of the curved X-cor specimen supported at the bottom and edge

Figure 67 depicts what the test specimens looked like at the far end of the curved portion. The ends were cut to be perpendicular to the facesheet and they were trimmed to remove all of the exposed foam core material. The flexural test, as shown in Figure 68, was performed with the Imada MX 500 load frame previously discussed in Chapter 2.



Figure 67: End condition for 6" radius flexural experiment. The sandwich was cut to be perpendicular to the facesheet material.

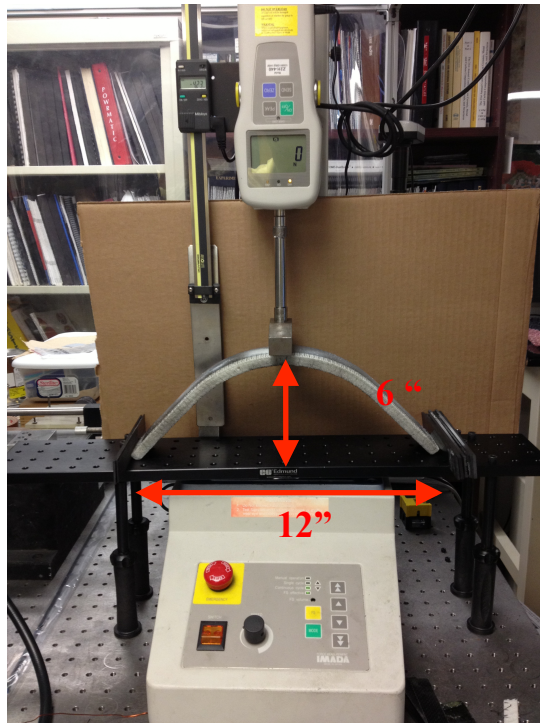


Figure 68: Imada load frame, specimen and caliper

In order to fully analyze the mechanical response of the 6 inch radius curved sandwich structures on the macro-mechanical scale, both 2D and 3D DIC images were utilized. 2D DIC measurements were taken at the edges of the specimen in order to examine the pin deformations in the through-thickness direction. 3D DIC measurements were made on one-half of the specimen with the cameras pointed

towards the facesheet surface. Figure 69 shows a schematic of what the 3D DIC image acquisition system looks like. Below that, Figure 70 shows the location where the specimen was actually imaged. These measurements were used to determine out-of-plane flexure. The expectation was to see anticlastic deformations near the load point.

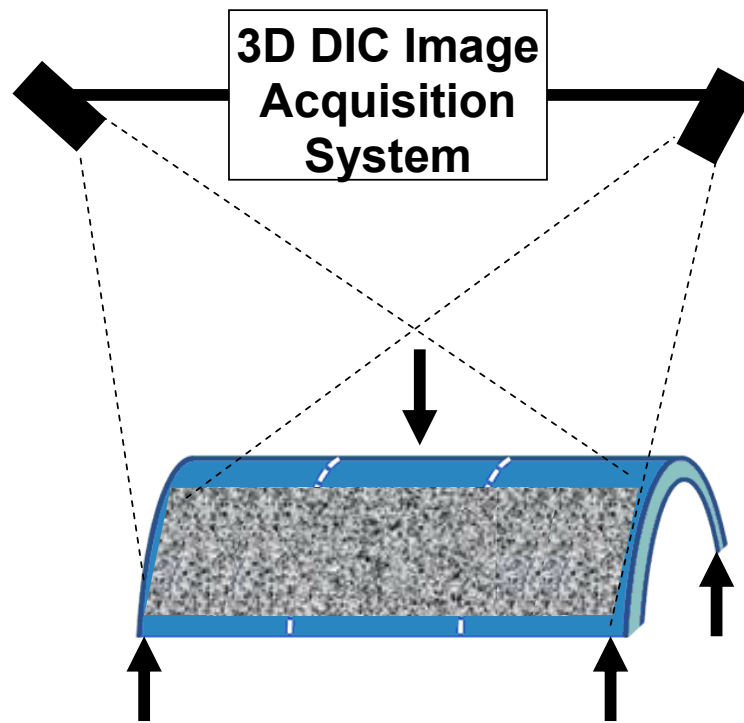


Figure 69: Diagram showing how the macro-mechanical DIC images were obtained.

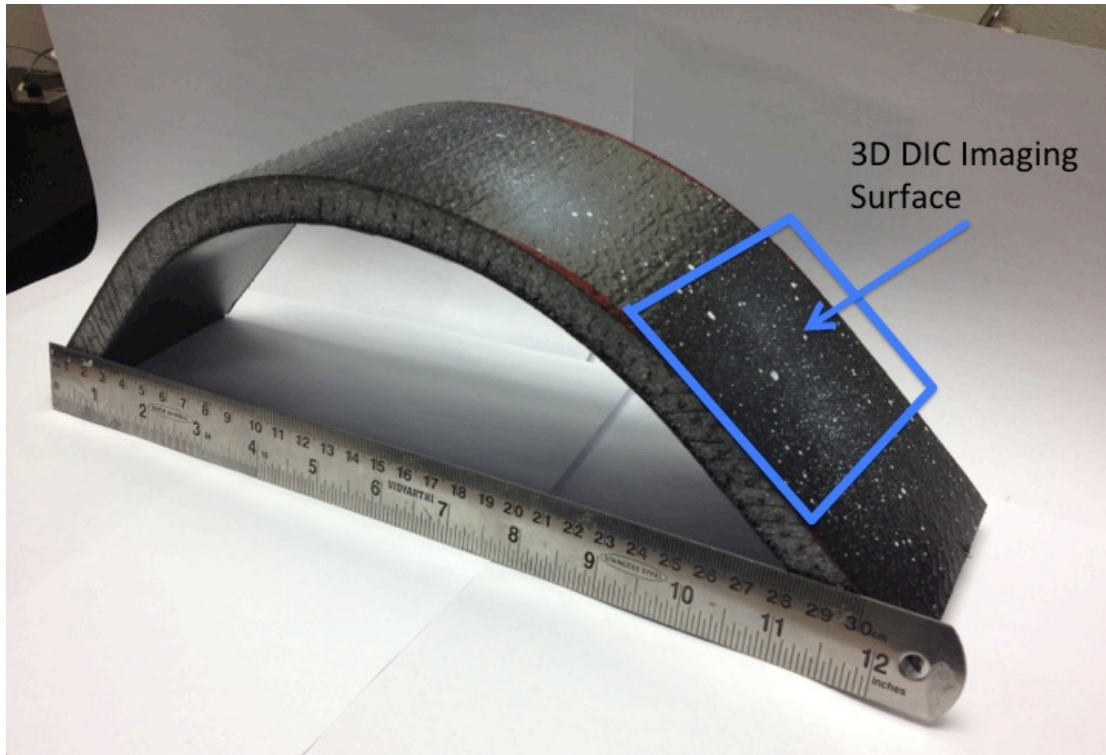


Figure 70: The location of the 3D imaging surface

6.2 Results

6.2.1 Load-Displacement Results

All of the flexural tests performed in this experiment each used specimens that were constrained on the bottom and on the facesheet edge. This boundary condition was chosen to mitigate the lateral motion of the sandwich during the test. If the specimen had moved during the test, the images would be out of focus. As determined in Chapter 5, the boundary conditions (supported at the bottom where only the bottom facesheet is supported, and supported at the bottom and edge where both facesheets are supported) do not significantly affect the global flexural response in terms of the flexural stiffness. They do, however, affect the load bearing capacity of the sandwich. Each specimen was tested with the foam core still intact. The global

stiffness of these large curved specimens (with foam) was found to be ~ 170 N/mm, as shown in Figure 71 below. The compressive strength was determined to be 20.2 MPa. Although a total of five specimens were tested, only the last three provided suitable load-displacement and DIC results.

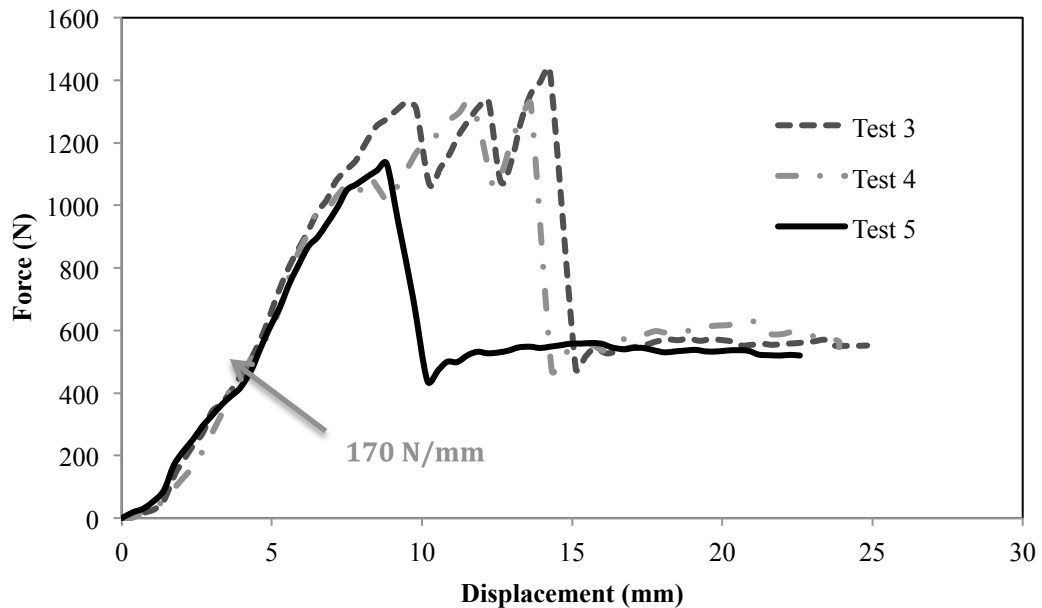


Figure 71: Load-displacement response of the curved (6" Radius) X-cor composite sandwich structure under flexure; the elastic stiffness is shown.

It is interesting to note that there is a pronounced plateau region for these experiments. The load-displacement curves show a typical elastic region followed by a sharp drop in force of $\sim 50\%$, leading to the inelastic deformation response. The curved sandwich structure material demonstrated obvious signs of failure almost immediately after the sharp drop in load. More precise information about the inelastic deformation and subsequent failure modes within this plateau region can be extracted from the 2D DIC strain data in *Section 6.2.2 2D DIC Results* below.

The global stress-strain response was also extracted for all of the 6 inch radius curved sandwich structure compression experiments. Only the results from Test 5 are

shown here because the forthcoming 2D and 3D DIC results all stem from that particular data set. Figure 72 shows the stress-strain plot for Test 5. The equations used to calculate stress and strain are given below the plot.

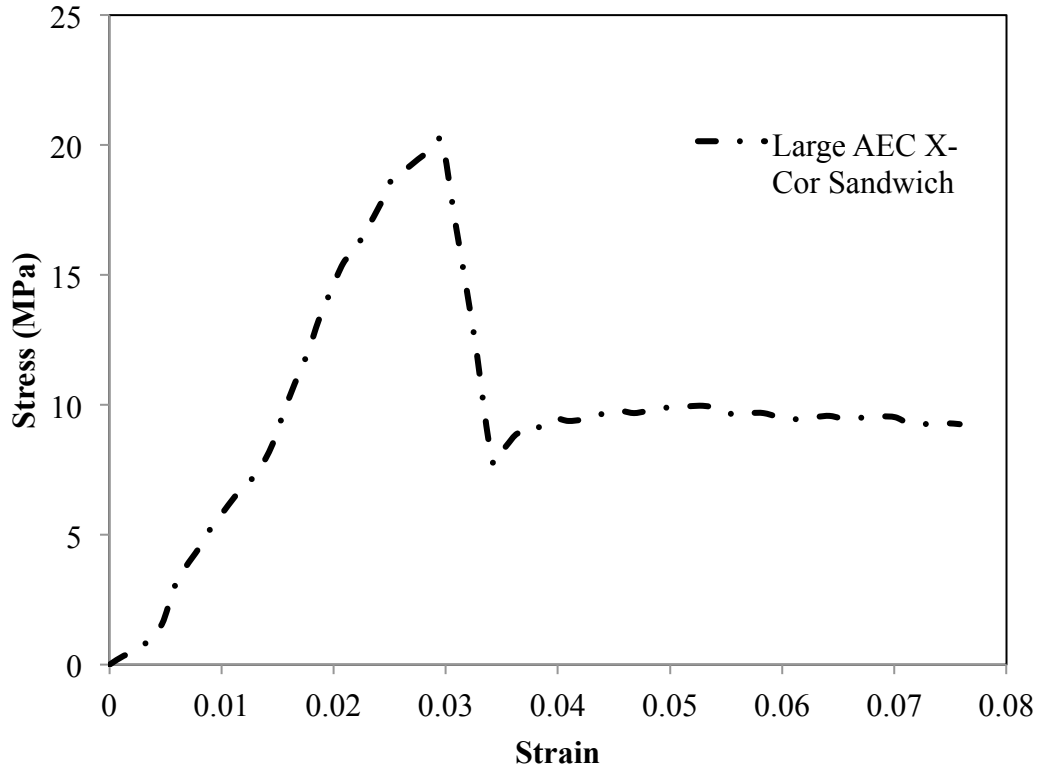


Figure 72: Global stress-strain results for Test 5 of the 6" radius curved sandwich structure

$\epsilon_f = \frac{6Dd}{L^2}$	(Eq. 10)
--------------------------------	----------

$\sigma_f = \frac{3PL}{2bd^2}$	(Eq. 11)
--------------------------------	----------

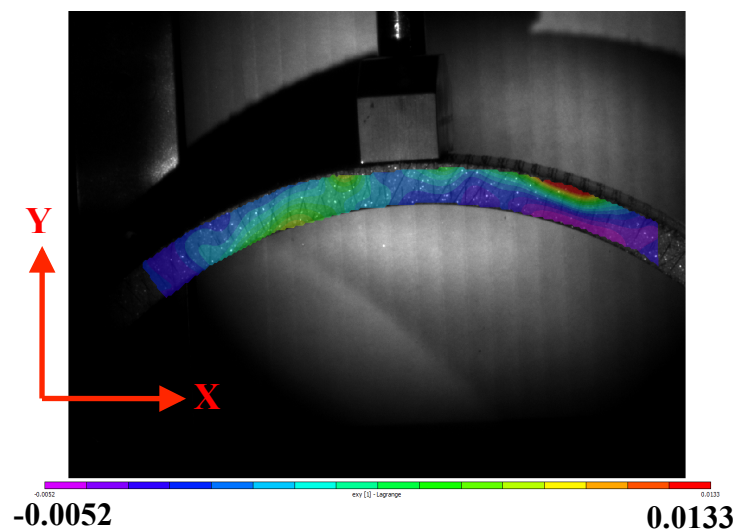
Equation 10 and 11 given above relate loads and displacements to stress and strain. In Eq. 10, D is the deflection measured by the Imada load frame, d is the width of the specimen and L is the span-wise length of the specimen. In Eq. 11, P is the

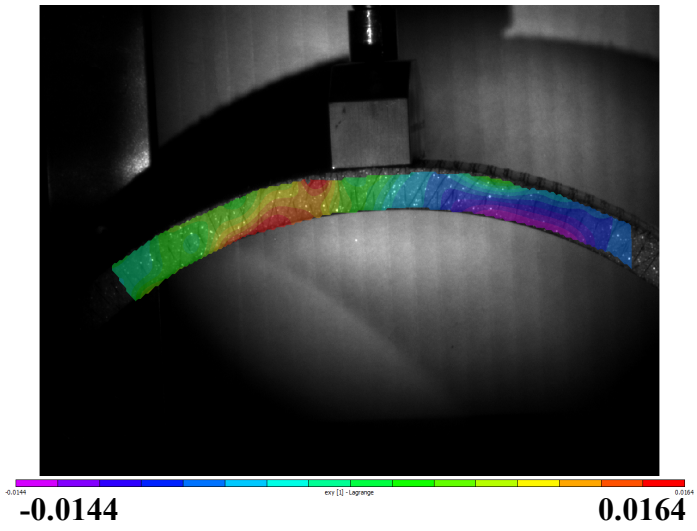
force measured by the Imada load frame, L is the span-wise length, b is the thickness of the specimen and d is the width of the test specimen. The compression stiffness was determined to be 728 MPa from the stress-strain diagram.

6.2.2 2D DIC Results

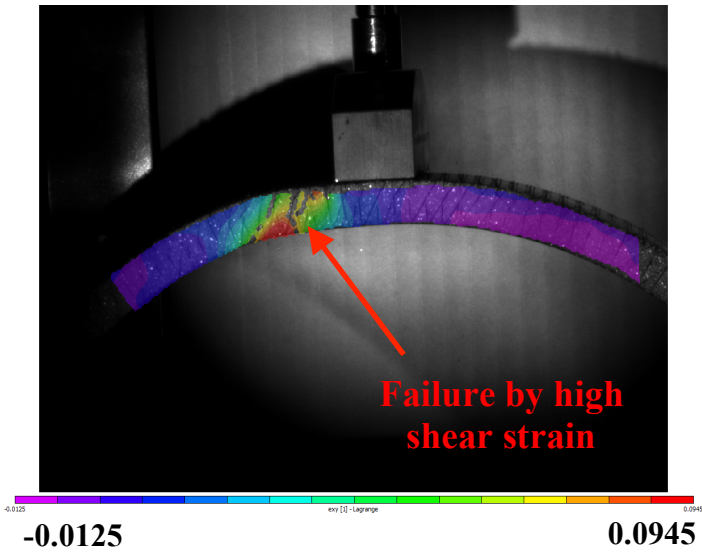
6.2.2.1 Strain Fields

The 2D DIC results from initial testing gave us some insight into how these curved sandwich structures actually fail. The strain fields determined by DIC can be used to identify dominant strain in the deformation, the failure initiation site and the failure mode by which the specimen failed. In this case, the failure initiation site is determined with the shear strain, and that specifically shows where the specimen failed via the core shear failure mechanism. Other failure modes (like facesheet delamination) can be determined by looking at axial strain. The shear strain fields on the front face of the specimen are depicted in Figure 73 for four regimes: (a) the elastic regime, (b) right before failure initiation, (c) right after failure initiation and (d) initiation of the plateau regime.





(b)



(c)

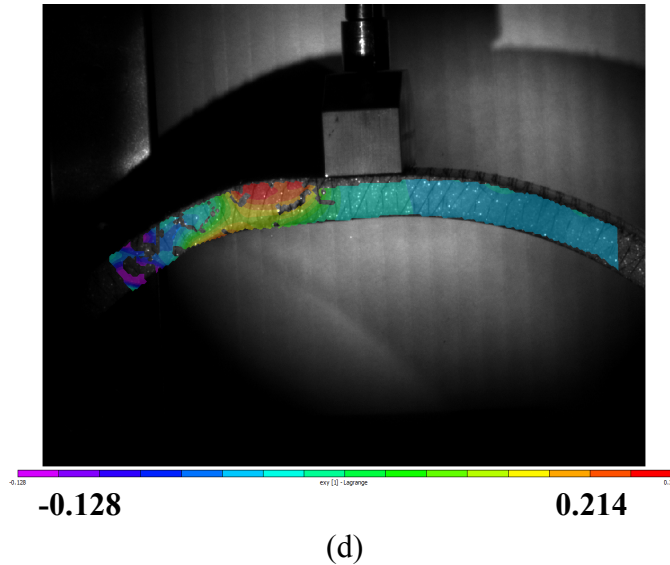


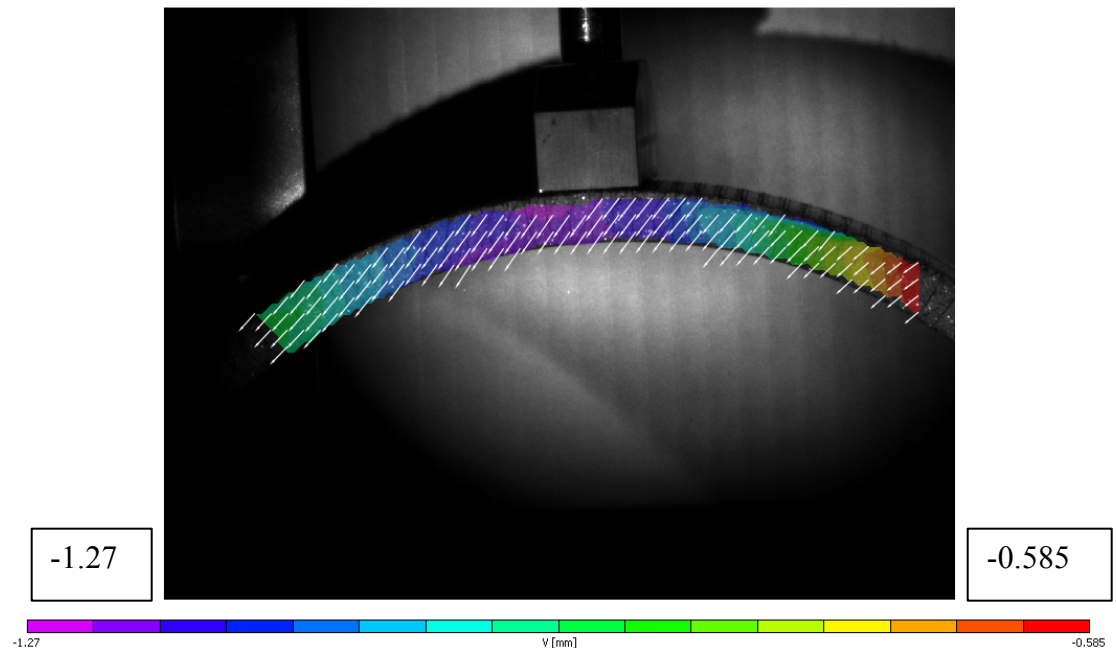
Figure 73: Shear strain fields on the X-Cor sandwich specimen as determined by DIC at (a) elastic regime, (b) before failure initiation, (c) failure initiation, and (d) start of plateau regime. The specimen fails by core shear.

The shear strain field during the elastic regime is aligned with the intuitive characteristics of the strain fields. The shear strain dominates and accumulates in an area between the central load point and the lower region of the sandwich. The shear strain reaches a value up to $\sim 1.5\%$ (Figure 73 (a,b)).

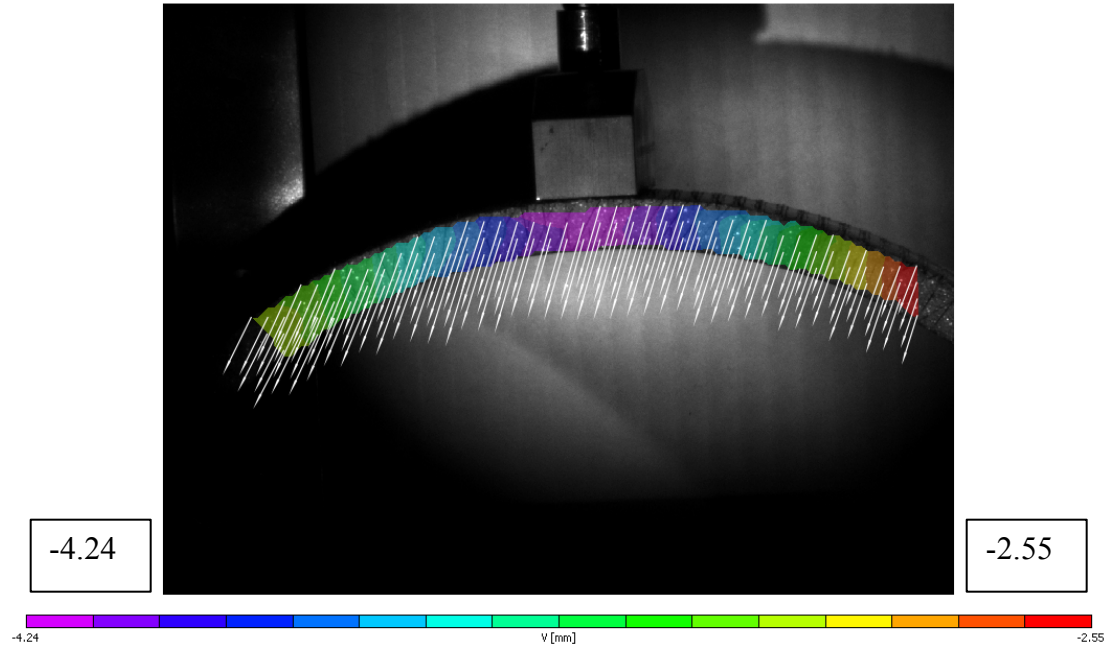
Around the failure initiation, a high magnitude of shear strain develops at the failure initiation site (Figure 73 (c)). The shear strain after failure initiation was found to be as high as 9.4% right after the shear failure. Due to the failure at the left side of the sandwich specimen, the material is required to redistribute the load to the other side of the sandwich. On the right side—where the failure did not occur—the shear strain is around -1.2% .

Beyond the failure initiation, the image becomes uncorrelated which indicates the discontinuity in the material and clearly identifies the failure initiation site (Figure 73 (d)). Observing the image of the failed specimen also confirms the failure site.

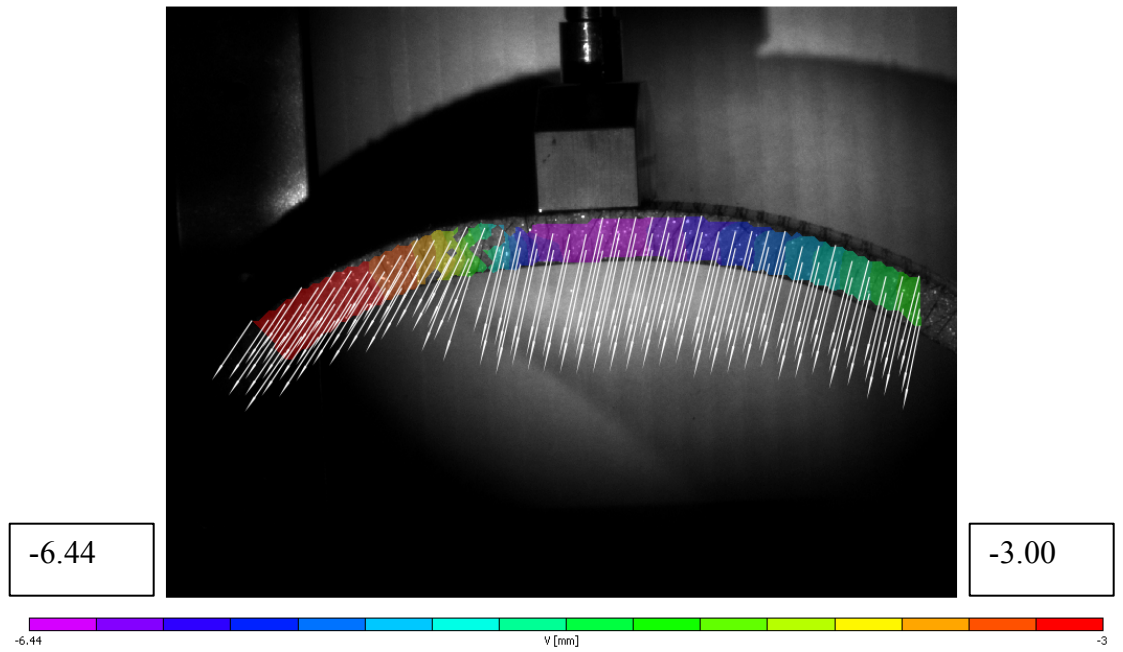
Global displacement data was also gathered within the elastic region, at the end of the elastic region and at failure. The full-field displacement images are given in Figure 74 below. The white arrows show the evolution of the displacement during the test. The length of the arrows indicates how much displacement the material experienced throughout the test and the actual values for displacement are all relative to the reference image in which there was zero displacement. For this particular experiment, the sandwich structure shifted down and to the left as the load was being increased. The maximum vertical displacement was consistently located underneath of where the load was being applied and directly in the center of the sandwich structure. The displacement was -1.27 mm and -4.24 mm in the elastic region, and end of the elastic region, respectively. Once the material experienced core shear failure and the core split apart, the maximum displacement became -6.44 mm.



(a)



(b)



(c)

Figure 74: Vertical displacement fields for a six inch radius of curvature sandwich at (a) elastic region (b) end of the elastic region and (c) failure

6.2.2.2 Strain and Displacement at a Specific Location

With 2D DIC, we can also extract the strain and displacement information for a specific point or area throughout the experiment. Choosing a point close to where the material failed shows how the strain accumulates throughout the compression test. The selected area shown in Figure 75 was chosen because the material failed by the core shear failure mechanism in that region.

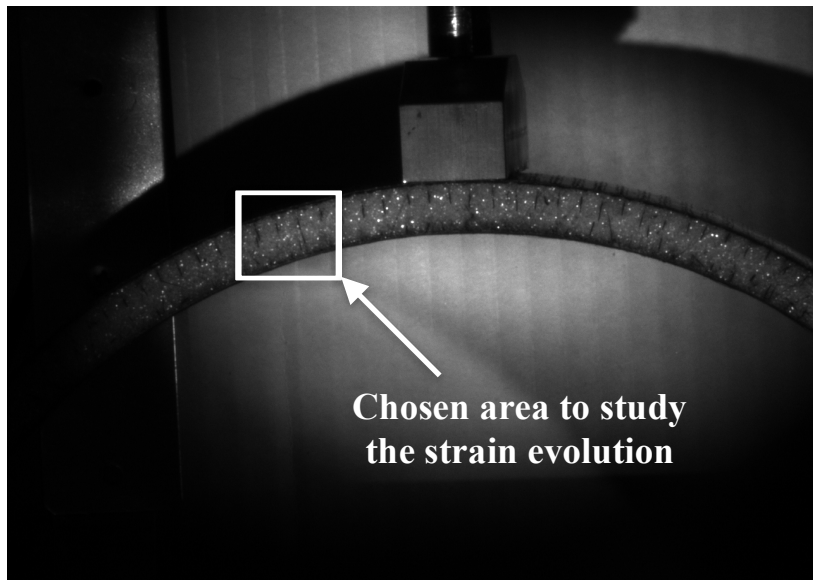


Figure 75: Chosen area for 2D DIC strain and displacement extraction

For this area, the plot of the strains versus DIC-calculated displacement is given in Figure 76. Strains in the x and y directions are given by e_{xx} and e_{yy} , respectively, and shear strain is given by e_{xy} .

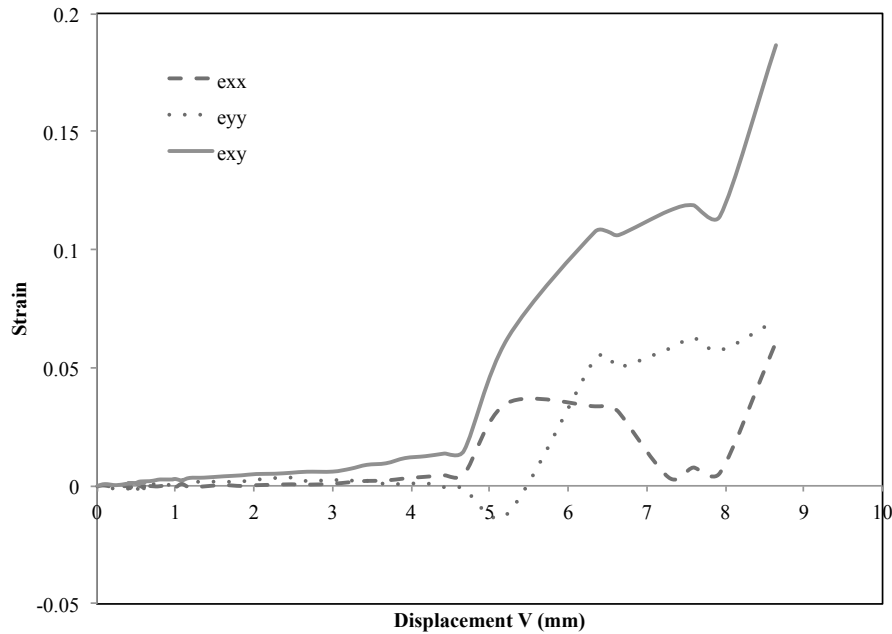


Figure 76: Strains in the x and y direction and shear strain plotted against vertical displacement.

This plot is consistent with the load-displacement graph in Figure 71. When the vertical displacement reaches 8 mm, the sandwich material experiences a high accumulation of shear strain and subsequently fails, just as the strain fields from Figure 73 (c) show.

Core shear failure seemed to be the dominant cause of failure in these tests. The DIC images and the strain-displacement plot from Figure 76 prove this to be true. Facesheet buckling and facesheet-core delamination were secondary sources of failure. Since all of the sandwiches were supported and constrained at the ends, buckling was inevitable. Most of the sandwiches buckled on the top facesheet and the foam core then proceeded to become detached from the facesheet surface (Figure 77).

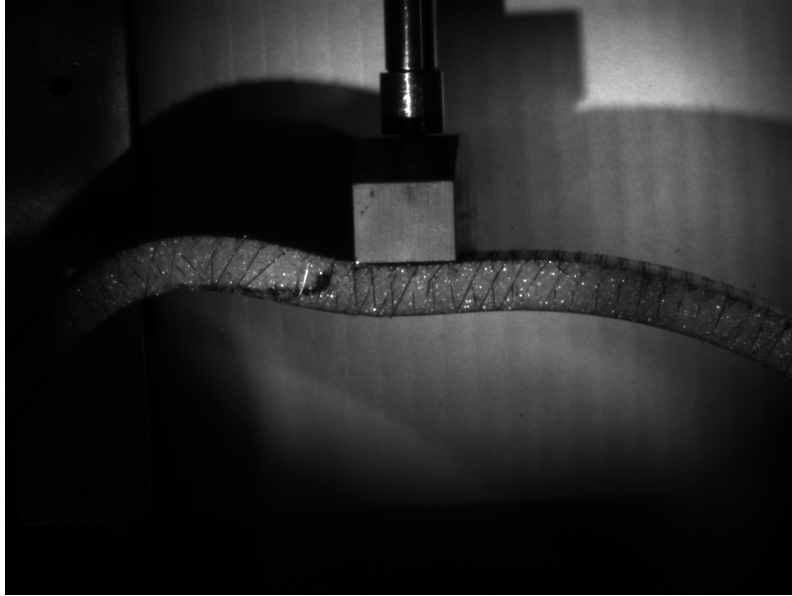


Figure 77: A sample specimen that failed by core shear failure and facesheet-core delamination

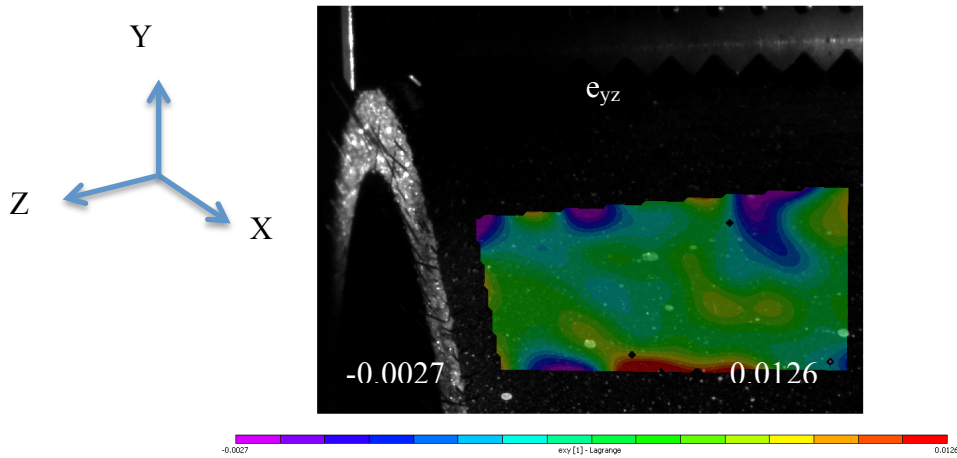
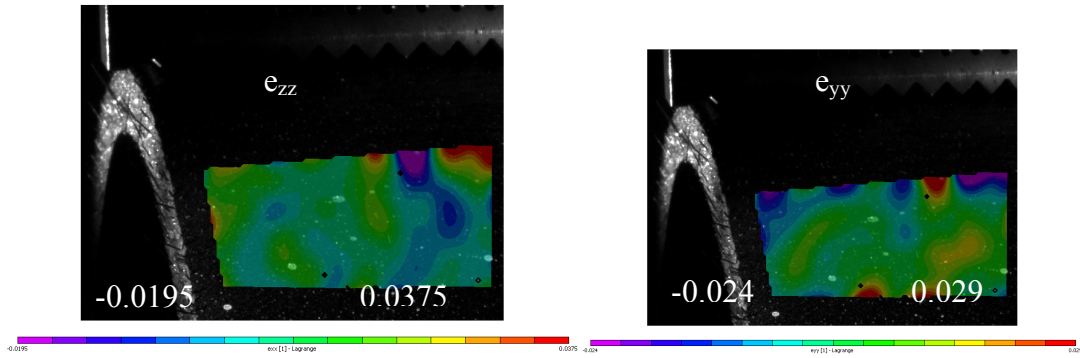
6.2.3 3D DIC Results

6.2.3.1 Strain Fields and Contour Plots

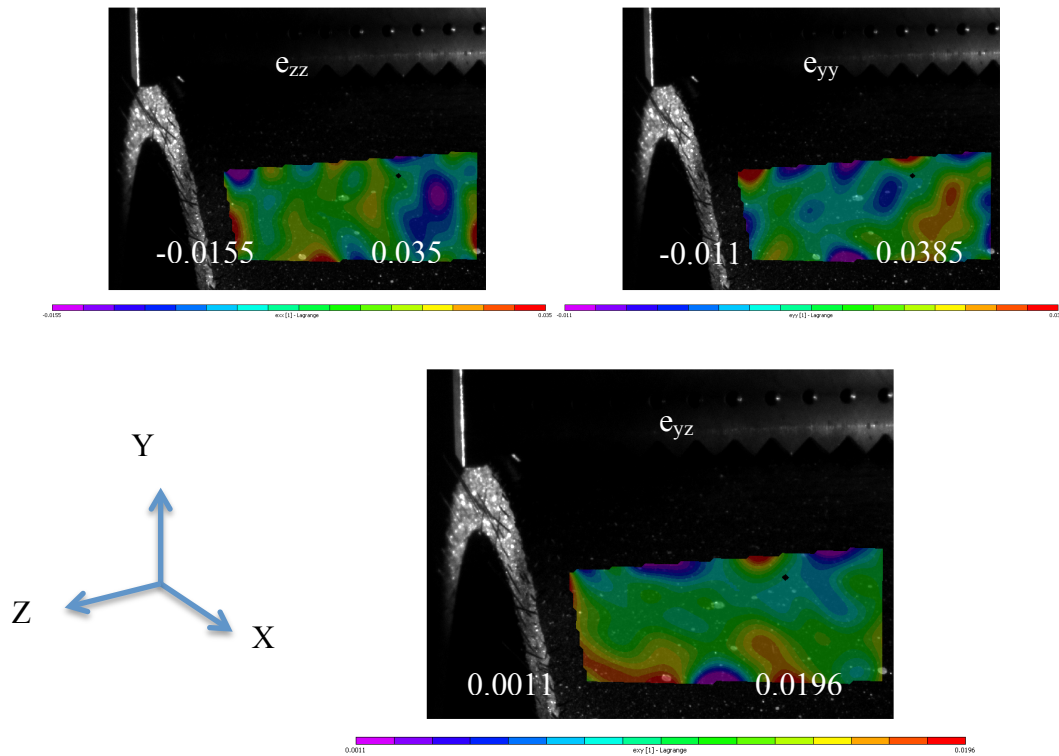
The experimental testing for the curved specimens was analyzed simultaneously with 2D and 3D DIC software programs. Results showing the strain fields and deformed 3D shapes obtained using DIC on the top facesheet during loading are given in Figure 78. The first set of 3 images was taken while the material was being loaded within the linear elastic regime. The second set of images shows what the strain field looks like just after failure initiated. Since this experiment required both 2D and 3D DIC, the coordinate system for the 3D tests is in accordance with the 2D. Therefore, the x-axis in the 3D system looks like the “out of plane” axis in the following diagram. In reality, the z-direction is the only out-of-plane axis.

When the sandwich structure was loaded in the linear elastic region (Force = 607 N), the out of plane strains (e_{zz}) dominate. It is important to note that these images were taken on the opposite side of where the core shear failure occurred. At

failure, the out of plane and transverse strains are quite similar. The maximum out of plane strain is 3.5% and the maximum transverse strain is 3.85%.



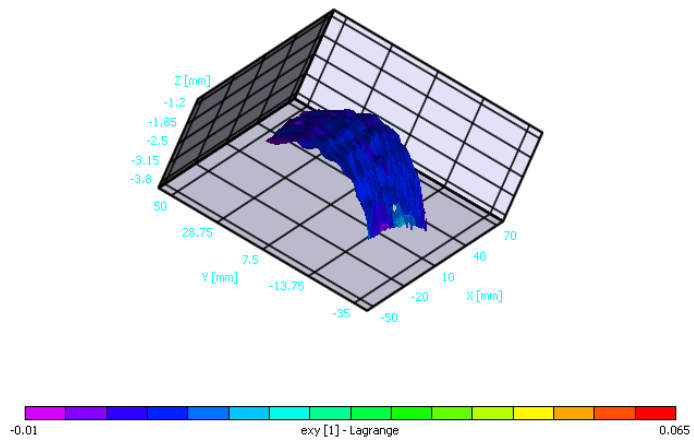
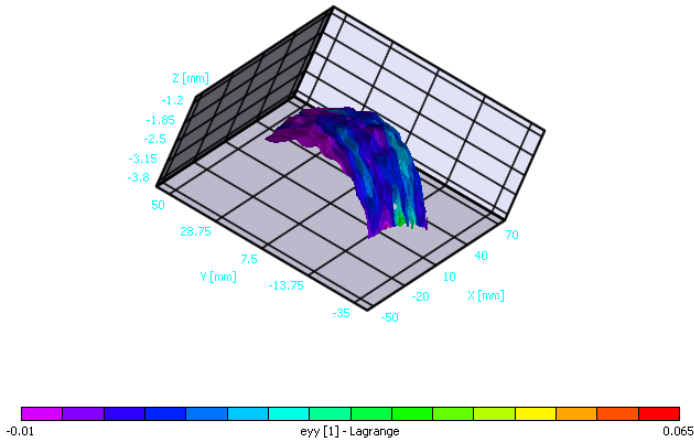
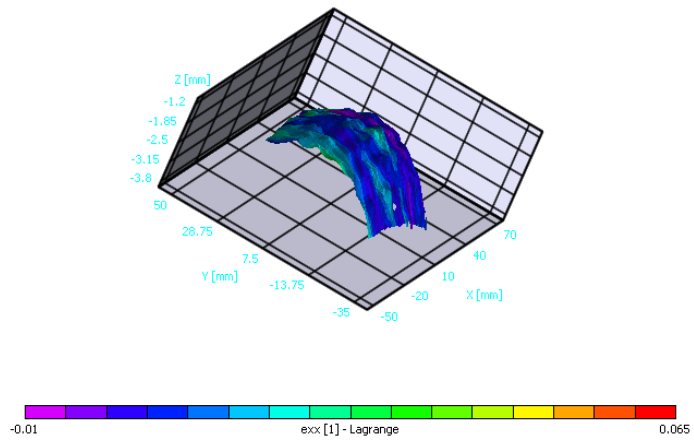
(a)



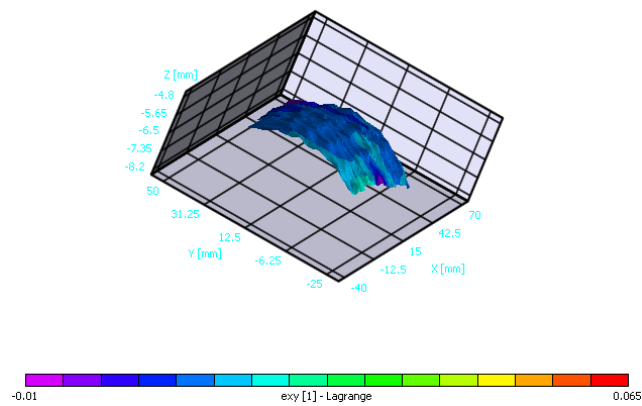
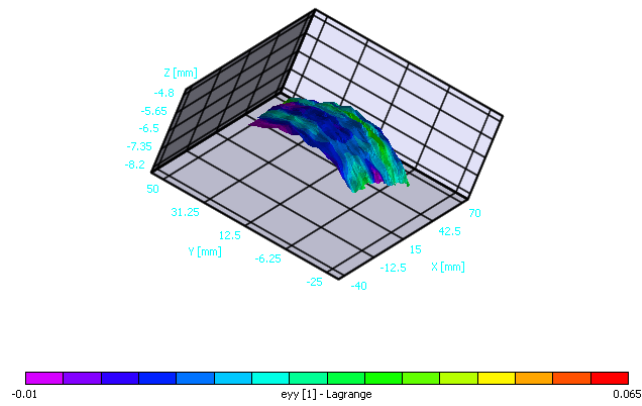
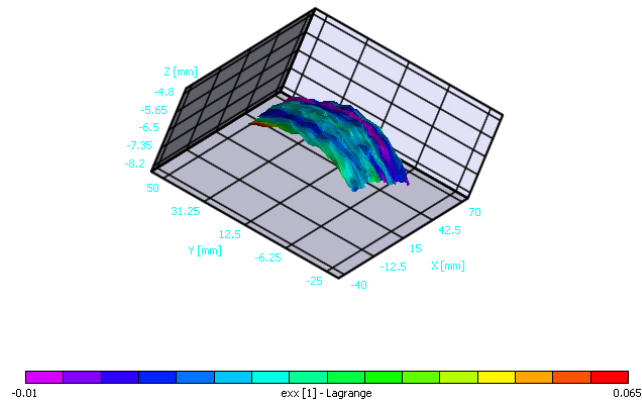
(b)

Figure 78: Strain fields, as determined by 3D DIC, for (a) within the elastic regime and (b) after the failure initiation.

With 3D DIC, the above strain fields can also be plotted as contours. The contour plots in the elastic region and at failure initiation are given in Figure 79 (a) and (b), respectively. Contour plots give a better visualization of the strain as they evolve over the deformed image than 2D DIC images. The axes are x, y, and z deformation directions, in millimeters. Upon close inspection, it is possible to see bumps on the facesheet surface. Presumably, the DIC is picking up on the pultruded carbon fiber pins that extend through the X-Cor sandwich facesheet.



(a)



(b)

Figure 79: Contour strain plots, as determined by 3D DIC, for (a) the elastic regime and (b) after the failure initiation.

6.2.3.2 Strain at a Specific Location

In a similar procedure as the 2D DIC results, an area can be chosen to extract the evolution of the strains in the facesheet during bending of the curved X-Cor sandwich composite. Figure 80 depicts the area that was considered along with the appropriate coordinate system.

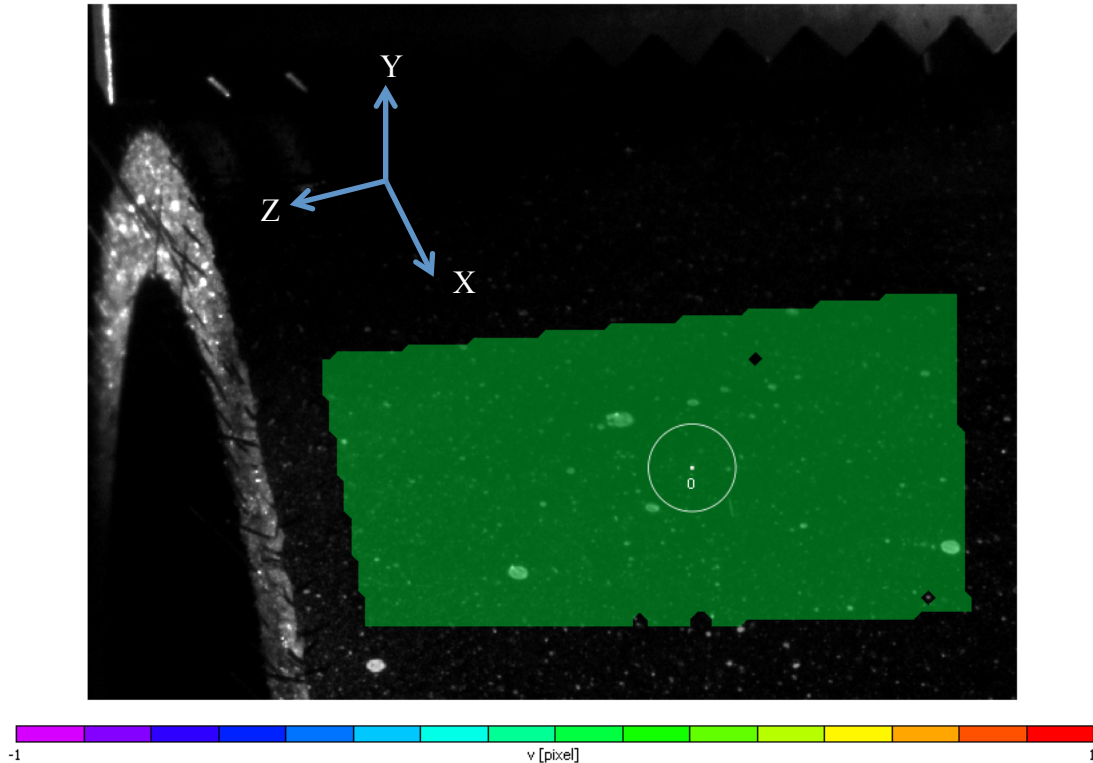


Figure 80: Representative image to show the area used to extract strains from 3D DIC.

The strain evolution in the facesheet during bending is shown in Figure 81 and Figure 82. Since the specimens were 3 inches wide, it is noted that the normal strain (ϵ_{zz}) in the out of plane direction is minimal, whereas the normal strain in the longitudinal direction (ϵ_{yy}) was the largest. The out of plane normal strain was as low as 1%, whereas the shear strain (ϵ_{yz}) and longitudinal normal strain (ϵ_{yy}) were much larger, at 2.5% and 5%, respectively. Consistent with the information gained from 2D

DIC, the shear strain accumulates up until the displacement reaches ~5 mm. Then, all three of the strains separate, with ϵ_{yy} reaching a maximum value of 5% DIC strain.

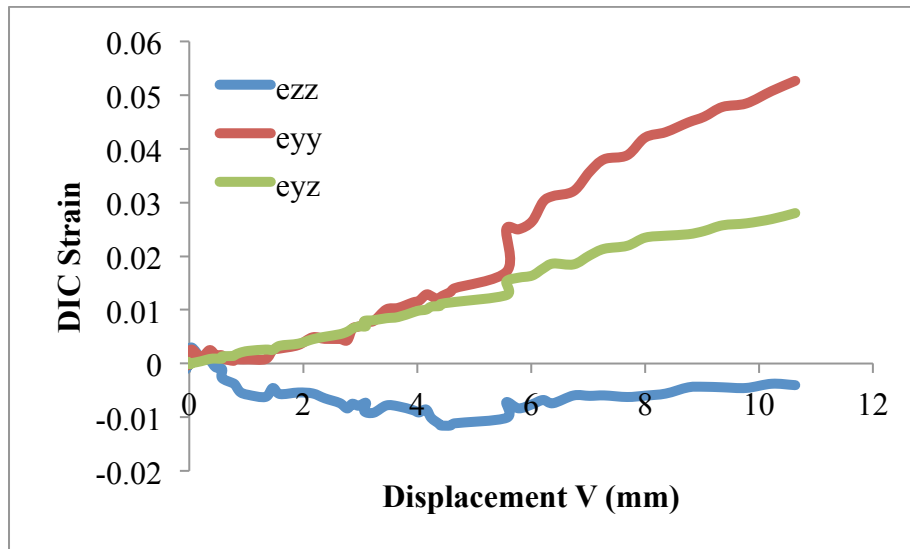


Figure 81: 3D DIC strain versus vertical displacement (ref. Figure 78)

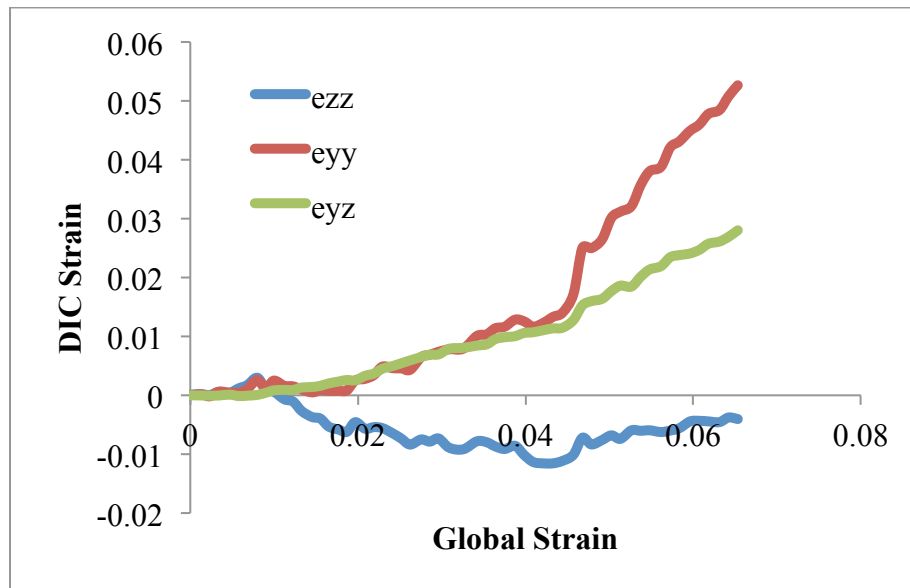


Figure 82: Plot of DIC Strain versus global strain (ref. Figure 78)

VIC 3D also allows for the calculation of curvature for these experiments. Like strain, curvature can also be calculated for any point in the specimen. Since these specimens are contoured, curvature is found to be an important value to

quantify. These results are presented simply for educational purposes. Hopefully, DIC will be used to determine the curvature for other sandwich specimens in the future. For the singly contoured 6" radius specimens, curvature has been calculated and plotted against load to show how the accumulation of load affects curvature over the surface at a specific point (Figure 83). The chosen point is the same as the one selected in Figure 80. Although there is some curvature, the sandwich structure is mostly flat for the chosen data point. This results in curvature values at or near zero, which is quite logical. Curvature has units of 1/mm.

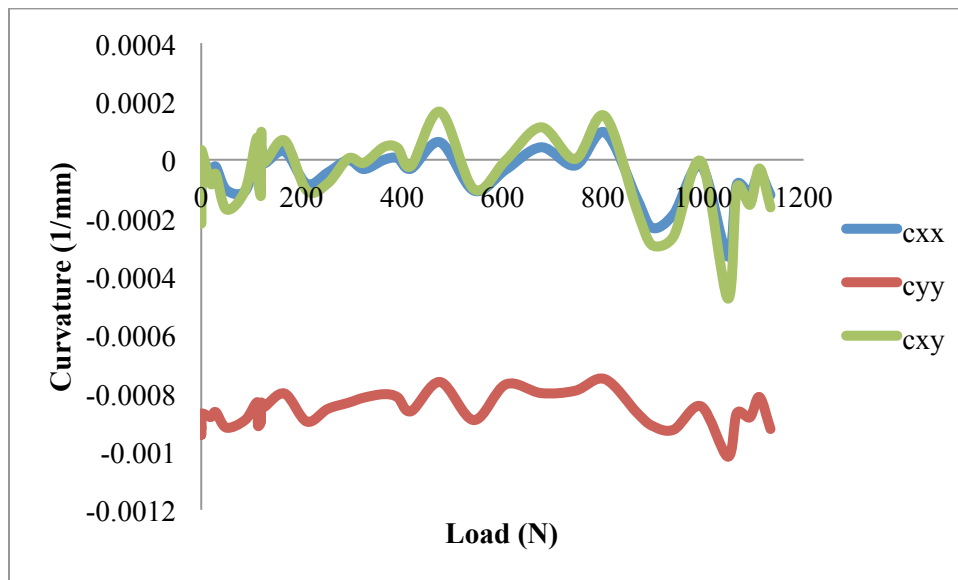


Figure 83: Plot of curvature versus macroscopic load

For added comparison, the values of curvature and radius of curvature are presented for both the small curved specimens prepared at UMD and the large curved specimens provided by AEC. At the most curved part of the large contoured sandwich the curvature is 0.007/mm. At the same location for the smaller sandwich, the curvature is 0.0072/mm. Since curvature and radius of curvature have an inverse

proportional relationship, it can be shown that the radius of curvature is 138.89 mm (5.47 in) for the small sandwich and 142.86 mm (5.62 in) for the large sandwich.

6.2.4 Comparison with Small Curved Specimen

There is significant variation in load-bearing capacity between the smaller curved specimens produced at UMD and the large curved materials provided by AEC (Figure 84). The maximum load withstood before failure by the small sandwiches was 400 N whereas the large sandwiches could hold up to 1100 N. Most likely, this is simply because of the size difference. Another significant distinction between the observed characteristic behaviors of these sandwiches is the plateau regime in the load-displacement response for the large curved sandwich specimens from AEC. As displacement increases, both of the sizes of curved specimens appear to have a decrease in load bearing capacity after failure initiation. The large sandwich structure has a response similar to the flat specimen as it exhibits a large drop in load bearing capacity immediately following the elastic region. The larger specimens had enough displacement to deform in the plateau regime, however the UMD curved specimen had less vertical space to displace. Because of this, the UMD specimen exhibited a compressive “crushing” behavior and the 6 inch radius curved specimen showed a constant force.

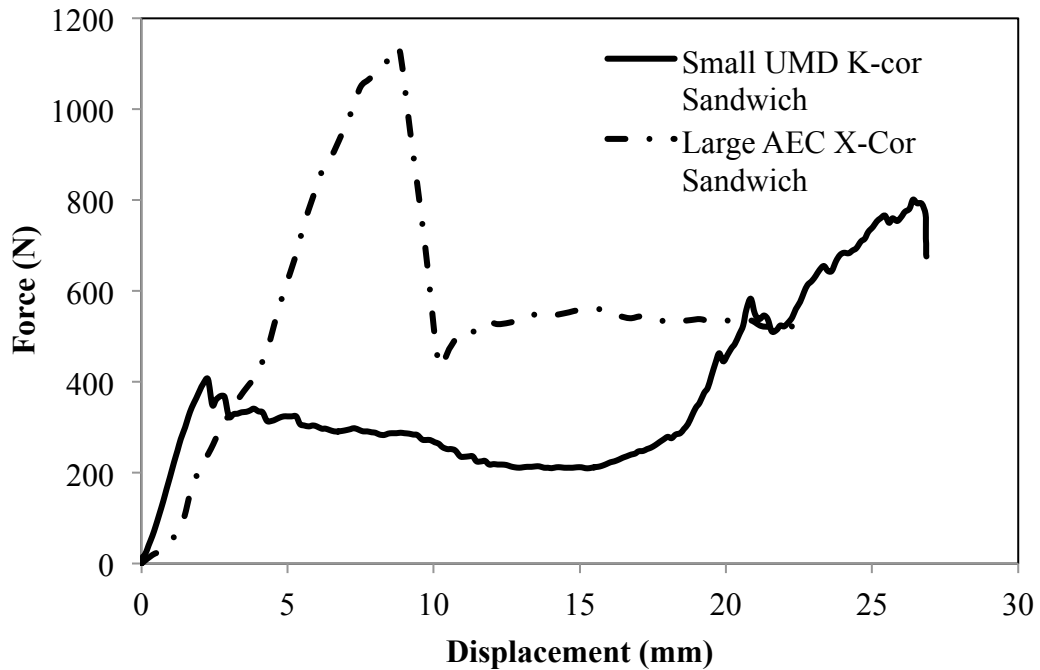


Figure 84: The non-normalized load-displacement response for small and large curved sandwich specimens.

In addition, the small specimens were K-cor sandwich structures and the large specimens were X-cor sandwich structures. X-Cor sandwich structures have pins that are attached directly into the facesheet, so the bonding was much stronger than the K-cor sandwiches. This difference could have played a role in the load bearing capacity of these sandwiches. The curved specimens from UMD exhibited the same failure modes as the AEC specimens.

Normalizing the load-displacement plot to adjust for size differences results in the stress-strain plot in Figure 85 below. The equations inside of the graph are the same ones from *Section 6.2.1: Load-Displacement Results*. From this plot, it is evident that the large X-Cor sandwiches can reach a maximum stress of 20 MPa and the smaller K-Cor sandwich can only attain 9.5 MPa. Although the smaller sandwich cannot hold as much stress as its larger counterpart, the K-Cor sandwich is able to

experience more strain. It is important to note that the small sandwich failed at a shear strain of -5.5% and the large sandwich failed at a shear strain of 9.4%, as calculated by 2D DIC.

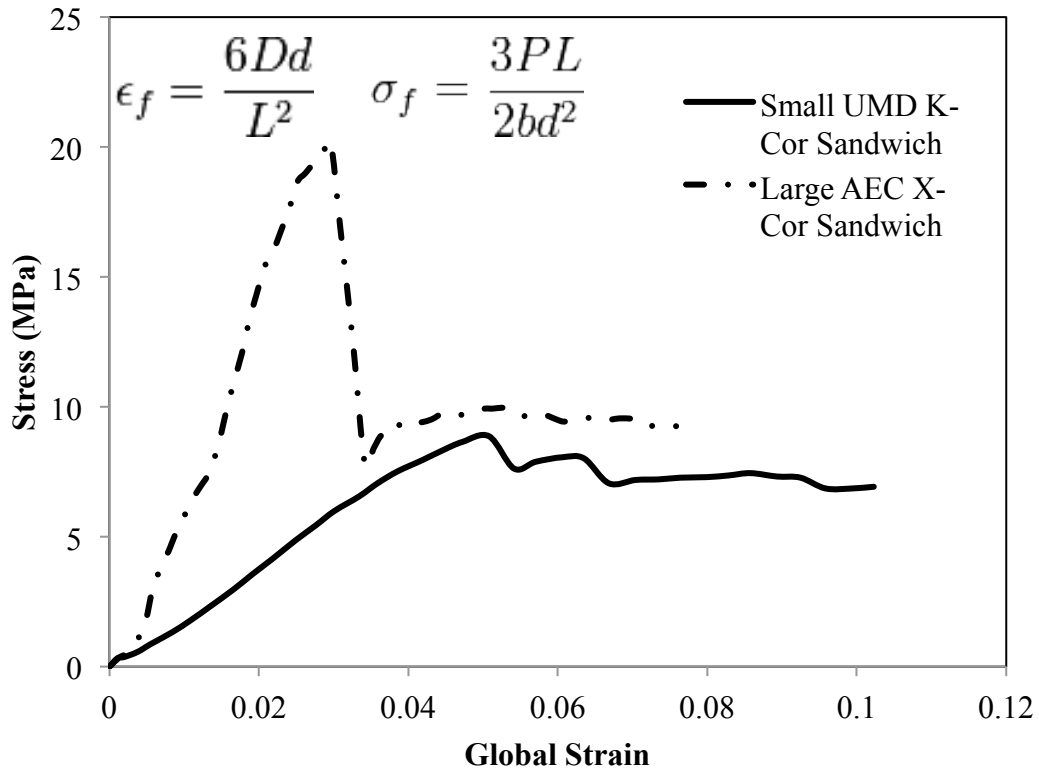


Figure 85: Stress-Strain plot to show the response of small K-Cor curved sandwiches prepared at UMD and large X-Cor curved sandwiches from AEC.

6.3 Discussion

In this final experiment, five 3-inch wide singly curved X-Cor sandwich structures with a 6-inch radius were tested under compressive loading. Upon closer inspection, it was determined that the actual radius of curvature is 5.5 inches. This relates to a curvature of 0.007/mm, which is very similar to the curvature of the small curved specimens manufactured at UMD. The load-displacement response for these larger curved structures is comparable to the curved K-cor

specimens manufactured at UMD. The main difference between these two is the load bearing capacity, but that is derived from the increased size of the larger specimen. The large X-Cor sandwich could withstand a maximum load of 1100 N before failure, whereas the small K-Cor sandwich could only hold 400 N. Flexural stiffness of the large curved sandwich composite specimens has been determined to be around 170 N/mm and the compressive strength was 20.2 MPa. The compression stiffness for these sandwiches was calculated to be 728 MPa. The maximum load that the test specimens could carry was between 1100 – 1400 N. Displacement for the large sandwich reached a maximum value of 25 mm during the test.

The main failure mechanisms for this large curved sandwich structure were core shear failure and facesheet buckling. Occasionally, both failure mechanisms would occur, but more often the sandwiches failed solely by core shear failure. The experimental testing for the curved specimens was analyzed simultaneously with 2D and 3D DIC software programs. The 2D DIC picked up on the concentrated shear strain in areas where the material failed by core shear failure. The maximum shear strain observed near the failure site was 9.4% at failure. After failure, the DIC images became uncorrelated and it was no longer possible to calculate strains and displacements. 3D DIC gave insight on how the sandwich structure material accumulates strain in the out-of-plane direction. At this time, no conclusions can be drawn about the pin-facesheet interaction playing a role in failure of these sandwich structures because no testing was conducted without the foam core removed.

3D DIC was also used to determine the curvature of the facesheet surface. For the section of the sandwich structure that was chosen, the facesheet was mostly flat. This resulted in very small curvature values, but this is to be expected.

Chapter 7: Conclusion

This research investigated the mechanical properties of pin-reinforced composite sandwich structures under compressive loading and three-point bending. 2-dimensional and 3-dimensional Digital Image Correlation was successful in calculating the full-field strains and displacements for these multi-scale experiments. Tests were conducted on small-scale cross pins, representative volume elements, flat sandwich structures, and singly curved contoured sandwiches. A brief summary of the findings from this research is given below, followed by a Contributions section and Future Work.

Multi-scale DIC results show that the strains in the facesheet are not quite as significant as the through-thickness strains. The previously described macrostress equation that was used to transform small-scale loads into macroscale stresses proved to be valid on the representative volume element level as well. There was close correlation between the material stiffnesses and strengths. This is a significant finding, because the small-scale specimens were not tested to failure like the RVEs were. We now know that the sandwich behaves in an elastic manner before failure and in an inelastic manner after failure. The contoured specimens that were tested show that the pin-reinforced composite sandwich structure exhibits the same evolution of loading as flat sandwich structures, but the load bearing capacity changes depending on the size of the sandwich.

7.1 Contributions

This work set out to accomplish several goals, including: property characterization, understanding the effect of carbon fiber pins, and the response of the macro-scale material. Through these experiments, all of these goals were accomplished. Property characterization was achieved by the use of compression and three-point bend testing. 3D DIC was used to analyze representative volume elements to understand how the carbon pins accumulate strain as load is being applied. These results were shown to be scalable by using the macroscale stress conversion equation given in (Eq. 8). The DIC characterization method proved to be successful in determining full-field strains and displacements in both the through-thickness and out-of-plane directions. Results from this research program show that large singly curved pin-reinforced composite sandwich structures can reach a maximum stress level of 20 MPa and can withstand compressive loadings of up to 1400 N. This research also shows that the compressive properties of pin-reinforced composite sandwich structures are scalable and that local pin deformation greatly affects the overall macroscale response.

7.2 Future Work

Before I give any advice on what future work can be done, I'd first like to give some recommendations and tips that will be helpful in conducting the future work experiments. Several of the experiments conducted during this research turned out to be inconclusive, in that they did not allow for any DIC data to be extracted. This occurred for many different reasons, but more often than not it was because of a

lighting issue. Large glares would show up over the pins, thereby blocking the cameras from viewing the speckle pattern. For future experiments, I recommend that the pins for these sandwich structures be painted with a non-reflective coating and then spray-painted to create a speckle pattern.

In order to understand the pin-facesheet interaction for shaped sandwich structures, the 6” singly curved specimens from AEC must be tested without the foam core intact. The deformation as a function of displacement must be determined in critical locations that are prone to failure, similar to what has done for the experiments presented in this thesis. This will aid MR&D in improving their micromechanics tool. It is possible that there will be a different response than what we saw in Chapter 5 because the AEC specimens are X-cor and the UMD small curved sandwiches are K-cor. To carry out this experiment on the micro-scale, it is recommended that lens extenders be used to capture the pin response to compressive loading. This will make it easier to visualize the speckle pattern with DIC and thereby calculate displacements and strains.

After the 6-inch radius curved sandwiches are fully characterized, the 12-inch singly curved sandwich structures from AEC should be tested.

The doubly curved hemisphere shaped shell structures should be tested next in order to verify these results and add more robustness to the micromechanical tool.

MR&D already has an idea for the size and shape of the specimens they wish to test.

These dimensions are as follows:

- X-Cor sandwich structure with a spherical shape (6” diameter, 0.5” thick)

- Pin density of 3 lb/ft³
- Facesheet should be 0/90 4-ply skins

As with any material, the pin-reinforced composite sandwich structure should also be tested for thermal and environmental reliability. In particular, it would be interesting to see the effect of increased temperature on thermal expansion, degraded elastic properties and nonlinear creep/viscoelastic effects on the load-bearing capacity of the composite sandwich.

Glossary

AOI: Area of Interest. This user-selected area defines what space will be inspected to calculate displacements and strains within the material with DIC.

Calibration images: This set of images is used to calibrate the two cameras that will be used for 3D DIC analysis. Without the correct calibration images embedded into the VIC 3D project file, the resulting data will be invalid. Calibration images can also be used for 2D DIC experiments, but is not necessary.

Core: Soft, lightweight inner layer of the composite sandwich structure; the “meat” of the sandwich. In these experiments, a Rohacell 31 foam was used as the core material.

DIC: Digital Image Correlation. This is the program that was used to analyze the image’s AOI and calculate displacement and strain.

Facesheet: Carbon fiber laminates; the “bread” of the sandwich structure

Pin Density: Weight of the pins contained inside of a unit volume of sandwich structure.

Reveal Length: The length of pins that extends beyond each surface of foam core

RVE: Representative Volume Element. The smallest unit for which a single unit cell can represent the full specimen on a micro-mechanical scale.

Speckle image: Images that are captured during the experiment; must include a speckle pattern in order for results to be calculated with DIC.

Speckle pattern: This pattern is applied to the material before testing; usually applied via spray paint. The pattern creates data points for DIC to track as it steps through each speckle image.

Bibliography

- [1] Plantema, F. J., Sandwich Construction: The Bending and Buckling of Sandwich Beams, Plates, and Shells, Jon Wiley and Sons, New York, (1966).
- [2] Virakthi, A., “Stiffness and Strength of K-Cor Sandwich Structures Under Compression and Shear Loading Conditions”, University of Maryland, (2011)
- [3] <http://www.onr.navy.mil/Science-Technology/Departments/Code-33/All-Programs/332-naval-materials/Solid-Mechanics.aspx>
- [4] Vinson, Jack, “Sandwich structures 7: Advancing with Sandwich Structures and Materials: Proceedings of the 7th International Conference on Sandwich Structures”, Aalborg University, Aalborg, Denmark, 29-31 August 2005, page 3-12
- [5] Boeing 707 Family.
<http://www.boeing.com/commercial/707family/index.html>
- [6] Boeing 767 Family.
<http://www.boeing.com/commercial/767family/background.html>
- [7] T. Kevin O’Brien, Isabelle L. Paris, “Exploratory investigation of failure mechanisms in transition regions between solid laminates and X-cor truss sandwich”, Composite Structures 57 (2002) p. 189–204
- [8] A. Nanayakkara, S. Feih, A.P. Mouritz, “Experimental analysis of the through-thickness compression properties of z-pinned sandwich composites”, Composites Part A (2011) 42: 1673–1680.
- [9] Mouritz, A.P., “Compression properties of z-pinned sandwich composites”,

Journal of Materials Science (2006), 41: 5771-5774.

- [10] Daniel, Isaac M., Gdoutos, Emmanuel E., “Failure Modes of Composite Sandwich Beams”, Major Accomplishments in Composite Materials and Sandwich Structures: An Anthology of ONR Sponsored Research, Springer (2009), 197-227.
- [11] Composites World. <http://www.compositesworld.com/products/foam-based-x-cor-and-k-cor-lightweight-structural-cores>
- [12] Bruck, Hugh A.; Lee, Sung A.; Sharkey, Curtis. “Tenth and Eleventh Progress Reports on ‘Mechanical Characterization and Modeling of X- and K-Cor panels’”
- [13] Marasco, Andrea I., Cartié, Denis D. R., Partridge, Ivana K., Rezai, Amir, “Mechanical properties balance in novel Z-pinned sandwich panels: Out-of-plane properties”, Composites: Part A (2006) 37: 295-302
- [14] The Composites Store. www.cstsales.com
- [15] Zhong, Reimerdes, “Stability Behavior of Cylindrical and Conical Sandwich Shells with Flexible Core”, Journal of Sandwich Structures and Materials (2007)
- [16] Göttner, Wilfried; Reimerdes, Hans-G., “Low Velocity Impact Investigations of Sandwich Panels with Different Cores”, Sandwich Structures 7: Advancing with Sandwich Structures and Materials (2005), 661–670.
- [17] Wallace, Brian T., Sankar, Bhavani V., Ifju, Peter G., "Pin Reinforcement of Delaminated Sandwich Beams under Axial Compression", Journal of Sandwich Structures and Materials (2001), Vol 3: 117-129.

- [18] Cartie, Denis D., Fleck, Norman A., "The effect of pin reinforcement upon the through-thickness compressive strength of foam-cored sandwich panels", *Composites Science and Technology* (2003), 63: 2401-2409.
- [19] Wang, Bing; Wu, Linzhi; Ma, Li; Sun, Yuguo; Du, Shanyi, "Mechanical behavior of the sandwich structures with carbon fiber-reinforced pyramidal lattice truss core", *Materials and Design* (2010), 31: 2659-2663.
- [20] Haldar, S., Gheewala, N., Grande-Allen, K.J., Sutton, M.A., Bruck, H.A., "Multi-scale Mechanical Characterization of Palmetto Wood using Digital Image Correlation to Develop a Template for Biologically-Inspired Polymer Composites", *Experimental Mechanics* (2011), 51: 575-589.
- [21] Rice, M.C., Fleischer, C.A., Zupan, M., "Study on the Collapse of Pin-Reinforced Foam Sandwich Panel Cores", *Experimental Mechanics* (2006), 46: 197-204.
- [22] Sutton, Michael A., Orteu, Jean-José, Schreier, Hubert W., "Image Correlation for Shape, Motion and Deformation Measurements: Basic Concepts, Theory and Applications", Springer (2009).
- [23] Carlsson, L.A., Kardomateas, G.A., "Structural and Failure Mechanics of Sandwich Composites", Springer (2011).
- [24] Marasco, Andrea I., Cartié, Denis D.R., Partridge, Ivana K., "Mechanical properties balance in novel Z-pinned sandwich panels: out-of-plane shear", Presentation at CompTest, September 21-23, 2004.